DEVELOPMENT AND CHARACTERIZATION OF A TISSUE ENGINEERED MULTICOMPONENT SKIN SUBSTITUTE AND A SKIN MODEL

A THESIS SUBMITTED TO
THE GRADUATE SCHOOL OF NATURAL AND APPLIED SCIENCES
OF
MIDDLE EAST TECHNICAL UNIVERSITY

BY

GÖZDE EKE

IN PARTIAL FULFILLMENT OF THE REQUIREMENTS
FOR
THE DEGREE OF DOCTOR OF PHILOSOPHY
IN
BIOTECHNOLOGY

FEBRUARY 2018

Approval of the thesis:

DEVELOPMENT AND CHARACTERIZATION OF A TISSUE ENGINEERED MULTICOMPONENT SKIN SUBSTITUTE AND A SKIN MODEL

submitted by **Gözde EKE** partial fulfillment of the requirements for the degree of **Doctor of Philosophy in Biotechnology Department, Middle East Technical University** by,

Prof. Dr. Gülbin Dural Ünver _____
Dean, Graduate School of **Natural and Applied Sciences**

Assoc. Prof. Dr. Can Özen _____
Head of Department, **Biotechnology, METU**

Prof. Dr. Vasıf Hasırcı _____
Supervisor, **Biological Sciences Dept., METU**

Prof. Dr. Nesrin Hasırcı _____
Co-supervisor, **Chemistry Dept., METU**

Examining Committee Members:

Prof. Dr. Ayse Ebru Abalı _____
Vocational School of Health, Baskent University

Prof. Dr. Vasıf Hasırcı _____
Department of Biological Sciences, METU

Prof. Dr. Ayşen Tezcaner _____
Department of Engineering Sciences, METU

Assoc. Prof. Dr. Halime Kenar _____
Arslanbey Vocational School, Kocaeli University

Assoc. Prof. Dr. Çağdaş Devrim Son _____
Department of Biological Sciences, METU

Date: 01.02.2018

I hereby declare that all information in this document has been obtained and presented in accordance with academic rules and ethical conduct. I also declare that, as required by these rules and conduct, I have fully cited and referenced all material and results that are not original to this work.

Name, Last Name: Gözde EKE

Signature:

ABSTRACT

DEVELOPMENT AND CHARACTERIZATION OF A TISSUE ENGINEERED MULTICOMPONENT SKIN SUBSTITUTE AND A SKIN MODEL

EKE, Gözde

Ph.D., Department of Biotechnology

Supervisor: Prof. Vasıf HASIRCI

Co-Supervisor: Prof. Nesrin HASIRCI

February 2018, 153 pages

The tissue engineered human skin substitute has the potential to fill large areas of skin loss caused by severe burns or chronic wounds. It can also serve as an alternative skin model to *in vivo* testing of drugs or cosmetic products. The aim was to construct a tissue engineered full-thickness human skin model mimicking the native tissue. To this end, this model was developed as epidermis, dermis and subcutaneous tissue of the skin. The feasibility of the dermis layer was tested by co-culturing fibroblasts and epithelial cells isolated from healthy human biopsies in two different scaffolds: An electrospun trilayer mesh and collagen sponge. Dermis substitutes mimicking the native dermis were characterized by scanning electron microscopy, histology, immunohistochemistry and mechanical testing. Decellularized human dermis and

native human skin were used as controls. As a subcutaneous tissue, photocrosslinked hydrogels were obtained and loaded with adipose derived stem cells that can be used to improve the regeneration of skin on difficult wound beds by stimulating rapid neovascularization. The photocrosslinkable hydrogels were achieved by first synthesizing methacrylated gelatin and hyaluronic acid. These polymers were then dissolved in media with adipose derived mesenchymal stem cells (ADSCs) and human umbilical vein endothelial cells (HUVEC), and afterward crosslinked to obtain a cell-laden hydrogel. These hydrogels provided a suitable microenvironment for stem cell proliferation, and HUVECs induced prevascularization. Empty and cell-laden gels were used in chick embryo *ex ovo* to demonstrate the angiogenic activity of the constructs. Penetration of poly(3-hydroxybutyrate-co-3-hydroxyvalerate) (PHBV) nanoparticles was studied in the trilayer electrospun dermal model. Penetration of the particles and release of a lipophilic dye was studied using Rhodamine as a model drug which was released at the epidermal layer and penetrated throughout the construct.

In conclusion, skin substitute and model produced in this thesis showed the desired proliferative and angiogenic properties essential to promote vascularization for wound healing and to improve survival of tissue engineered skin substitute. It is also possible to use the tissue engineered skin construct as an *in vitro* model for drug delivery studies or cosmetic products instead of *in vivo* animal models.

Keywords: Skin tissue engineering, Neovascularization, Skin substitute, Photocrosslinking, Nanoparticles, Transdermal drug delivery, Epithelial cells, Mesenchymal stem cells

ÖZ

DOKU MÜHENDİSLİĞİ İLE ÜRETİLMİŞ ÇOK BİLEŞENLİ BİR YAPAY DERİ EŞLENİĞİ VE DERİ MODELİ GELİŞTİRİLMESİ VE KARAKTERİZASYONU

Eke, Gözde

Doktora Tezi, Biyoteknoloji Bölümü

Tez Yöneticisi: Prof. Dr. Vasıf Hasırcı

Ortak Tez Yöneticisi: Prof. Dr. Nesrin Hasırcı

Şubat 2018, 153 sayfa

Doku mühendisliği ürünü insan deri eşleniği, şiddetli yanık ya da kronik yaralar sonucunda oluşan geniş yüzeyli deri kayıplarını telafi etme olanağı sağlayabilecektir. Bu yapay deri aynı zamanda ilaç ya da kozmetik ürünlerin *in vivo* testlerinin yerine de kullanılabilir. Bu çalışmanın amacı doğal dokuya çok yakın özellikler taşıyan bir tam kalınlıkta yapay insan derisi geliştirmektir. Bu amaç doğrultusunda, öncelikle bu model epidermis, dermis ve subkütan doku olarak geliştirildi. Dermis katmanının yapılabilirliğini sınamak amacıyla, sağlıklı insan derisinin biyopsilerinden elde edilen fibroblastlar ve epitel hücreler, iki farklı doku iskelesi içinde yetiştirilmişlerdir: Elektroeğirme ile üretilen üç katmanlı ağ yapısı ve kolajen sünger doku iskelesi içerisinde kültür edilmiştir. Taramalı elektron mikroskopisi (SEM), histoloji, imunohistokimya ve mekanik test sonuçları doğala çok benzeyen bir dermis eşleneğinin elde edilebildiğini göstermiştir. Çalışmalarda, kontrol yapılar olarak

sağlıklı insan derisi ve hücrelerinden arındırılmış bir dermis kullanılmıştır. Subkütan doku olarak, çapraz bağlanmış hidrojeller tasarlanıp, bu hidrojellere adipoz kökenli kök hücreler yüklenmiştir. Aynı zamanda kök hücre yüklü hidrojeller, hızlı bir damarlaşmaya yol açarak derin yara yatakları üzerindeki derinin de iyileşmesini sağlamaktadır. Hidrojeller, öncelikle metakrilat jelatin ve hiyalüronik asit sentezleyerek elde edildi. Bu polimerler daha sonra ortamda yağ dokusundan elde edilen mezenkim kök hücreler (ADSCs) ve insan umbilikal damar endoteli hücreleri (HUVEC) ile karıştırılarak, hücreyle yüklü bir hidrojel elde etmek için çapraz bağlandı. Hidrojellerin kök hücre çoğalması için uygun bir mikro ortam sağladığı ve HUVEC hücrelerinin damar oluşumunu başlattığı gözlendi. Hücre yüklü veya hücresiz jeller, *ex ovo* civciv embriyolarında, yapıların anjiyojenik aktivitesini göstermek için kullanıldı. Poli(3-hidroksibütirat-ko-3-hidroksivalerat) (PHBV) nano parçacıklarının deri içerisinden nüfuz etmesi üç katmanlı dermis modelinde incelendi. Nanoarçacıkların deri modeline nüfuz etmesi ve ilaç salımı incelenmiştir. Lipofilik yapıda olan Rhodamine boyası, epidermis katmanında salınmış ve yapı boyunca nüfuz etmiştir.

Sonuç olarak, bu tezde üretilen deri eşleniği ve modeli, yaranın iyileşmesi için gereken damarlaşmayı teşvik edici ve yapay derinin hayatta kalması için gerekli proliferatif ve anjiyojenik özellikleri göstermiştir. Doku mühendisliği yöntemi ile tasarlanmış bu deri modeli ayrıca *in vitro* modeli olarak, ilaç salım çalışmaları ya da kozmetik ürünlerin testleri için, *in vivo* modeller yerine de kullanılabilir.

Anahtar kelimeler: Deri doku mühendisliği, Damarlaşma, Deri eşleniği, Çapraz bağlama, Nanoparçacıklar, Transdermal ilaç salımı, Epitel hücreler, Mezenkimal kök hücreler

Dedicated to my beloved family…

ACKNOWLEDGEMENTS

I would like to express my most sincere gratitude to my supervisor Prof. Vasıf Hasırcı for his continuous guidance, encouragement, motivation and support throughout my thesis. I am grateful for his patience, and effort to improve my scientific experience during my graduate years. I am very thankful to him for allowing me to participate in his lab team, giving me a chance to work with him. Prof. Hasırcı has been my inspiration as I hurdle all the obstacles in the completion this research.

I am very grateful to my co-supervisor Prof. Nesrin Hasırcı who has been a significant role model to me and has kind consideration regarding my academic requirements. I was fortunate for her mentoring and valuable advices which improved my scientific experience to an international level.

I would like to express my gratitudes to Prof. Sheila MacNeil for giving me a chance to experience an international research environment and her guidance during my experiments in University of Sheffield. Time and effort she spent on my studies were so valuable to me. I am very thankful to her students Naside Mangir, Sabiniano Roman who guided my experiments with an unfailing support. I would like to thank Brenda Narice, Marcela Garcia Martinez and MehRi Be for making my life in England fruitful, warm and full of memory. I would like to express my deep sincere to Antony Bullock for his limitless help during my studies.

I would also like to thank my thesis monitoring committee members, Prof. Dr. Ayşe Ebru Abalı and Assoc. Prof. Halime Kenar for all their collaboration, suggestions, and useful discussions.

I am deeply thankful to my partner in crime and love in life Alper Çevik who is the greatest gift life has given to me. He brightens everything around him. Thank you for introducing love, hope and faith to my life and future.

I offer my deepest blessings to my family who supported me in any respect during my life. I owe my deepest gratitude to my mother, Asiye Eke, my father Uğur Eke and my precious beloved sister Özge Eke for their endless love and continuous help in every possible way. I feel very lucky to be raised in their hands. Life would be meaningless without sharing with them.

I am indebted to my dear friends and companions Menekse Ermis for making everything nicer she touches, Çağla Mirasyedioğlu for her support during my long term experiments.

I am very thankful to Kaan Kirdeciler and Seçkin Öztürk for their valuable friendship and showing a great patience during SEM analysis.

I would like to thank to all my labmates and graduates Aylin Kömez, Deniz Sezlev, Arda Büyüksungur, Senem Büyüksungur, Gökhan Bahçecioğlu, Ezgi Antmen, Cemile Bektaş, Tuğba Dursun, Esen Sayın, Ayşe Selcen Alagöz, Dilara Tamay, Aysel Kızıltay, Tuğba Endoğan Tanır. Our technician Zeynel Akın for his patience and help throughout these years.

Lastly, I gratefully acknowledge TUBITAK (Scientific and Technological Research Council of Turkey) for the 2211-C Ph.D. scholarship and 2214-A research fellowship programmes.

TABLE OF CONTENTS

LIST OF TABLES

TABLES

LIST OF FIGURES

FIGURES

LIST OF ABBREVIATIONS

µm	micrometer
2D	Two Dimensional
3D	Three Dimensional
Ab	Antibody
ADSC	Adipose Derived Stem Cell
BSA	Bovine Serum Albumin
CA	Contact Angle
CAM	chorionic allantoic chick membrane
CLSM	Confocal Laser Scanning Microscopy
CO_2	Carbon Dioxide
Col	Collagen
CPD	Cyclobutane Pyrimidine Dimer
d	days
Da	Dalton
DAB	diaminobenzidine
DAPI	4', 6-diamidino-2-phenylindole
DED	Decellularized and De-epidermized Dermis
DHT	Dehydrothermal
DMEM	Dulbecco's Modified Eagle Medium
DMF	Dimethylformamide
DMSO	Dimethyl Sulfoxide
DS	Degree of Swelling
E	Young's Modulus
ECM	Extracellular Matrix
EDTA	Ethylenediaminetetraacetic Acid

EE	Encapsulation Efficiency
EGF	Epidermal Growth Factor
EGM-2	Endothelial Growth Medium
FBS	Fetal Bovine Serum
FDA	Food and Drug Administration
FITC	Fluorescein Isothiocyanate
g	gram
Gel	Gelatin
GelMA	Methacrylated Gelatin
h	hour
H_2O_2	Hydrogen Peroxide
HA	Hyaluronic Acid
HAMA	Methacrylated Hyaluronic Acid
HBV	Hepatitis B Virus
HIV	Human Immunodeficiency Virus
HUVEC	Human Umbilical Vein Endothelial Cells
IL	Interleukin
IPS	Pluripotent Stem Cells
i3T3	Irradiated 3T3 Murine Fibroblasts
kDa	Kilo Dalton
kPa	Kilo Pascal
KGF	Keratinocyte Growth Factor
M	Molarity
mg	milligram
min	minute
mL	milliliter
mm	millimeter

mM	millimolar
MMP	Matrix Metalloproteinase
MPa	Mega Pascal
MSCs	Mesenchymal Stem Cells
MW	Molecular Weight
NaOH	Sodium Hydroxide
nm	Nanometer
NP	Nanoparticles
P	Passage
PCL	Poly(caprolactone)
PDI	Polydispersity Index
PDMS	Poly(dimethylsiloxane)
PE	Polyethylene
Pen/Strep	Penicillin/Streptomycin
PET	Poly(ethylene terephthalate)
PGA	Poly(glycolic acid)
PHAs	Polyhydroxyalkanoates
PHBV	Poly(3-hydroxybutyrate-co-3-hydroxyvalerate)
PHB	Poly(3-hydroxy butyrate)
PIPES	Piperazine-N, N'-Bis(Ethanesulfonic Acid)
PLA	Poly(lactic acid)
PLGA	Poly(lactic acid-co-glycolic acid)
PLA	Poly(l-lactic acid)
PMMA	Poly(methyl methacrylate)
PS	Polystyrene
PVC	Poly(vinyl chloride)
Rho	Rhodamine

RP	Retinyl Palmitate
ROS	Reactive Oxygen Species
s	second
SEM	Scanning Electron Microscopy
TCPs	Tissue Culture Polystyrene
TGF-β	Transforming Growth Factor-beta
TNF	Tumor Necrosis Factor
UTS	Ultimate Tensile Strength
UV	Ultraviolet
VEGF	Vascular Endothelial Growth Factor
w	weight
w/v	weight/volume ratio
w_d	Dry Weight
w_s	Swollen Weight

CHAPTER 1

INTRODUCTION

1.1 Problems related with skin

Skin lesions may be generalized or localized to one or several sites of abnormality appear on the skin (Sneddon 1971). Rash, nevus, pigmentation or the increase in epidermis thickness are the signs of lesions on the skin. Many patients with skin diseases believe that these signs are on the surface and therefore it would be easily cured without applying any special care. However, this approach reduces the rate of correct diagnosis and treatment and leads to a social isolation and depression of patients.

Patients who lost larger than 4 cm in diameter of their full thickness skin require an autologous split thickness skin graft from elsewhere on their body. Large areas of skin loss might be caused by severe tissue deficits, extensive burns or chronic wounds and they represent a different kind of challenge in their treatment. These wounds usually involve a large surface area have a high incidence in the general population and thus have enormous medical and economic impacts. In the US and Europe, more than 25 million chronic wounds and burn injuries occur each year (Supp and Boyce 2005; Fink

et al. 2018). These problems result in 1 million hospitalizations and 100,000 deaths each year. It has been estimated that chronic wounds affect 120 per 100,000 people age between 45 and 65 years and rises to 800 per 100,000 people age over 75 years (Romanelli et al. 2017). These lethal cases are much more common and remain a major healthcare problem in underdeveloped countries. The only permanent treatment for these patients is 'skin grafting'. Split-thickness grafts that contain all of the epidermis but only part of the dermis is generally removed from the healthy areas of the body and used to treat damaged areas. Patients will rebuild an epidermis from the source sites if there are sufficient epidermal cells remaining in the residual dermis (MacNeil 2007). If the wound is too deep, it is covered with wound closure materials such as silicone to prevent the fluid loss.

Skin constantly undergoes renewal and maintain the capacity for repair of wounds. In order to begin to understand treatment of skin problems, it is first necessary to consider the structure of the skin and the principles of wound healing.

1.2 Skin structure and organization

The skin is the largest organ in the body, and the main function is to protect the body from the external environment such as microorganisms, UV radiation, toxic agents and shearing forces (Ro and Dawson 2005). It prevents the loss of water and electrolytes and helps to control the temperature of the body.

Skin consists of three layers: epidermis, dermis and subcutaneous layer (hypodermis or subcutis) (**Figure 1.1**). Epidermis is the outer layer and serves as a barrier between the body and the environment. The dermis, which gives the skin its mechanical strength, is the thickest component of the skin and consists of collagen fibers and glycoprotein filaments embedded in amorphous connective tissue.

Capillaries in the dermis serve the exchange of substances between blood and skin. The deepest subcutaneous layer mainly composed of loose connective and fat tissue which helps to conserve the heat and act as a shock absorber.

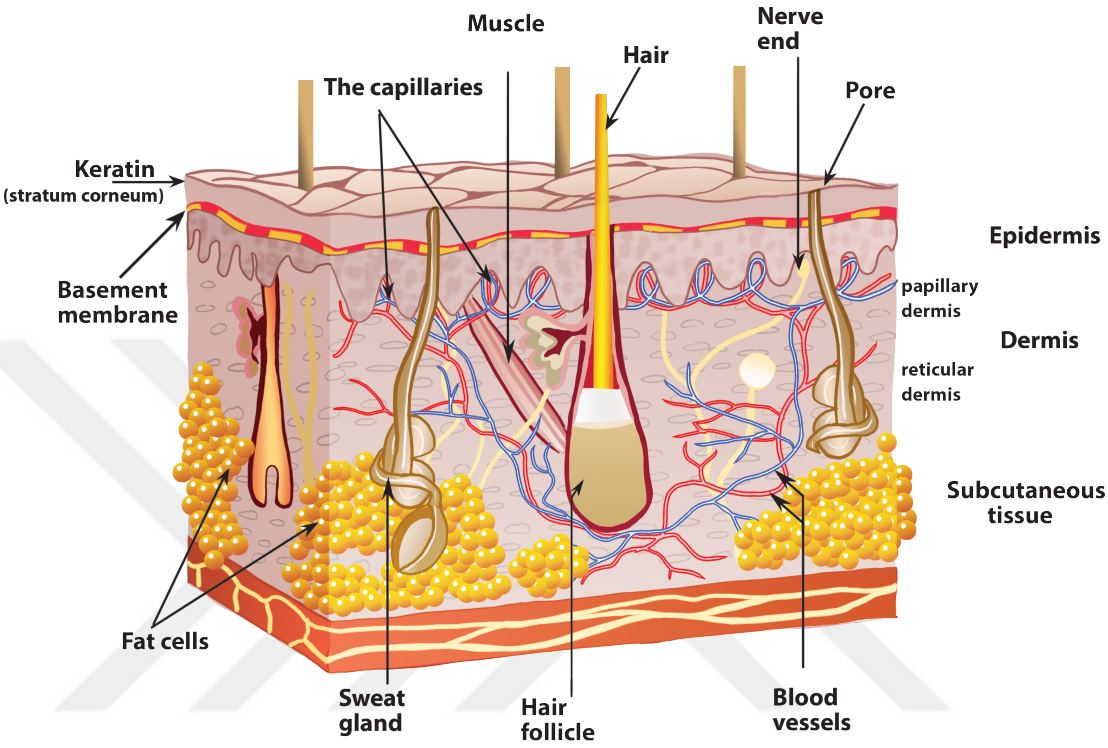

Figure 1.1 Schematic representation of skin structure showing three layers of skin. The epidermis is the outer layer and serves as a barrier against the environment The dermis layer is made of dense, irregular connective tissue that contains blood vessels, hair follicles, sweat glands, and other structures. The subcutaneous tissue which contains fat tissue and functions as insulation and as an energy source.

1.2.1 Epidermis

The epidermis is a stratified, keratinized, non-vascular layer, composed of epithelial cells. It is divided into five layers; the stratum corneum, stratum lucidum, stratum granulosum, stratum spinosum and stratum basale (**Figure 1.2**).

The stratum basale is the germinal layer, consisting of one or two layers of cylindrical cells with large nuclei. The stratum spinosum consists of several layers of prickle cells united to each other by filamentous processes. These cells are in the process of growth and early keratin synthesis. Stratum granulosum contains lamellar granules. The stratum lucidum is only present in very thick skin. It consists of a homogeneous layer of flattened cells that contain profilaggrin. The stratum corneum consists of several layers of flattened non-nucleated keratinocytes (Jean et al. 2009; Duangjit et al. 2011) and it has a very low water content. This water is found in the corneocytes (Sloan, Wasdo, and Rautio 2006; Park et al. 2008).

In addition to the keratinocytes, which make up 95% of the cell mass of human epidermis (Chakrabarty et al. 1999), three other cell types are found in this layer. These are the melanocytes, Merkel cells and Langerhans cells (**Figure 1.2**).

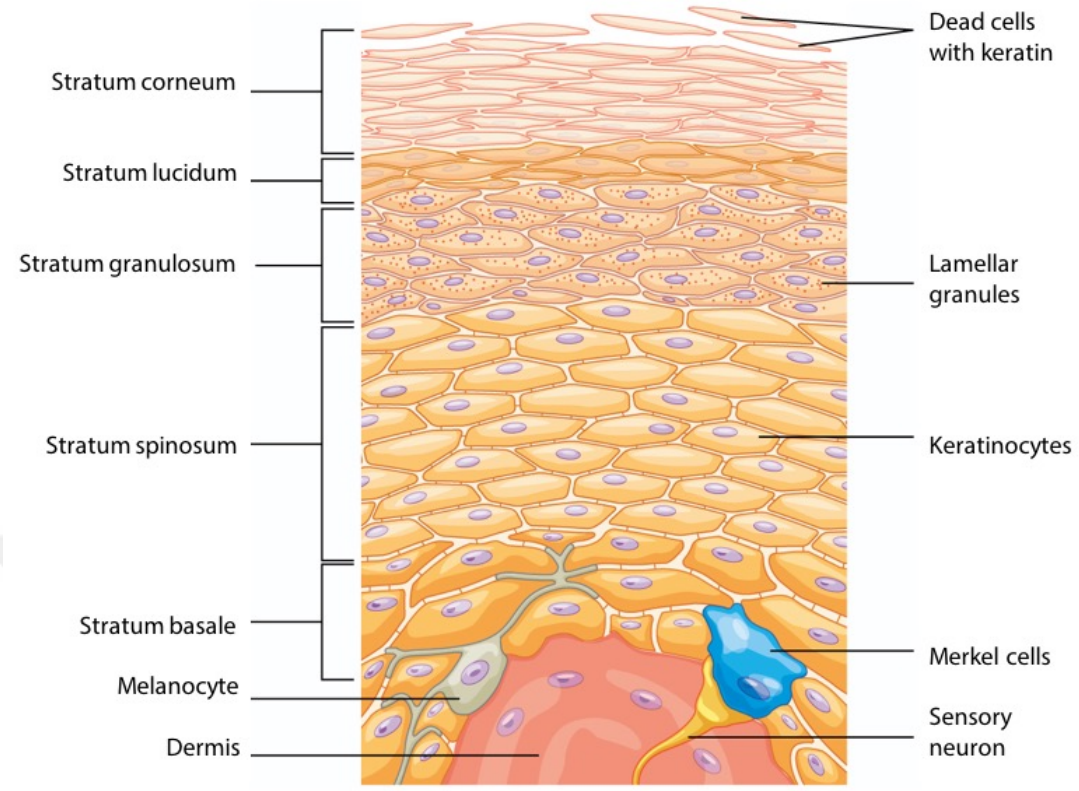

Figure 1.2 Layers of epidermis. The cells in the different layers of the epidermis originate from basal cells located in the stratum basale, however the cells of each layer are distinctively different (Adapted from http://philschatz.com/anatomy-book/contents/m46060.html)**.**

1.2.2 Dermis

The dermis is the tough, fibrous layer of the skin and the thickness is 1-2 mm which is divided into two layers: the papillary dermis and the underlying reticular dermis. The upper surface of the papillary layer is tightly connected to the epidermis, the most upper layer of the skin through the basement membrane (**Figure 1.1**).

This layer provides resistance against frictional forces. The reticular layer continues deep to the papillary layer. It consists of collagen fibers (collagen types I and III), elastic fibers, ground substance (glucosaminoglycans), fibroblasts, dermal dendrocytes (skin dendritic cells known as Langerhan cells), mast cells, histiocytes, blood vessels, nerves, and lymphatics (Supp and Boyce 2005; Harrison et al. 2007). Fibroblasts isolated from the papillary dermis exhibit greater proliferative potential in vitro, than those isolated from the reticular dermis, whereas reticular dermis fibroblasts appear to have the intrinsic ability to synthesize more collagen (Sahota et al. 2003).

1.2.3 Subcutaneous tissue

Beneath the dermis there is a layer of connective and fat tissue called subcutaneous fat layer, functions as insulation layer and as an energy source. Subcutaneous fat protects the body from cold, stores nutrition, and cushions the body from physical trauma (Groeber et al. 2011). It contains blood vessels that provide nutrition and control the body temperature, and nerves that provide sensations. This layer contains fat cells and there is a rich capillary blood supply available in the subcutaneous tissue to transport solutes like drugs that diffuse out of the follicle. Epidermal appendages such as hair follicles, sweat and sebaceous glands originate from downward projections of the epidermis into the underlying dermis and subcutaneous tissue (Stern, McPherson, and Longaker 1990; Boyce et al. 1999).

1.3 Wound healing

A wound is defined as damage or disruption of the normal anatomical structure and its functions (Broughton, et al. 2006). This can range from a simple break in the epithelial integrity of the skin or it can be deeper, extending into subcutaneous tissue with damage to other structures such as tendons, muscles, vessels, nerves, parenchymal organs and even bone (Velnar, Bailey, and Smrkolj 2009; Wang et al. 2017)

Definition of the wound is important for injury management and wound treatment. Therefore, wounds can be clinically defined as acute and chronic according to their structure and time frame of healing. Wounds that repair themselves and that proceed normally by following a timely and orderly healing pathway, with the end result of both functional and anatomical restoration, are defined as acute wounds. The time course of healing usually ranges from 5 to 10 days, or within 30 days. Acute wounds can be acquired as a result of traumatic loss of tissue or a surgical procedure. Chronic wounds are, however, that fail to progress through the normal stages of healing and cannot be repaired in an orderly and timely manner. These factors which fails the wound healing process include infection, tissue hypoxia, necrosis, exudate and excess levels of inflammatory cytokines (Velnar, Bailey, and Smrkolj 2009).

The healing of acute wounds passes through the phases of hemostasis, inflammation, proliferation and maturation. The ideal result for a healed wound is a fine scar with minimal fibrosis or wound contraction, and return to near normal tissue architecture and function (Myers and Ghanem 2015).

Healing of chronic wound occurs by the same processes as acute wound healing, but often occurs with the formation of granulation tissue and excessive fibrosis leading to contraction and loss of function. The typical shift in M1 to M2 macrophages seen in acute wounds is dysregulated in chronic wounds (Demidova-Rice, Hamblin, and

Herman 2012). In the early inflammatory stage of an acute wound, macrophages engulf neutrophils that complete their function. In the later stages, macrophages switch phenotype and are predominantly M2 macrophages (**Figure 1.3A**). In a chronic wound, macrophages are predominantly M1 that are unable to consume neutrophils (**Figure 1.3B**).

At the chronic wound margin, approximately 80% of cells are pro-inflammatory (Hesketh et al. 2017). This leads to the enrollment of more macrophages and an increase in inflammation.

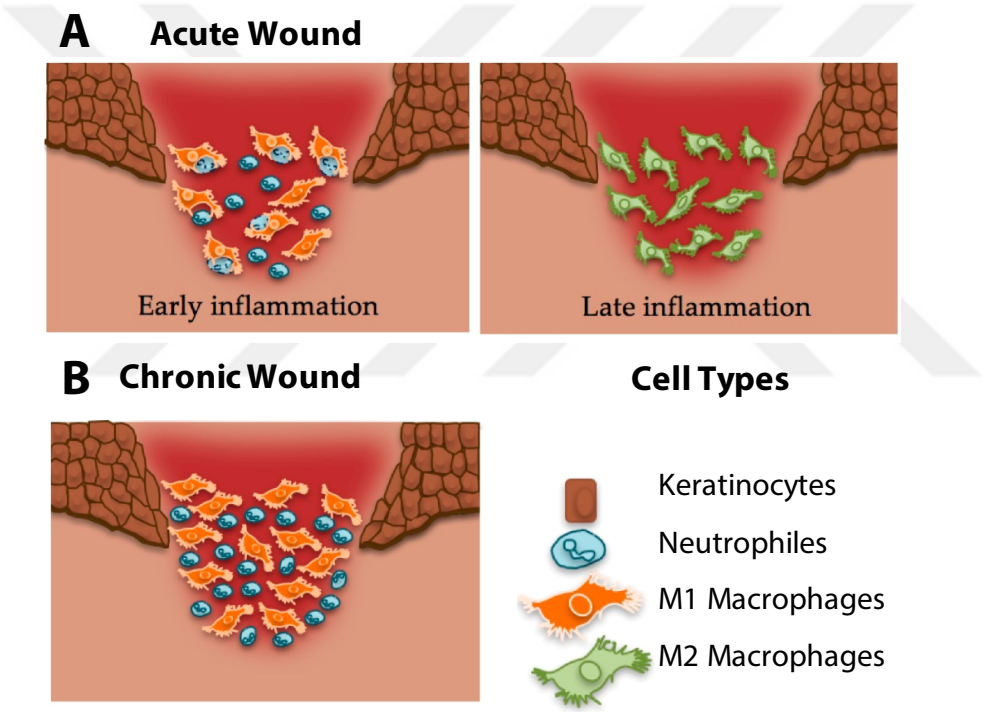

Figure 1.3 Schematic illustration of acute and chronic wounds. A) Late stages of acute wounds macrophages are predominantly M2 macrophages. B) In chronic wounds, the typical shift in M1 to M2 macrophages dysregulated and macrophages are generally M1 that leads to an increase in inflammation (Adapted from Hesketh et al. 2017).

After tissue injury, hemostasis and inflammation start immediately, in which cytokines, growth factors, and reactive oxygen species (ROS) are produced to recruit cells to the wound site (**Figure 1.4**). The next proliferative phases of wound healing include angiogenesis and re-epithelialization, where new tissue is formed by endothelial cells, fibroblasts, and keratinocytes. The final phase is tissue remodeling.

In chronic wound healing, the inflammation is prolonged and it is important to note that the epidermis fails to re-epithelialize due to non-migratory keratinocytes, compared to acute wounds (**Figure 1.4**). (Broughton et al. 2006; Eke et al. 2017; Wang et al. 2017).

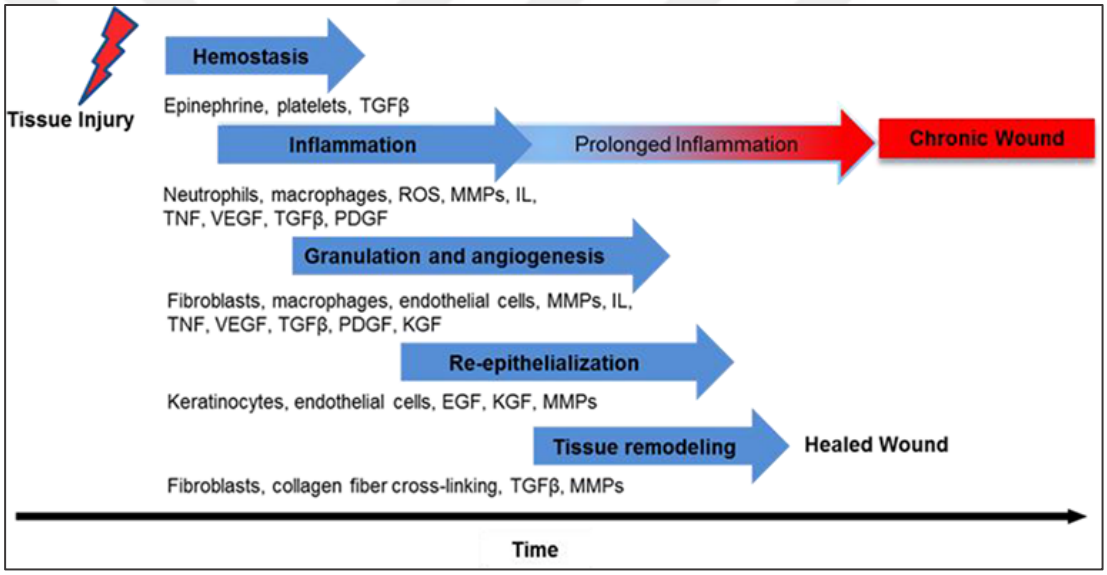

Figure 1.4 The phases of wound healing. EGF (epidermal growth factor), IL (interleukin), KGF (keratinocyte growth factor), MMPs (matrix metalloproteinases), PDGF (platelet-derived growth factor), ROS (reactive oxygen species), TGF-β (transforming growth factor-beta), TNF (tumour necrosis factor), VEGF (vascular endothelial growth factor). Adapted from (Nguyen et al. 2016).

1.4 Tissue engineering of skin

Tissue engineering is a branch of the biomaterials that aims to produce healthy equivalents for the injured or diseased tissues by using a combination of cells and neosynthesized or reconstituted extra cellular matrix (ECM) (Langer and Vacanti, 1993).

Skin repair research is an active field in tissue engineering and it has encouraging prospects for clinicians to restore various skin defects (Harrison et al. 2007; Chakrabarty et al. 1999; MacNeil 2007; Bhardwaj, Chouhan, and Mandal 2018). Tissue engineered skin is although one of the most advanced tissue constructs, it lacks several important components such as hair follicles, sebaceous glands, sweat glands, and dendritic (immune) cells. Therefore, skin replacements have been a challenging task for surgeons since the first introduction of skin grafts by Reverdin in 1871.

Tissue engineering of skin aims to treat and fill the skin loss caused by excessive burns or chronic wounds as well as to study the biology of skin. The general approach in skin tissue engineering is to obtain a biopsy (preferably from the patient himself), harvest skin cells from the biopsy, proliferate and seed them on a suitable biodegradable cell carrier and after culturing and maturation, implant it to the patient (**Figure 1.5**). The cell carrier, known as the scaffold, should mimic the cell microenvironment, provide space for cell attachment, proliferation, migration and ECM production. Over time, the implanted reconstructed tissue is vascularized, ingrown by the surrounding healthy natural tissue and eventually the carrier degrades in the body, leaving only the seeded and infiltrated cells and the ECM produced by these cells (Kinikoglu et al. 2015).

Tissue engineered skin may further serve as a model and an alternative to *in vivo* testing of drugs and cosmetics products without using any animal application (**Figure 1.5**).

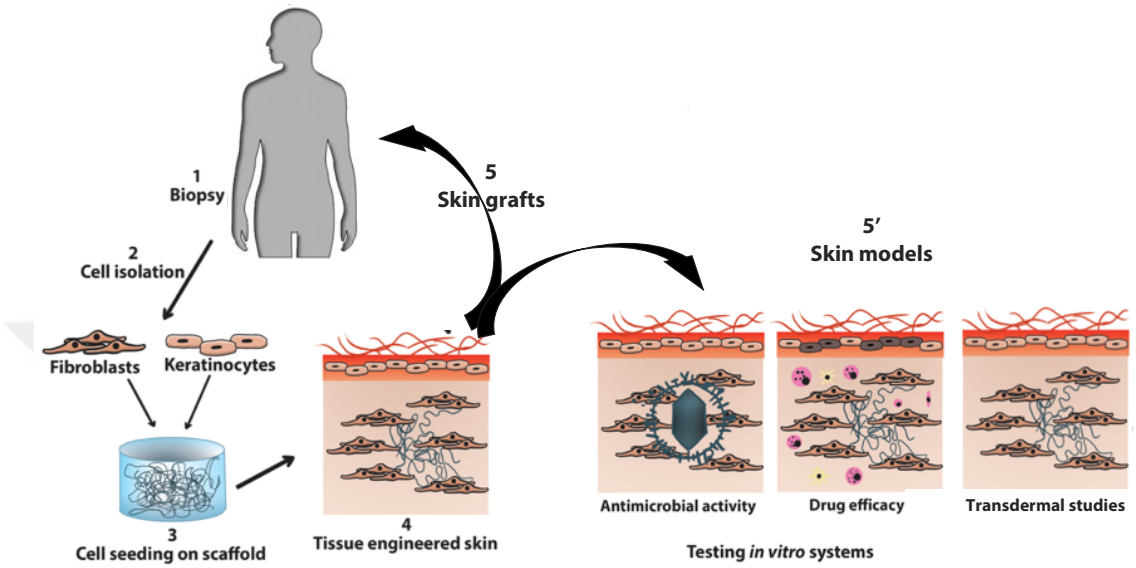

Figure 1.5 Schematic illustration of human skin tissue engineering. Primary keratinocytes and fibroblasts are isolated from human biopsy, proliferated prior seeding to the appropriate scaffolds. The tissue engineered skin can serve as skin graft (arrow 5) or can be used as *in vitro* human-cell based test systems (arrow 5').

1.5 Tissue Engineered Skin Substitutes

The most important expectation from a tissue engineered skin is to restore the barrier function to patients whose skin tissue is severely compromised. Any loss of full thickness skin of more than 4 cm in diameter will not heal without a graft or a skin substitute (MacNeil 2007).

Tissue engineered cell-free and cell-loaded skin substitutes provide a possible off-the-shelf solution to the problem of donor graft shortage. These bioengineered skin substitutes offer protection from fluid loss and microorganismal contamination, while also delivering dermal matrix components, cytokines, and growth factors to the wound bed. **Figure 1.6** shows the wounded parts of a patient to which a tissue engineered skin was applied.

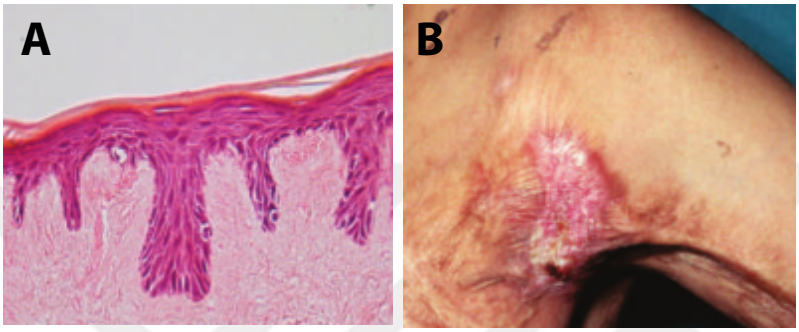

Figure 1.6 An example of clinical use of a tissue engineered skin substitute. A) Micrograph of a reconstructed human skin made from sterilized de-epidermized, acellular donor dermis to which keratinocytes and fibroblasts were added. B) The appearance of this reconstructed skin 2 months after its application to correct the contraction of the tissue of a patient who had suffered severe skin contractions as a result of earlier burn injuries. Adapted from Sahota et al. 2003.

In addition to the clinical uses of tissue engineered skin in the treatment of various skin problems there are many nonclinical applications for tissue engineered skin, especially as 3D skin models. These studies aim decreasing the number of *in vivo* animal experiments (Groeber et al. 2011), investigate cell-to-cell and cell-to-extracellular matrix interactions (Harrison et al. 2007), skin penetration of nanoparticles and chemicals (Duangjit et al. 2011), wound healing (Chakrabarty et al.

1999; Mutlu et al. 2018), angiogenesis (Seder et al. 2015), regulation of pigmentation, skin contraction (Sahota et al. 2003) and investigation of skin diseases such as melanoma invasion, psoriasis and skin blistering disorders (Bye et al. 2013).

1.5.1 Decellularized Skin Substittutes

Skin grafts are clinically meaningful if they are vascularized, maintain shape and dimensions, and remodel with the host (Shores, Gabriel, and Gupta 2007). There are currently available skin grafts in the market produced with decellularized skin substitutes. These can be categorized as epidermal layer replacements and dermal layer replacements (**Table 1.1**).

Decellularized skin substitutes remain in the wound during healing. Cell free decellularized skin substitutes can be used in combination with autografts to support their take (Lorenti 2012) or to improve graft engraftment in areas of mechanical stress (joints and arm pit) (Böttcher-Haberzeth, Biedermann, and Reichmann 2010). However, in contrast to autografts, decellularized skin grafts might have the risk of transmitting viruses such as hepatitis B Virus (HBV) or Human Immunodeficiency Virus (HIV). One advantage over autologous skin substitutes is that they have reduced manufacturing costs.

Table 1.1 Commercially available decellularized skin substitutes.

Product	Cell Source	Material Type	References
Epidermal Substitutes			
Permacol (Tissue Science Laboratories)	–	Porcine skin that provides a temporary wound dressing	(Jarman-Smith et al. 2004)
Epidex (Modex Therapeutics)	Autologous keratinocytes	Cell sheets cultured from the patient's hair follicles.	(Tausche et al. 2003)
Dermal Substitutes			
Donor skin	–	Acellular skin as a permanent source of allodermis	(Hermans 1989)
Integra (Integra LifeSciences)	–	Split thickness skin graft made up of polysiloxane, xenogenic tendon collagen	(Stern et al. 1990)
Alloderm (Lifecell)	–	Freeze-dried human donor dermis	(Wainwright et al. 1996)

Today, the most commonly used plastic surgery technique is the decellularized skin grafts. However, the amount of donor skin area is often limited. The development of synthetic or biological products as skin substitutes is therefore of interest.

1.5.2 Tissue Engineering Based Substitutes

Tissue engineered constructs are made up of nonbiological molecules and polymers that are not present in normal skin. These constructs are designed to be biodegradable or permanent depending on the use and have to provide an appropriate environment for the regeneration of tissue. They are expected to maintain their 3D structure for at least 3 weeks to allow ingrowth of blood vessels, fibroblasts, keratinocytes and epithelial cells. If designed for skin therapy, biodegradation should occur after this period. Foreign body reactions should be absent or minimal during biodegradation of the skin substitutes (Böttcher-Haberzeth, Biedermann, and Reichmann 2010).

1.5.2.1 Cell types and sources used in skin tissue engineering

Cell lines and primary cells are the two main groups of cells used in skin tissue engineering, but mostly primary cells isolated from healthy tissue biopsies are preferred due to the potential adverse effects of cell lines (antigenicity, tumorigenicity, etc.). Microenvironment in which the cells will be placed and responses to the signals generated by this environment is also important (Lorenti 2012).

Cells, depending on their source, are classified as autologous, allogeneic and xenogeneic (Cotsarelis 2006). Autologous cells are from patient himself and they do not cause immunologic reactions. However, creating new wounds on patient body, limits their use. Allogeneic cells are from different members from the same breed. The main advantage is getting more cells with a suitable cost. However, there are risks of immune response on patient and transfer of infection elements (Shores, Gabriel, and Gupta 2007).

Another cell resource is xenogeneic cells which are received from different species. In this cell group there are advantages of suitable cost and easy access but disadvantages of immune response, the risk of transferring pathogens.

Cells, depending on their type, that can be used in tissue engineering are: stem cells, progenitor cells, or differentiated primary cells and these can be isolated from adult or embryonic tissues. Stem cells have very high proliferation capacity. Progenitor cells are found in the bone marrow or could arise from embryonic stem cell lines cultured in vitro. Their differentiation and proliferation potentials are high. However, it could be cultured for shorter periods of times than stem cells (Metcalfe and Ferguson 2007; Ziane et al. 2012). Differentiated primary cells are directly derived from adult, differentiated and functional tissues or organs.

Skin tissue engineering application requires a specific source or combination of cells. Mostly stem cells are the best option, as they can be differentiated into a variety of cell types (Spotorno et al. 2006). Indeed, epidermis of skin was shown to contain stem cells. These cells are in the basal layer of the epithelium. The basal cells were reported to express stem cell related markers, PCNA, Ki-67, cytokeratins K5/14, K19, integrins (α2, α3, α6, β1 and β4), neurotrophin receptor p75, but not differentiation markers, K1/10 and K4/13 (Igarashi et al., 2008). Stem cells are also important to produce immunocompetent skin equivalents.

Skin substitutes have epithelial cells either alone or with fibroblasts. The presence of fibroblasts is important considering the influence of their interactions with epithelial cells on the repairment of the developing tissue. In fact, besides epithelial cells; melanocytes, Langerhans cells, Merkel cells, and lymphocytes also exist in the native skin (**Figure 1.7**) (Nestle et al. 2009).

Skin equivalents consisting of Langerhans cells, melanocytes, adipose cells and endothelial cells were previously reported (Auxenfans et al. 2009). Similar approaches may be undertaken to reconstruct skin substitutes using induced pluripotent stem cells (IPS).

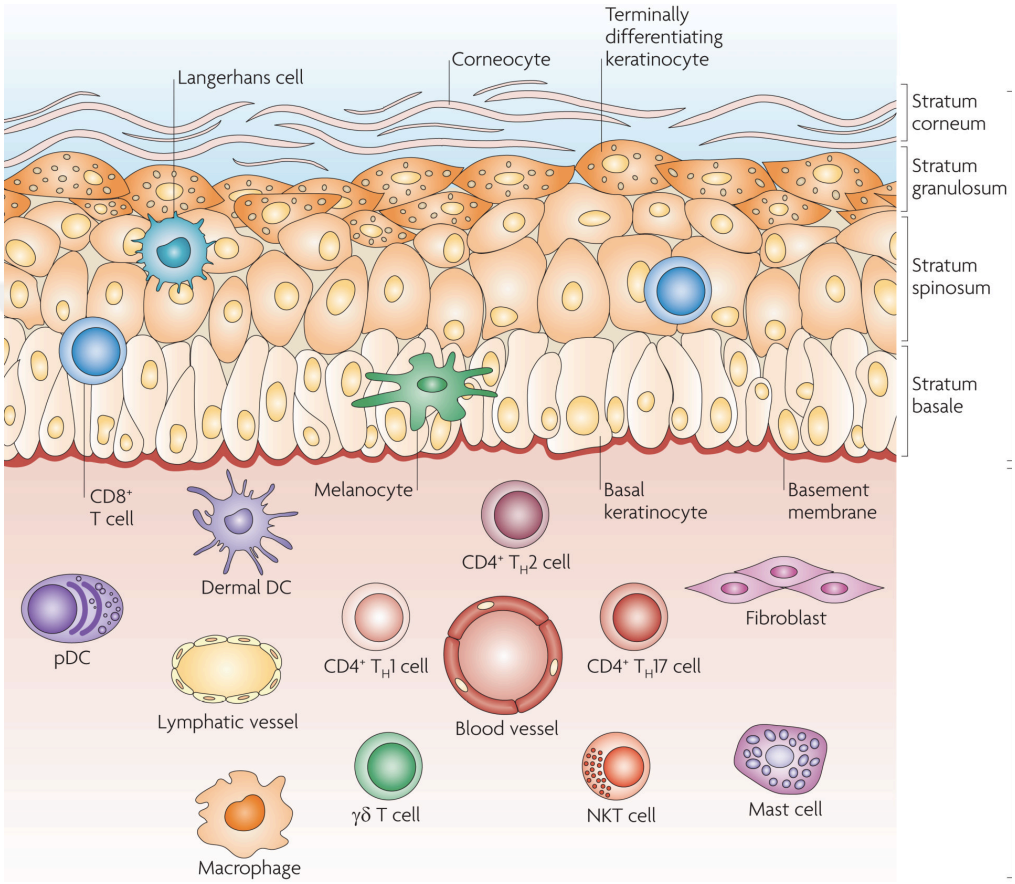

Figure 1.7 Cell types in skin structures. Specialized cells in the epidermis include melanocytes, which produce pigment (melanin), and Langerhans cells. T cells, can be found in the stratum basale and stratum spinosum. Dermis contains dermal dendritic cells (DC), T cells including CD4+ T helper 1 (TH1), TH2 and TH17 cells, γδ T cells and natural killer T (NKT) cells. In addition, macrophages, mast cells and fibroblasts are present. Adapted from Nestle et al. 2009.

1.5.2.2 Materials used in skin tissue engineering

One of the important parameters of tissue engineering, is the material used for seeding the cells on. The ideal materials to be used in skin engineering must not induce a toxic or immune response or result in excessive inflammation. It should be slowly biodegradable, support the reconstruction of normal tissue and have similar mechanical and physical properties to the skin it replaces. The materials used are chosen from biological or synthetic sources or blend of them.

The artificial nature of the skin substitutes has some distinct advantages and disadvantages when compared to decellularized skin structures. The composition and properties of the product can be much more precisely controlled. Various additives such as growth factors and matrix components can be added to enhance their healing effect. These products could also avoid complications due to disease transmission. However, these synthetic skin substitutes generally lack a basement membrane and their architecture does not resemble native skin (Halim, Khoo, and Yussof 2010).

Different synthetic or biological scaffolds can be used for skin tissue engineering. Many synthetic biocompatible polymers, biodegradable or not, can be used as supports for fibroblast culture during the production of dermal or epidermal equivalents. They differ by their structure (porous, mesh or layer), or by their composition (polyglycolic acid (Cooper et al. 1991; Contard et al. 1993) poly-L-lactide, poly(ethylene oxide), polybutylene terephthalate (Beumer, Blitterswijk, and Ponec 1994). After adhesion and proliferation, cells synthesize and deposit an extracellular matrix thus forming a 3D tissue closely resembling normal human dermis.

Currently available tissue engineered skin substitutes can be categorized into three groups: (a) Those to replace the epidermal layer, (b) those that substitute the dermis (c) those having both layers. Also, in some clinical conditions (such as non-healing ulcers and superficial burns) simply transferring cells can help the patients. The treatment of major full thickness burns, however, requires the replacement of both the dermis and epidermis; thus a bilayer structure is needed (MacNeil 2007). Examples of currently available material based skin replacements are given in **Table 1.2**.

Beside these commercially available tissue engineered skin products, various natural or synthetic biomaterials are being studied for use in tissue engineering. Some of them are electrospun silk fibroin (Min et al. 2004), PEG reacted with cysteine containing peptide sequence sheets (Wetering et al. 2005), gelatin scaffolds carrying epidermal growth factor (EGF) (Ulubayram et al. 2001; Dogan et al. 2009). It was reported that the wound dressings prepared from Heparin- Chitosan Alginate demonstrated very effective antibacterial property against *S. Epidermidis* (Aksoy et al. 2015).

Current research in the field of tissue engineering is making a good progress, with the ultimate goal being tissue engineered skin that matches the quality of the autologous skin graft.

Table 1.2 Commercially available material based tissue engineered skin substitutes.

Product/ Company	Cell Source	Material Type	References
Epidermal Substitutes			
Epicel (Genzyme Tissue Repair)	Autologous keratinocytes	A biopsy of the patient's cells is grown into an integrated sheet	(Wright et al. 1998)
Myskin (CellTran)	Autologous keratinocytes	Cells are delivered to the patient on silicone surface	(Haddow et al. 2003)
CellSpray (Clinical Cell Culture)	Autologous keratinocytes	Cells are delivered to the patient as a spray	(Navarro et. al. 2000)
Dermal Substitutes			
Dermagraft (Advanced Biohealing Inc.)	Allogeneic neonatal fibroblasts	Allogenic ECM and PGA/PLA composite conditioned with donor fibroblasts	(Marston et al. 2003)
Transcyte (Advanced Biohealing Inc.)	Allogeneic neonatal fibroblasts	Silicone film, nylon fabric and porcine collagen	(Kumar et al. 2004)
Epidermal and Dermal Substitutes			
Apligraf (Organogenesis)	Allogenic keratinocytes and fibroblasts	Bovine collagen with allogenic keratinocytes and fibroblasts	(Bello and Falabella 2003)
Orcel (Ortec International Inc.)	Allogenic keratinocytes and fibroblasts	Bovine collagen with allogenic keratinocytes and fibroblasts	(Lipkin et al. 2003)
Cincinnati skin substitute or Permaderm (Cambrex Inc.)	Autologous keratinocytes and fibroblasts	Comprises bovine collagen. A permanent skin substitute for burns patients	(Boyce et al. 1995)

1.6 Nanoparticles for transdermal drug delivery

One major reason for the construction of tissue engineered skin was to study permeability of skin to various pharmaceutical formulations without having to retort to *in vivo* experiments achieved on animals. So, a number of drug delivery approaches have been studied for skin treatment applications.

Transdermal drug applications are frequently used because of the effectiveness of the localized treatment, low cost, relatively low side effects, maximum drug availability at the target site, and avoidance of the systemic circulation. Many bioactive agents, however, do not have the necessary physicochemical properties for satisfactory efficacy when applied topically (Sloan, Wasdo, and Rautio 2006). Transdermal skin treatment requires the absorption of drug through the skin into the body. If drug is applied in free form, it can be washed away before complete penetration. In order to prolong the bioavailability and enhance permeability, the most suitable delivery systems are the nanoparticulate carriers. One of the biggest challenges in developing an effective system is the transfer of the drug through the tightly structured stratum corneum when the skin is not compromised (Eke et al. 2015). The three layers of skin needs to be crossed by the nanoparticles or bioactive agents, and each layer has a different role as mentioned in *Section 1.2*. The lipid matrix and the corneocytes, together, create a barrier, which is broken by hair follicles (**Figure 1.8A**) and sweat glands (**Figure 1.8B**). These components cover less than 1% of the surface area, and are believed to serve as a route of entry for nano sized drug carriers. There is a rich capillary blood supply available in the subcutaneous layer to transport solutes like drugs that diffuse out of the follicle (Wosicka and Cal 2010; Prow et al. 2011). As a result, there is substantial interest in targeted follicular delivery via nanoparticles loaded with drugs.

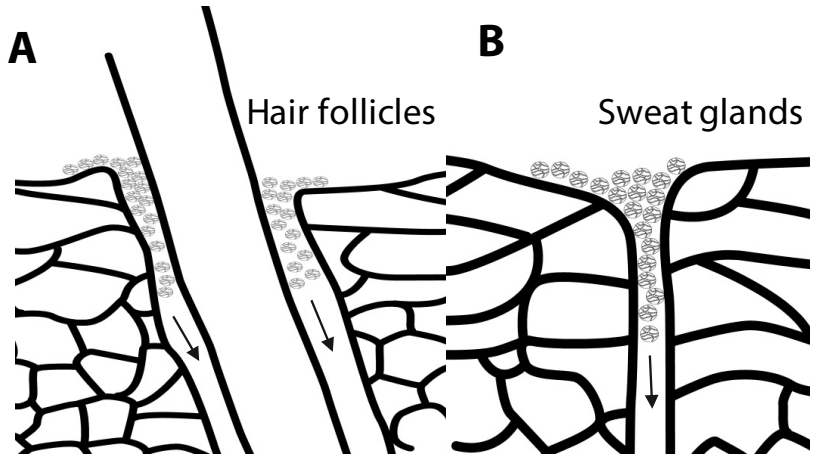

Figure 1.8 Penetration of nanoparticles through stratum corneum. Penetration through A) hair follicles, B) sweat glands.

Nanocarriers have three important properties as delivery systems: High rate of release due to the high surface-to-volume ratio, extravasation leading to release of the drugs in regions with compromised vasculature, and ease of transportation across cell membranes. With the developments in nanotechnology and their introduction to the biomaterials field, various types of nano sized drug delivery systems such as nanocapsules, nanospheres, liposomes, dendrimers and emulsions were developed (**Figure 1.9**). The use of nano sized drug carriers constructed from biodegradable polymers are also increasingly used because even if they penetrate untargeted tissues they do not stay there long but disintegrate by time (Yin Win and Feng 2005; Hasirci et al. 2006; Boyandin et al. 2012).

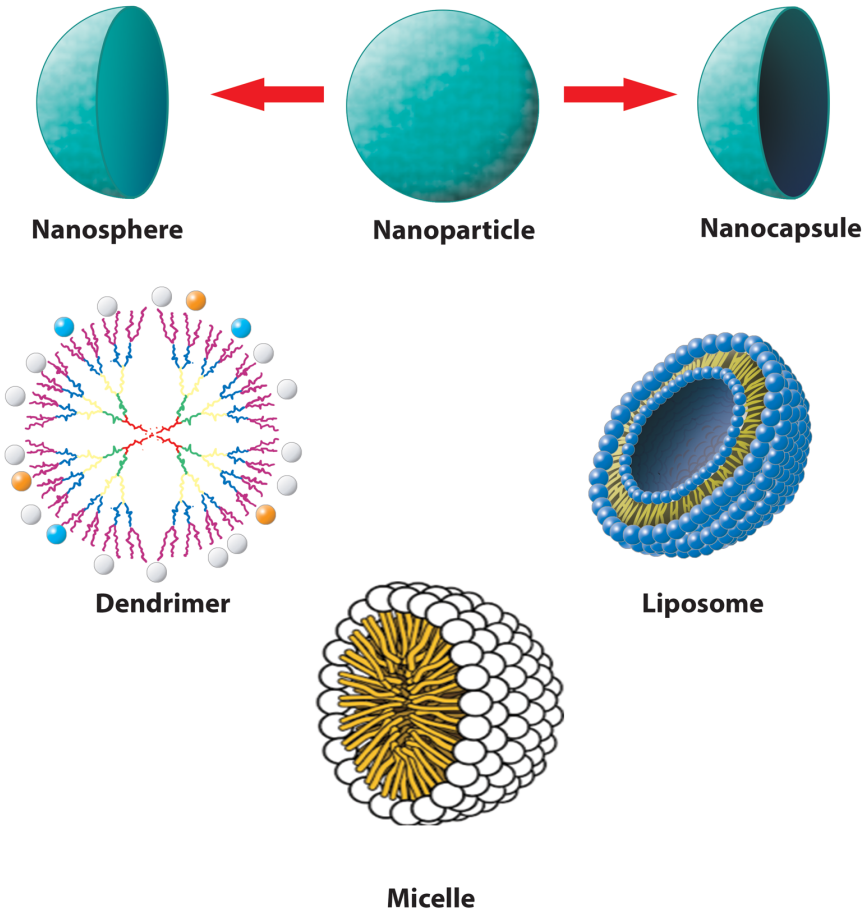

Figure 1.9 Nanoparticulate drug carrier systems. Within the broad category of nanoparticles, nanospheres refers to spherical particles with full interior while nanocapsules apply to particles which have a core-shell structure.

Biodegradable polymers are preferable as drug carriers. The widely used Food and Drug Administration (FDA) approved polymers are poly(lactic acid) (PLA), poly(glycolic acid) (PGA), poly(lactide-co-glycolide) (PLGA), poly(ε-caprolactone) (PCL), alginate and chitosan and their blends (Hasirci et al. 2017).

Polyhydroxyalkanoates (PHAs) are among the natural polymers preferred for the production of drug delivery vehicles, because they can be produced in a range of compositions and properties, such as degradation rate, elasticity or mechanical strength (Errico et al. 2009; Sahin et al. 2018). PHAs are linear, semicrystalline, thermoplastic and biocompatible polymers of microbiological origin which have a biodegradability in the body (Hasirci et al. 2006; Shishatskaya et al. 2011; Volova et al. 2017). Their biological origin is an advantage over the other major polyester group, the polylactides, which are petroleum based. The most abundantly studied PHAs are poly(3-hydroxybutyrate) and its copolymers with 3-hydroxyvalerate, poly(3-hydroxybutyrate-co-3-hydroxyvalerate) (PHBV), with varying HV contents (**Figure 1.10**). PHBV has been used for the production for drug delivery systems to diffuse into the skin (Eke et al. 2014; Eke et al. 2015; Mutlu et al. 2018).

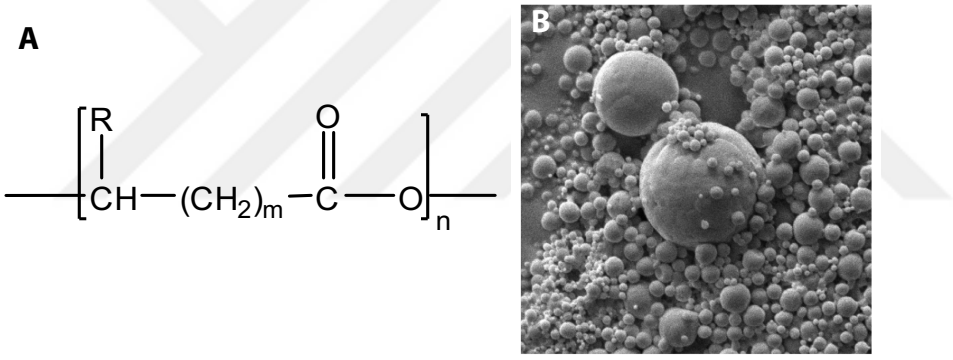

Figure 1.10 Polyhydroxyalkoanoates**.** A) General molecular structure. When m=1, and R=CH_3, the product is poly(3-hydroxybutyrate) (P3HB), and when R=CH_2CH_3 the product is poly(3-hydroxyvalerate) (PHV). B) SEM micrographs of spherical drug carriers produced from PHBV.

1.7 Approach in this study

Current clinical practice is that poorly vascularized wound beds are first treated with natural extracellular matrix products (e.g. Integra) followed by a second stage operation for skin grafting. In this study, a tissue engineered skin substitute that mimics the structural and cellular organization of the normal human skin is aimed. This model was designed to be implanted into patients in a one or two staged operation, depending on the vascularization status of the wound bed. This tissue engineered skin substitute was also designed to be used as a 3D model in skin research to decrease the number of animal use. The utility of this model in transdermal drug penetration was studied instead of *in vivo* applications.

In this study, dermis is designed to be porous, so that fibroblasts cultured on layer could act as a feeder layer. ECM of the natural dermis is mostly made of interconnected collagen, for additional strength and stability. In order to mimic the natural dermis structure, two approaches were used: dermis made of natural ECM (collagen) in collagen sponge/PLA-PHBV bilayer mesh and dermis made of synthetic ECM (PLA) in a PLA-PHBV-PLA trilayer mesh. PHBV fibers were produced to act as a barrier due to their slow degradation rate and higher mechanical strength compared to collagen. PHBV fibers on a scaffold may also provide a natural polymeric basement membrane and it would be advantageous to give the cells a framework to start producing the required extracellular matrix. Since collagen is derived from animals, it has a major limitation of disease transmission when used in human patients. To avoid this, PLA-PHBV-PLA trilayer electrospun mesh were produced. Drug penetration studies were also performed on this model. De-cellularized de-epidermized dermis (DED) and natural human skin were used as positive controls. Human keratinocytes and fibroblasts isolated from donated skin were sequentially seeded onto these models.

To form the epidermis, keratinocytes were exposed to air- liquid interface and cultured until they differentiated, since in natural epidermis, the majority of the cells are the keratinocytes.

The subcutaneous tissue consists mainly of fat tissue, which functions as insulation and as an energy source. Two UV crosslinkable polymers, methacrylated gelatin (GelMA) and methacrylated hyaluronic acid (HAMA) were synthesized to form a transparent hydrogel loaded with adipose derived stem cells (ADSCs) to serve as a biodegradable subcutaneous tissue. The hydrogels were designed to provide a suitable microenvironment for ADSC proliferation. *Ex ovo* studies demonstrated the hydrogels carrying stem cells provide newly formed blood vessels on the chick embryo (chorioallontoic membrane, CAM) and chick aorta. Such a stem cell containing hydrogel would also be valuable in stimulating blood vessel formation in poorly vascularized chronic wounds which is a growing burden for patients.

This biomimetic tissue engineered skin design was also used for transdermal drug penetration studies. Skin penetration tests were carried out with Retinyl Palmitate and Rhodamine loaded PHBV nanoparticles by using this 3D model. Retinyl Palmitate is the most stable form of Vitamin A and generally used in the field of anti-ageing pharmaceutical preparations (Teixeira et al. 2005). Rhodamine, on the other hand is a hydrophobic dye and used in the penetration studies into the tissue engineered skin as a fluorescent stain in this study.

PHBV was selected as the delivery vehicle material as it was demonstrated that PHBV nanoparticles have penetrated into the fibroblastic cells and healthy mice skin in our previous *in vitro* and *in vivo* studies, respectively (Eke et al. 2014).

CHAPTER 2

MATERIALS AND METHODS

2.1 Materials

PHBV (HV content 5% M), hyaluronic acid (HA), porcine skin gelatin type A(100 bloom), methacrylic anhydride, cell culture inserts (CellCrown 12 well plate inserts), 4,6-diamidino-2-phenylindole dihydrochloride (DAPI), topro3, paraformaldehyde (37%), neutral buffered formalin (10%), sodium azide (ReagentPlus®, ≥99.5%), sodium cacodylate (pH 7.4), glutaraldehyde (25%), amphotericin B, Piperazine-N,N′-bis(2-ethanesulfonic acid) (PIPES), trypsin-EDTA (0.25%), 100 U/mL penicillin and 100 µg/mL streptomycin, ethylenediaminetetraacetic acid (EDTA, 0.02%), collagenase type I, apo-transferrin, hydrocortisone, human recombinant epidermal growth factor, ascorbic acid-2-phosphate and cholera toxin, smooth muscle actin antibody (a-SMA) were purchased from Sigma-Aldrich (USA).

Endothelial growth medium-2, DMEM High Glucose, DMEM High glucose colorless, HAMF12 cell culture media, Fetal bovine serum (FBS), Fetal calf serum (FCS), L-glutamine, ascorbic acid were purchased from Lonza (USA).

Polyvinyl alcohol (PVA, MW $1.5x10^4$), 1,1,1,3,3,3-hexafluoroisopropanol (HFIP), bovine serum albumin (BSA) and penicillin/streptomycin were obtained from Fluka (Switzerland).

Total DNA quantification kit PicoGreen dsDNA assay, Alexa Fluor 488 goat anti-mouse IgG, Alexa Fluor 532 goat anti-mouse IgG, Alexa Fluor 647 goat anti-mouse IgG, Alexa Fluor 488 goat anti-rabbit IgG, Alexa Fluor 532 goat anti-rabbit IgG, Alexa Fluor 647 goat anti-rabbit IgG, Alexa Fluor 488 Phalloidin, Alexa Fluor 532 Phalloidin, Alexa Fluor 647 Phalloidin and Collageanse Type I were purchased from Invitrogen (USA).

Immunofluorescent stains Griffonia Simplicifolia Lectin I, isolectin B4 were from Vector Laboratories, Burlingame, USA; Genomic DNA Purification Kit was obtained from Promega (USA). Matrigel® Basement Membrane Matrix was from Corning®, USA.

Triton X-100 was purchased from AppliChem (USA). VEGF Vascular endothelial growth factor was from Cell Signaling Technologies (Netherlands). Difco-Trypsin 1:250 was obtained from Difco Laboratories, USA.

Mouse anti-involucrin monoclonal antibody (Clone SY5), mouse monoclonal antibody against involucrin and monoclonal mouse anti-human Ki-67 antibody was purchased from Abcam, USA. Avidin-biotin and 3,3'-diaminobenzidine tetrahydrochloride (DAB) were from Vector Labs, UK.

Alexa Fluor® 488 anti-human CD31, CD45 and Mouse IgG1κ; and Alexa Fluor® 647 and CD90 antibodies were bought from BioLegend (USA). Human umbilical vein endothelial cells (HUVECs) were purchased from PromoCell, UK.

Collagen Type I was isolated from Sprague-Dawley rat tails and were a kind gift from GATA Animal Experiments Laboratory, Turkey.

Fertilized leghorn chicken eggs (Gallus gallus domesticus) were obtained from Henry Stewart Co. Ltd (UK).

Human skin was obtained from patients undergoing routine abdominoplasties and breast reductions in the Department of Plastic Surgery, Northern General Hospital, UK. The majority patients were female (95%) and aged 25-45, as these patients form the typical patient group undergoing breast and abdominal reduction surgery.

2.2 Methods

2.2.1 Epidermis and Dermis

Two different scaffolds were produced as dermis layer of the model skin. 1) PLA-PHBV-PLA trilayer electrospun fiber mesh (**Figure 2.1A**) Collagen sponge/PLA-PHBV bilayer electrospun fiber mesh (**Figure 2.1B**). As a positive control, de-cellularized de-epidermized dermis (DED) was used. Keratinocytes were seeded to form epidermis.

In skin tissue engineering applications, 2D or 3D biomaterials are used for the replacement of the skin's dermal layer. To form the epidermal layer keratinocytes are exposed to air and differentiated. Therefore, epidermis is not mentioned as a separate layer throughout this thesis.

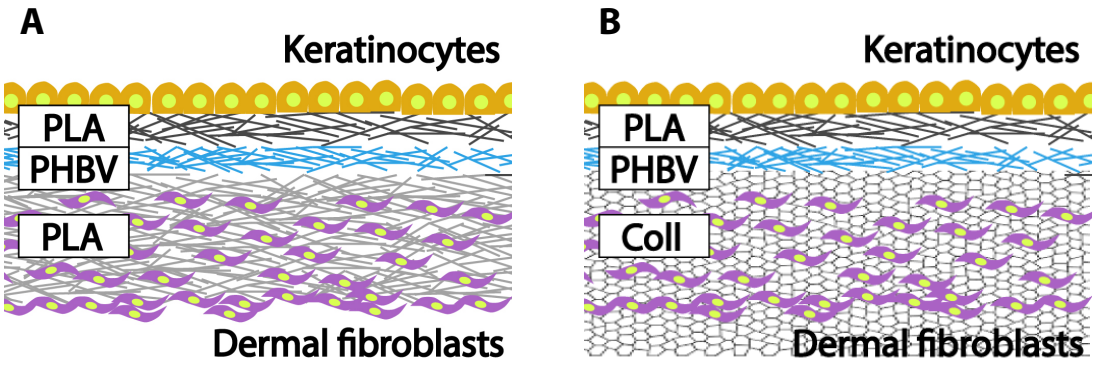

Figure 2.1 Illustration of two different scaffolds produced to serve as dermis layer; A) PLA-PHBV-PLA trilayer electrospun fiber mesh seeded with keratinocytes and dermal fibroblasts, respectively. B) Collagen sponge/PLA-PHBV bilayer electrospun fiber mesh. De-cellularized de-epidermized dermis (DED) was used as a control.

2.2.1.1 Preparation of collagen sponges

In the preparation of collaged sponges, collagen which was isolated from rat tail was used.

2.2.1.1.1 Collagen Type I Isolation from rat tail

Collagen Type I was isolated from Sprague-Dawley rat tails according to Bahcecioglu et al. 2014; Kilic et al. 2014. The tendons were dissolved in 0.5 M acetic acid (2-3 days) at 4°C. The suspension was filtered through glass wool, dialyzed at 4°C against phosphate buffer (pH 7.2), centrifuged (Sigma 3K30, Germany) (16,000 g, 10 min) at 4°C. The pellet was kept overnight in 0.15 M acetic acid, precipitated by addition of 25 g NaCl and centrifuged. Dialysis and centrifugation steps were repeated.

The collagen pellet was maintained in 70% alcohol for 2 days for sterilization. After centrifugation, the product was lyophilized (Labconco Freezone 6, USA).

2.2.1.1.2 Preparation of collagen sponge

A solution of Sprague-Dawley rat tail collagen type I in acetic acid (1% w/v, 0.5 M) was prepared with a vigorous mixing at room temperature. The solution was added into PDMS molds in 12 well plates, frozen at -80°C for 24 h and lyophilized under vacuum for 8 h. The lyophilized sponge was then physically crosslinked with dehydrothermal (DHT) treatment by keeping the samples under vacuum at 140°C for 24 h.

2.2.1.2 Preparation of electrospun fibers

2.2.1.2.1 Electrospinning of PLA and PHBV monolayers

PLA (Goodfellow, Huntingdon, UK, MW: 10,100 g/mol) solution (10% w/w) was prepared by dissolving the polymer in dichloromethane (DCM). PHBV12 (88:12 HB:HV, Goodfellow, Huntingdon, UK) solutions (5% and 10% w/w) in DCM:methanol (90:10) were prepared. These solutions were loaded into 4 x 5 mL syringes (20 mL in total), fitted with blunt tip needles (0.6 mm ID), and placed onto a single syringe pump (40 µL/min, Genie Plus, Kent Scientific, USA). A mandrel (w: 20 cm, d: 10 cm), coated with aluminum foil and rotating at 200 rpm was used as the collector. Working distance from the needle tip to the mandrel was 17 cm for PLA and 10 cm for PHBV, to produce micro and nano fibers, respectively. A potential of +17 kV was used (73030P, Genvolt, Shropshire UK).

2.2.1.2.2 Electrospinning of PLA-PHBV-PLA trilayers

Electrospun trilayer membranes were designed to be used to separate keratinocytes from fibroblasts. A nanofibrous membrane (PHBV) which is permeable to nutrients was coupled on both sides with PLA to support the proliferation of different cell types either side, but prevent migration of cells across the barrier. PHBV is in between the two PLA layers, because it acts as a barrier due to its nanofibrous structure.

Trilayer membranes were electrospun by consecutively spinning first a PLA layer then on top of that a PHBV layer. A final layer of PLA was spun on the exposed PHBV face using the conditions above (**Figure 2.2**). This method produced a uniform PHBV layer sandwiched between PLA layers (Bye et al. 2013).

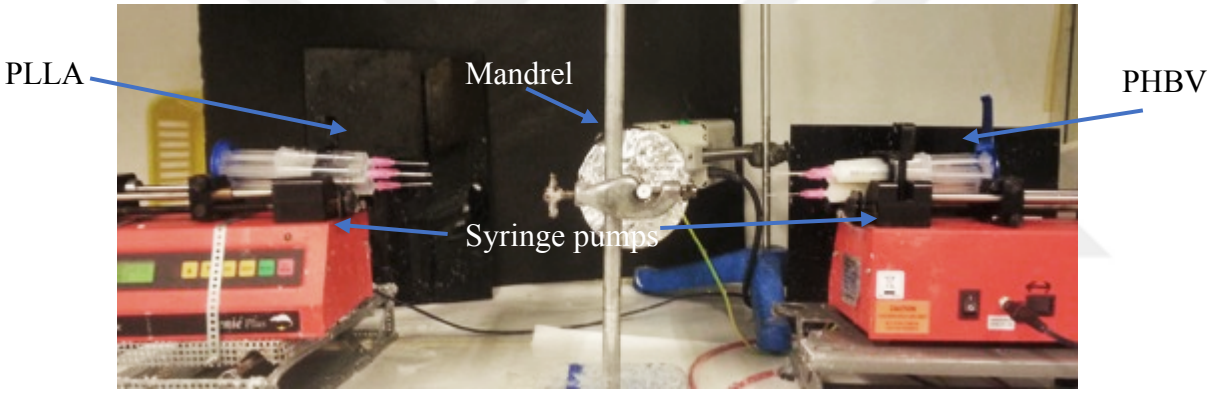

Figure 2.2 The electrospinning setup. A trilayer of PLA-PHBV-PLA fiber mesh production using a rotating mandrel placed in between syringe pumps carrying PLA and PHBV solutions. (The mandrel spin rate was 200 rpm. Working distance was 17 cm for PLA and 10 cm for PHBV. Potential was +17 kV.

2.2.1.3 Preparation of decellularized and de-epidermized dermis (DED)

2.2.1.3.1 Harvesting skin biopsy from a patient

Skin to use isolation of the cells was obtained from patients undergoing routine abdominoplasties and breast reductions at the Department of Plastic Surgery, Royal Hallamshire Hospital, Sheffield, UK. Full informed consent was obtained from the patients pre-operatively in accordance with the ethics permission under a protocol approved by Sheffield University Hospitals NHS Trust Ethics Committee (04/Q2306/29). Full thickness skin was harvested by surgery using an aseptic approach and split thickness skin was obtained from this full thickness skin (thickness of 0.6-0.8 mm) using a modified Watson knife (**Figure 2.3**). Specimens were placed into sterile tubes containing PBS, 0.625 µg/mL amphotericin B, 1% penicillin/streptomycin 100 unit and 100 µg/mL streptomycin and stored in the refrigerator at 4ºC. Cell isolation was performed within 2 days of harvesting.

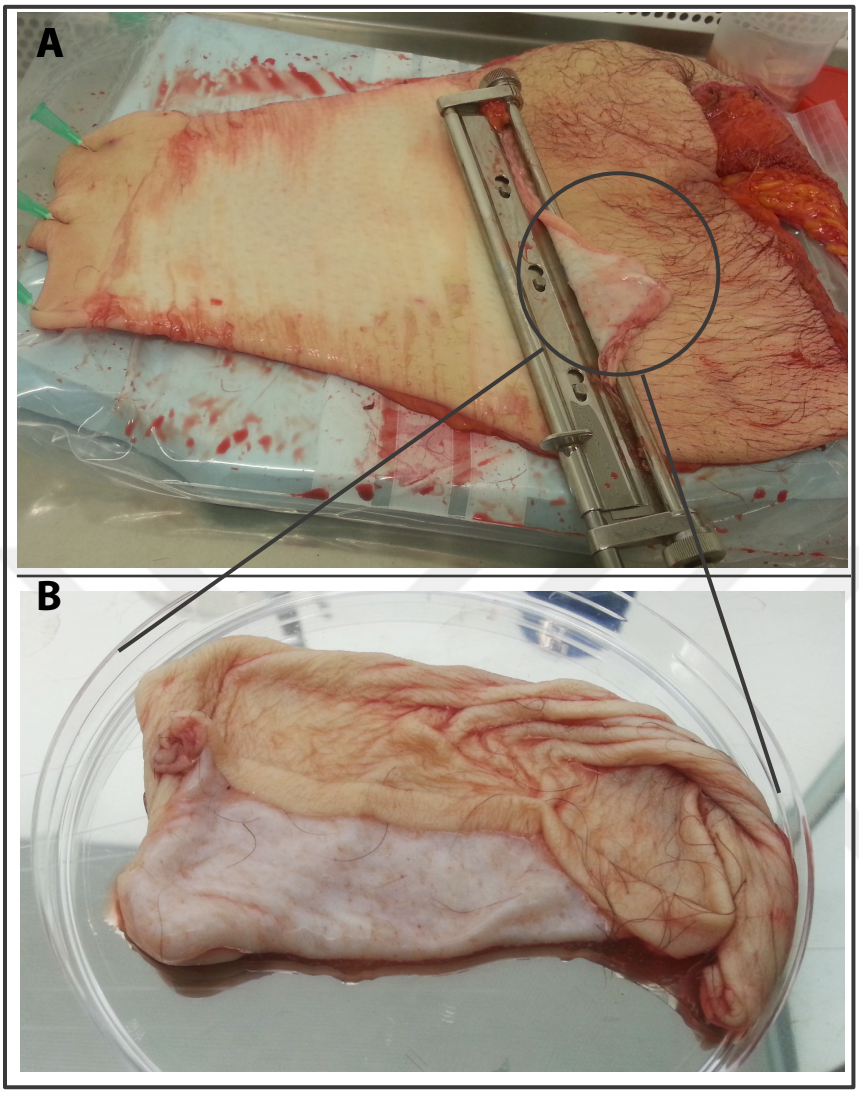

Figure 2.3 Representative images of human skin after abdominoplastic surgery. A) Full thickness skin is harvested by a modified Watson knife, B) Split thickness skin with of a 0.6-0.8 mm thickness.

2.2.1.3.2 De-epidermization of cadaver skin

Sterilized cadaver skin (Research and Development Unit of Sheffield University Hospital) removed from the vacuum sealed packs and hydrated in sterile PBS for 24 h at 37ºC. Skin was then kept in an excess of sterile NaCl solution (1 M) at 37ºC overnight. Epidermis was gently removed with forceps. Remaining de-epidermised dermis (DED) was rehydrated in Greens medium (*Section 2.2.1.5.1*) for 48 h in a CO_2 incubator at 37ºC to ensure that no residual NaCl leached from the DED.

2.2.1.3.3 Decellularisation of cadaver skin

After de-epidermisation with NaCl solution (1 M) for 16-18 h, the dermis was completely acellular and no further processing was required. Biopsies of the dermis were taken for confirmation of acellularity by haematoxylin and eosin stain (H&E).

2.2.1.4 Characterization

2.2.1.4.1 Characterization of isolated collagen with SDS-Page

Collagen purity was assessed by using sodium dodecyl sulfate-polyacrylamide gel electrophoresis (SDS-PAGE). Briefly, collagen isolated from Sprague-Dawley rat tail was treated at 95°C for 5 min in mercaptoethanol, then the solution was loaded on 10% (w/v) gels and the bands were visualized by staining with 0.2% (w/v) Coomassie Brilliant Blue solution.

2.2.1.4.2 Analysis of morphology with SEM

Morphology of scaffolds were studied with scanning electron microscopy (SEM). Cell seeded and unseeded PLA/PHBV/PLA electrospun trilayer fibers, collagen sponges and deepidermized decellurized dermis were examined by SEM. Cell seeded SEM specimens were washed twice with PIPES (piperazine-N,N'-bisethanesulfonic acid) buffer (Sigma Aldrich, USA), and fixed in 4% paraformaldehyde solution for 5 min. After washing with PIPES buffer, the samples were freeze-dried for 6 h. Scaffolds were coated with Au-Pd under vacuum and examined with the SEM (400F Field Emission SEM, USA).

Porosity, pore size distribution and average pore size of the collagen sponges and the mean diameters of the PLA-PHBV-PLA electrospun fibers were determined from the SEM micrographs ($n \geq 6$) using ImageJ program (NIH, USA). The mean diameters of pores and electrospun fibers were calculated using results from 15-20 measurements from three randomly selected fields.

2.2.1.4.3 Mechanical tensile testing

Uniaxial tensile testing was performed for cell seeded and cell-free scaffolds. As a positive control, human skin was tested under the same conditions. For the cell seeded scaffolds, all samples were stored in the medium until testing. Samples were cut, dimensions were measured and then the moist samples were clamped in the tensiometer.

Samples were cut (5 mm × 20 mm) and their thickness were measured using a micrometer and then tested with a mechanical tester (Bose Electroforce 3100, USA).

Tension test was applied at a rate of 0.5 mm/s with a maximum displacement of 8 mm using a 22 N load cell (**Figure 2.4A**). The first failure point or plateau was recorded as the load at failure (ultimate tensile strength, UTS), and the displacement at this point was recorded as maximum strain (at ultimate tensile strength).

The typical stress-strain curve is presented in **Figure 2.3B** and the slope of this plot gives the Young's modulus (or elastic modulus, E).

Since the collagen sponges take up water, the mechanical properties of the unseeded scaffolds were also measured in the wet state after storing in PBS.

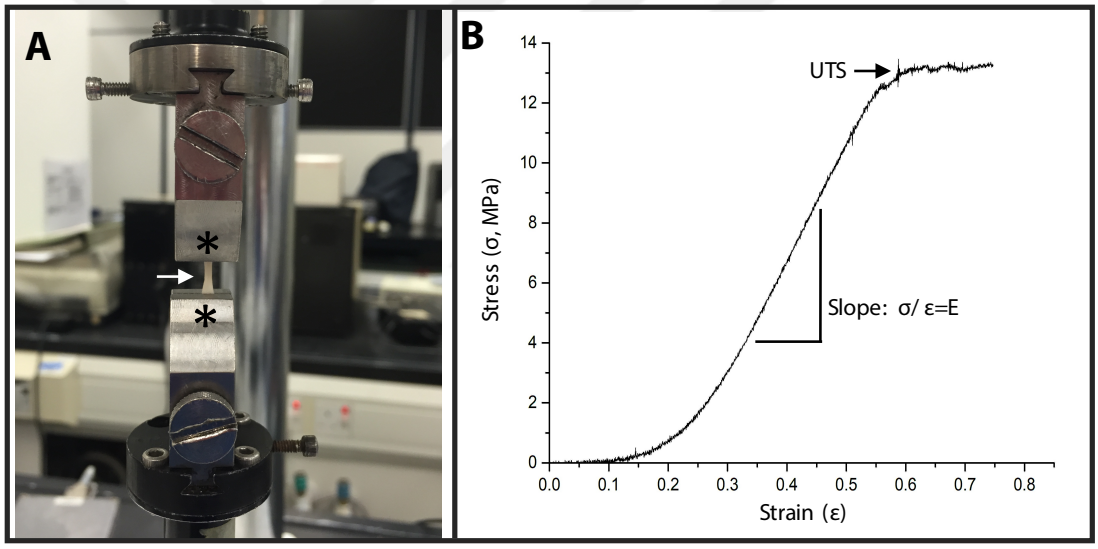

Figure 2.4 Mechanical testing. A) Clamps (marked with asterix) holding the specimens in stretched form. B) Typical stress vs. strain curve resulting from testing of the dermis. The elastic modulus was calculated from the linear region as the slope.

2.2.1.5 In vitro studies

2.2.1.5.1 Isolation and culture of keratinocytes from a split thickness human skin

Split thickness skin was removed from the full thickness skin as mentioned in *Section 2.2.1.3.1* and approximately 5 mm x 10 mm pieces were cut. These pieces were transferred into Difco-Trypsin (0.1 w/v, 15 mL) and kept at 4ºC overnight. Then skin was put in a petri dish with the dermal side down and medium was added to stop the enzymatic activity. Epidermis was peeled off with sterile forceps and keratinocytes were scraped from both the top side of the dermis and the under the epidermis with a scalpel (No. 22). The scraped dermis fragments were then used in fibroblast isolation.

Keratinocytes were suspended in Greens medium (DMEM:Ham's F12 3:1 supplemented with 10% FCS, 10 ng/mL EGF, 0.4 µg/mL hydrocortisone, 10-10 mol/L cholera toxin, $1.8x10^{4}$ mol/L adenine, 5 µg/mL insulin, 5 µg/mL transferrin, $2x10^{-3}$ mol/L glutamine, $2x10^{-7}$ mol/L triiodothyronine, 0.625 µg/mL amphotericin B, 1% penicillin/streptomycin 100 unit and 100 µg/mL streptomycin) and centrifuged at 10,000 rpm for 5 min. Then, freshly isolated keratinocytes in suspension (with the density of $2x10^{6}$) were seeded onto a precoated feeder layer of lethally irradiated 3T3 fibroblasts (i3T3) in Greens medium. Cells were cultured until approximately 70-80% confluent, usually for 6-9 days (**Figure 2.5**).

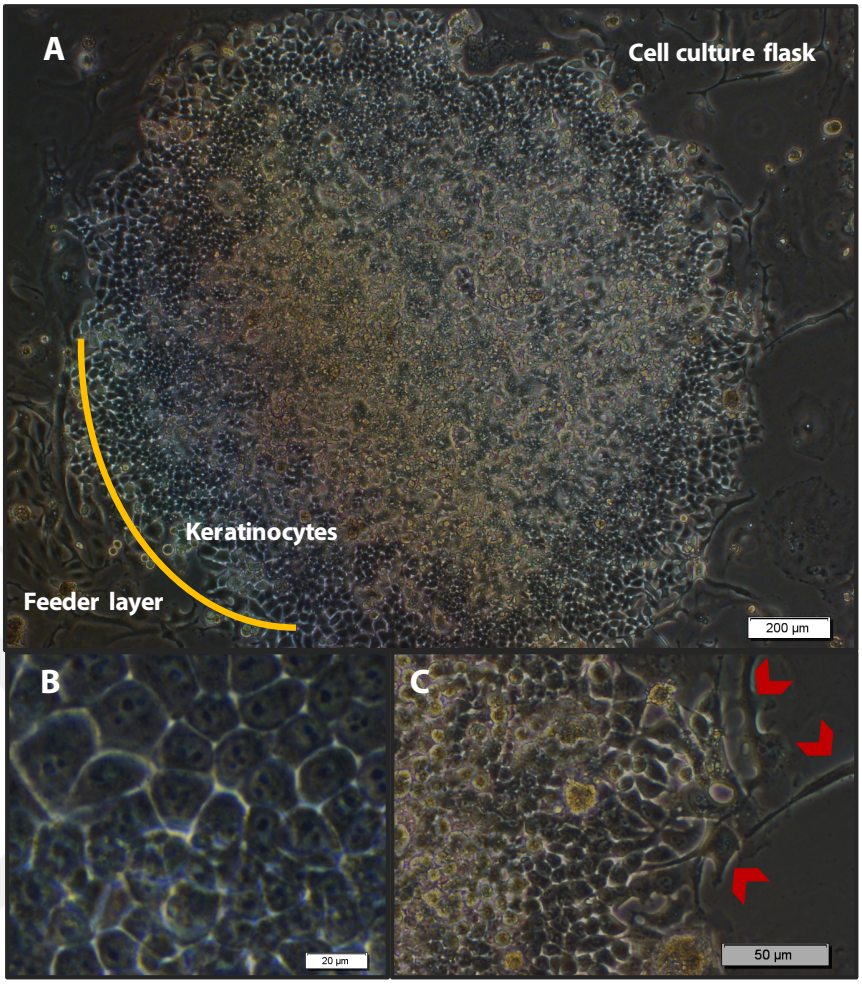

Figure 2.5 Isolation and culture of human keratinocytes. A) Keratinocytes migrating over radiated 3T3 fibroblasts in the cell culture flask (Scale bar: 200 µm). The interface between the keratinocytes and i3T3 cells are shown in yellow. B) Magnified view of typical polygonal morphology of keratinocytes (Scale bar: 20 µm). C) Spindle like i3T3 cells, indicated with red arrows, bridging between the keratinocytes and TCPS surface was observed in a close up (Scale bar: 50 µm).

Before seeding the keratinocytes, the i3T3 cells were removed from the culture flask with 0.02% EDTA. Then keratinocytes were detached from the flask with Trypsin solution (Difco-Trypsin 0.1 w/v, 3 mL) for 5 min. Then the culture medium (Greens medium) was added to the flask to inhibit trypsin activity. The cell suspension was centrifuged (10,000 rpm, 5 min) and the pellet was resuspended in the medium. The cells were counted with a hemocytometer (Blau Brand, Germany). Passage 1 was used for each experiment.

2.2.1.5.2 Isolation and culture of fibroblasts from a split thickness skin

After keratinocyte isolation from the split thickness skin (*Section 2.2.1.5.1*), the remaining dermis was minced using a scalpel (No. 22). Collagenase A (10 mL, 0.5% w/v in DMEM and 10% FCS, 1% penicillin/streptomycin) solution was added and the whole suspension was incubated at 37ºC for 12-18 h. Following centrifugation (20,000 rpm for 10 min) of the resulting tissue digest, the cells in the pellet were resuspended in DMEM supplemented with FCS (10% v/v), 1% penicillin/streptomycin 100 unit and amphotericin B (0.5 μg mL^{-1}). Cell suspension was then seeded in a T25 flask and cultured in a CO_2 incubator at 37ºC until 80% confluency.

For the cell seeding, fibroblasts were detached from the flask bytreating Trypsin solution for 5 min, culture medium (DMEM with 10% FCS, 1% penicillin/streptomycin) was added, and centrifuged for 5 min at 10,000 rpm. Then cells were resuspended in the medium and counted with a hemocytometer (Blau Brand, Germany). $1x10^6$ cells were seeded onto each scaffold. Fibroblasts used were between passages 4-9.

2.2.1.5.3 Irradiation of 3T3 murine fibroblasts

The J2 clone of the NIH strain of murine fibroblasts was used as a feeder layer for proliferating keratinocytes. Once sufficient cell number was reached by culture and passage, the 3T3 cells were irradiated by using a cobalt-60 source. Briefly, cells of known concentration in 10% DMEM medium were aliquotted into falcon tubes. They were then exposed to γ-rays from a cobalt-60 source for 24 minutes achieving a total radiation dose of 60 Grays (3T3 cells need 60 Grays in order to achieve growth arrest). Cells were then cryopreserved until use.

$$Dosage = \frac{Duration\ (in\ seconds)}{seconds\ per\ Gray} \quad (1)$$

2.2.1.5.4 Cell seeding on scaffolds

2.2.1.5.4.1 Keratinocyte and fibroblast seeding on de-epidermized dermis (DED)

In the experiments, DED from a single donor was used to reduce the effect of variation in skin characteristics and differences in dermal thickness. DED samples cut into 2 cm^2 pieces and placed in 6 well plates. A stainless steel ring (ID 1 cm) was placed on top of the each sample (**Figure 2.6A)**. Human dermal fibroblasts isolated were seeded inside the steel rings at a density of 1×10^6. Then DMEM medium (3 mL) was added, cultured for 48 h, rings were removed and the samples were incubated with fibroblasts for 10 days. After incubation, keratinocytes were seeded on DED at a density of 3×10^5.

Greens medium (3 mL) was added and cells were cultured for 1 week, and the samples were raised to an air-liquid interface with metal grids and maintained in this form for 14 days (**Figure 2.6B**). Medium was changed every 2-3 days. They were assessed for their histological morphology.

De-epidermized dermis (DED) incubated with cells is named as 'allograft' throughout this thesis.

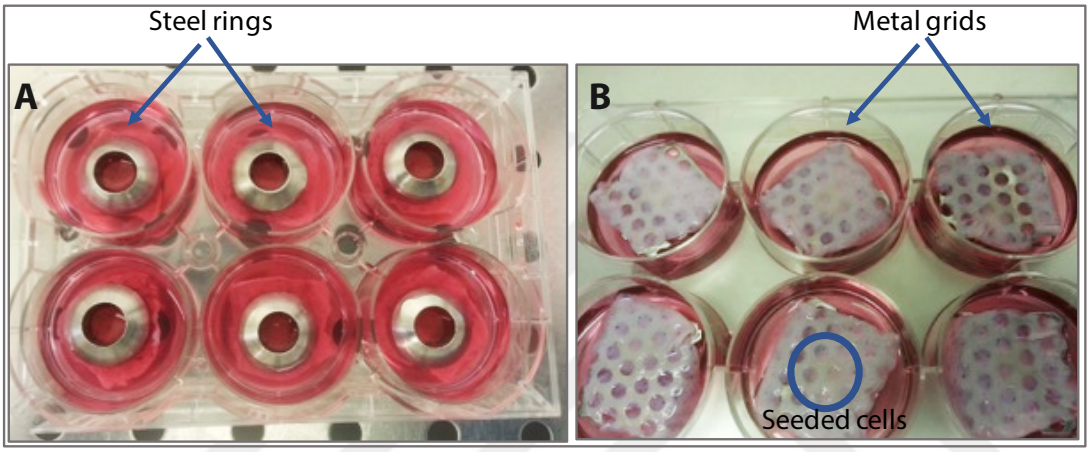

Figure 2.6 Cell seeding on de-epidermized dermis (DED) samples. A) Fibroblasts (1×10^6) were seeded inside the stainless steel rings and then keratinocytes (3×10^5) were added on them. B) After 4 days samples were raised to air-liquid interface with metal grids. Circle shows the cells seeded in the steel rings.

2.2.1.5.4.2 Keratinocyte and fibroblast seeding on trilayer meshes

Trilayer PLA-PHBV-PLA meshes (2 cm^2) were sterilized in alcohol (70%) for 3 h and washed with PBS. They were then placed in 6-well plates. Stainless steel rings (ID 1 cm) were placed on top of the scaffolds as described in the previous section (**Figure 2.6**). Isolated human dermal fibroblasts (1×10^6) were seeded inside the steel rings and

medium was added up to 3 mL. The scaffolds were incubated at 37°C in CO_2 incubator for 10 days. Then, scaffolds were turned over. Isolated human keratinocytes (3×10^5) were seeded on the reverse side of the scaffold. The steel rings were removed on Day 4 of incubation, scaffolds were raised to an air-liquid interface on metal grids and incubated for 14 days (**Figure 2.6B**). Medium was changed every 2-3 days. They were assessed for their histological morphology.

2.2.1.5.4.3 Keratinocyte and fibroblast seeding on collagen sponges

Collagen sponges (2 cm^2) were sterilized with UV for 15 min, and then placed in 6-well plates. Fibroblasts and keratinocytes were seeded as mentioned in *Section 2.2.1.5.4.2*. They were then further assessed for their histological morphology.

2.2.1.6 Histology

All samples were fixed with 10% formalin after cell culture studies, and put into a tissue processor (Leica ASP300 S) which dehydrates the sample with a series of increasing methylated spirits (IMS) and immerses them into xylene and then paraffin wax.

Paraffin embedded samples were cut in 6 μm sections with a microtome (Minot Microtome Leica RM 2145). After keeping at room temperature for air dry, samples from each group were processed for H&E staining and immunostaining.

2.2.1.6.1 H&E staining

The simplest method of assessing histological studies is to use haematoxylin and eosin staining of paraffin-embedded sections. Haematoxylin stains nuclei as well as cellular material while eosin stains the cytoskeleton.

The wax on the slides was removed by submerging the slides in xylene for 10 min. Xylene was removed by immersing the sections in descending grades of alcohol (99%, 95% and 70%) and then into water. The slides were stained with haematoxylin for 3 min and excess stain was removed by rinsing with tap water. To remove haematoxylin, slides were dipped in 1% HCl for 20 s and then stained with eosin. Excess stain was removed by rinsing with tap water. Dehydration was achieved in ascending grades of alcohol (70%, 95% and 99%) and xylene.

Mounting medium was added on the dehydrated samples and cover slips were mounted on the slides for microscopical analysis. The H&E staining provides purple cell nuclei with pink cytoplasm and connective tissue (Fischer et al. 2008).

2.2.1.6.2 Immunohistochemistry

Immunohistochemistry was performed by staining the samples for Involucrin and Coll-IV. Involucrin is a structural component of mature squamous epithelial cells. Anti-involucrin monoclonal antibody identifies terminal differentiation of the keratinocyte. Collagen IV antibody targets the collagen synthesized by fibroblasts.

2.2.1.6.2.1 Involucrin staining:

Removing the wax from the slides was performed as described in Section 2.2.1.6.1. Sections were placed in warm PBS to rehydrate. Trypsin antigen retrieval was used for involucrin unmasking. Slides were incubated in trypsin solution (0.5 % calcium chloride and 0.05% trypsin in distilled water, pH 7.8) for 14 minutes at 37ºC. After antigen retrieval, the slides were placed in TRIS-Buffered Saline pH 7.8 and Tween (5 µL) for 10 min then incubated with blocking buffer (1:25 horse serum in TBS/Tween) to eliminate background staining. The blocking buffer was removed and anti-human involucrin monoclonal antibody (1:100 in 0.05M TRIS-HCl buffer) was added (60 min at room temperature). After washing, the slides were incubated with goat anti-mouse IgG-AP conjugate (1:50 in 0.05M TRIS-HCl buffer) for 15 min.

The hydrogen peroxide Avidin-Biotin Complex kit and diaminobenzidine (DAB) substrate kit (brown colour end-point) were used as described by the manufacturer. The sections were washed in running water, stained with haematoxylin (20 s), immersed in acid/alcohol, followed by rinsing in running tap water, dehydrated in ascending grades of alcohol and xylene, and mounted for microscopic examination.

2.2.1.6.2.2 Coll IV staining:

De-waxing of the sections was performed as described in Section 2.2.1.6.1 and then slides were placed in distilled water at 37°C, followed by Tris-Buffered Saline pH 7.8 and Tween, and then blocking buffer (1:25 horse serum in TBS/Tween) to decrease background staining. The blocking buffer was removed and COL94 anti-human collagen IV monoclonal antibody (1:100 in PBS containing 3% bovine serum albumin) was added and kept at room temperature for 60 min.

After washing, they were incubated with goat anti-mouse IgG-AP conjugate (1:50 in 0.05M TRIS-HCl buffer) for 15 min. Further processing of the sections was performed in the hydrogen peroxide Avidin-Biotin Complex kit, diaminobenzidine (DAB) substrate kit (brown color end-point) and haematoxylin.

2.2.2 Subcutaneous Tissue

Two UV crosslinkable polymers, methacrylated gelatin (GelMA) and methacrylated hyaluronic acid (HAMA) were synthesized (Eke et al. 2017) to form a transparent hydrogel loaded with adipose derived stem cells (ADSCs) to serve as a biodegradable subcutaneous tissue.

2.2.2.1. Synthesis of methacrylated gelatin (GelMA)

Methacrylated gelatin was synthesized according to the method reported by Nichol et al. 2010. Briefly, porcine skin gelatin type A was dissolved in a phosphate buffer (10 mM, pH 7.4) at 50^{o}C solution of (10%, w/v) in phosphate buffer (10 mM, pH 7.4) was prepared. Methacrylic anhydride (20%) was added dropwise into the gelatin solution at 50^{o}C and stirred for 1 h. Then, the mixture was diluted 5 fold with warm phosphate buffer (40^{o}C), filtered and dialyzed against distilled water for 1 week and lyophilized after freezing at -80^{o}C (Labconco Freezone 6, USA) (**Figure 2.7A**). The white porous foam obtained was stored at +4˚C until use.

2.2.2.2 Synthesis of methacrylated hyaluronic acid (HAMA)

Methacrylated hyaluronic acid was prepared as described by Messager et al. 2013. A solution of hyaluronic acid in distilled water (0.5 w/v, %) was prepared and DMF (dimethylformamide) was added to obtain a ratio of 3:2 H_2O:DMF. Methacrylic anhydride (1%) was added dropwise while stirring on a magnetic stirrer at +4˚C. During the initial 4 h, the pH was adjusted to ca. 8-9 with NaOH (0.5 M). Then, it was incubated overnight at +4˚C with continuous stirring, and dialyzed against distilled water for 3 days. After dialysis, the solution was frozen at -80˚C and lyophilized and stored at +4˚C until use (**Figure 2.7B**).

2.2.2.3 Preparation of GelMA/HAMA hydrogels

Lyophilized GelMA and HAMA polymers were dissolved in cell culture media (GelMA:HAMA 15:1). Photoinitiator 2-hydroxy-1(4-(hydroxyethox)pheny)- 2-methyl-1-propanone (Irgacure 2959; 0.3% w/v) was added into the solution and mixed at 40^{o}C on a magnetic stirrer to achieve a homogeneous distribution. Then the solution was placed in a PDMS mold (i.d. 1 cm), exposed to 365 nm UV with power of 18W/cm^2 (Omnicure s1000) for 40 s. After release from the molds, the hydrogels were washed with PBS (**Figure 2.7C**).

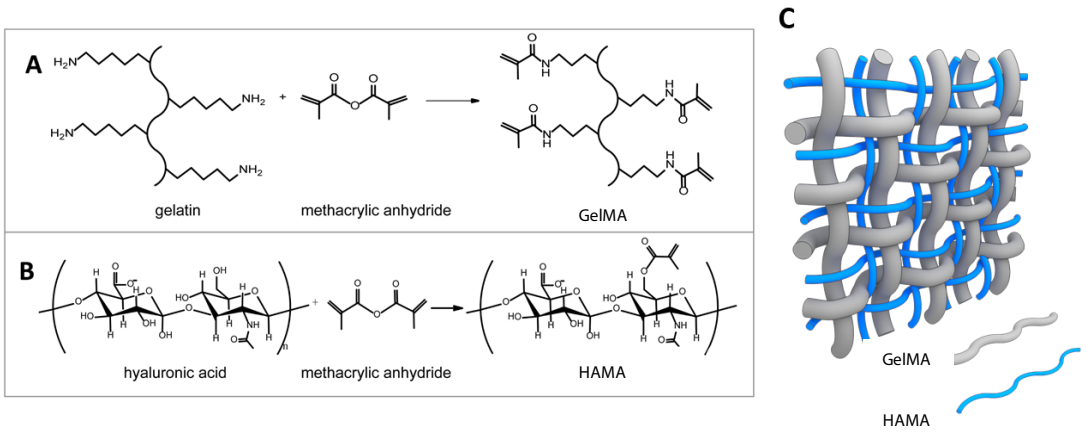

Figure 2.7 Synthesis of gelatin/hyaluronic acid hydrogel network. The binding of methacrylate groups to the: A) primary NH_2 groups of gelatin, B) hydroxyl groups of hyaluronic acid were used for methacrylation. In order to create a hydrogel, a solution consisting of methacrylated gelatin and methacrylated hyaluronic acid was crosslinked using UV irradiation. C) GelMA and HAMA polymer chains crosslinked to form the hydrogel. Gray: GelMA, Blue HAMA.

2.2.2.4 Characterization of the hydrogels

2.2.2.4.1. NMR spectra of GelMA and HAMA hydrogels

Proton nuclear magnetic resonance (^{1}H NMR) was used to characterize GelMA and HAMA, and to determine the methacrylation degree. High resolution (^{1}H-NMR) spectra of the GelMA and HAMA were obtained at room temperature on a Bruker DPX 400 spectrometer operating at ^{1}H resonance frequency of 400 MHz and 16 scans were acquired for signal-to-noise averaging. The methacrylated biopolymer samples were dissolved in Deuterium oxide (D_2O, 30 mg/mL).

The methacrylation degree of gelatin is defined as the number of methacrylate groups per amine group on unreacted gelatin.

The methacrylation degree of hyaluronic acid is defined as the number of methacryloyl groups per HA disaccharide repeat unit.

2.2.2.4.2. Analysis of morphology and porosity by SEM

SEM micrographs were obtained for cell seeded and unseeded hydrogel samples. Cell seeded hydrogel specimens were washed twice with PIPES (piperazine-N,N'-bisethanesulfonic acid) buffer (Sigma Aldrich, USA), and fixed in 4% paraformaldehyde solution for 10 min. Then the samples were frozen in liquid nitrogen, lyophilized, sputter coated with Au-Pd under vacuum and examined with QUANTA 400F field emission SEM (Netherland). Porosity and pore sizes were calculated with Image J software (NIH). Each group had 3 samples, 5 images from each sample were randomly selected and 5 measurements from each image were made (total 150 images).

2.2.2.4.3. Compressive mechanical testing

Compressive mechanical tests were performed on a universal test machine (Shimadzu AGS-X, Japan, 50 N load cell) at room temperature. Hydrogels were kept in PBS to swell before testing, then cut and the dimensions were measured using a micrometer. The cross-head speed was 1 mm/min.

$$\sigma = \frac{F}{A}\ , \tag{2}$$

$$\varepsilon = \frac{\Delta l}{l} \tag{3}$$

$$E = \frac{\sigma}{\varepsilon} = \frac{F}{\Delta l} x \frac{l}{A} \tag{4}$$

The applied force (F, N), cross-sectional area (A, mm^2), initial sample length (l, mm) and the displacement (Δl, mm) measured during the experiments were used to calculate the stress (σ, MPa), the strain (ε) according to equation (2) and (3). Compressive modulus (E, MPa) was calculated from the equation (4).

A representative stress strain curve of the GelMA/HAMA hydrogel for compressive mechanical test is given in **Appendix A**.

2.2.2.4.4 Contact angle measurements

Water contact angles of GelMA/HAMA hydrogels were measured using a goniometer (*Attension*, *Biolin* Scientific, *Sweden)*. Drop of distilled water (7 µL) was placed on 4 independent samples and wetting angle was calculated using Young-Laplace equation:

$$\gamma_{sv} = \gamma_{sl} + \gamma_{l\,v}\ cos\theta \tag{5}$$

where γ_{sv}, γ_{sl} and γ_{lv} were solid-vapor, solid-liquid, and liquid-vapor interfacial tensions respectively and θ is the wetting angle.

2.2.2.4.5 Transparency

Transmittance (T) of the GelMA/HAMA hydrogels was measured in the UV-Vis range 250-700 nm with 5 nm intervals (n=5) using a UV-Vis spectrophotometer (Thermo Scientific, USA).

2.2.2.4.6 In situ degradation

Each hydrogel formulation was gelled by exposing to UV and then weighed. The hydrogels were placed in sterile PBS in a rotary incubator at 37°C for 3 weeks to study in situ degradation. During this time, the samples were removed daily, washed with dH_2O, lyophilized to complete dryness and weighed. The test was performed according to ASTM F 1635-04a (Standard test method for in vitro degradation testing of hydrolytically degradable polymer resins and fabricated forms for surgical implants). The amount lost was calculated from the gravimetrical measurements.

2.2.2.4.7. Swelling

The degree of swelling (DS) of the GelMA/HAMA hydrogels were calculated from the weights of the samples in dry and wet states after immersion in PBS for 48 h. DS was calculated according to equation (6).

$$\text{DS}\ (\%) = \frac{w_s - w_d}{w_s} \times 100 \qquad (6)$$

where w_s: wet sample weight, and

w_d : dry sample weight

2.2.2.5 *In vitro* studies

2.2.2.5.1 Cell culture

2.2.2.5.1.1 Isolation and culture of human adipose derived stem cells (ADSCs) from patient subcutaneous fat

Human subcutaneous fat was selected as the source of ADSCs (**Figure 2.8A**). Biopsies from skin splits, on an anonymous basis under a research tissue bank license (number 08/H1308/39) under the Human Tissue Authority.

Samples were placed in Petri dishes, with 10 mL of PBS and 0.1 mL penicillin (100 units/mL) and streptomycin (100 µg/mL). Samples were minced with a scalpel (**Figure 2.8B**), 10 mL of fat were collected in falcon tubes, and washed with PBS (supplemented with 1% penicillin/streptomycin) by centrifugation at 1300 rpm for 8 min. The tissue (pellet) was collected in a 50 mL falcon tube and twice of the volume of the samples was added for HANK solution.

HANK solution is a saline solution to which collagenase A (0.1%), albumin bovine serum albumin (BSA, 0.1%) and 1% penicillin/ streptomycin were added. Tissues in HANK solution were incubated at 37ºC for 40 min and were periodically shaken for chemical disaggregation. Digested tissues were centrifuged (1300 rpm, 8 min). The floating fractions consisting of adipocytes were discarded and the pellets representing the stromal vascular fraction were resuspended in DMEM medium. ADSCs were collected by centrifugation (1300 rpm, 8 min) and placed in 25 T flasks. Cells up to passage 5 were used.

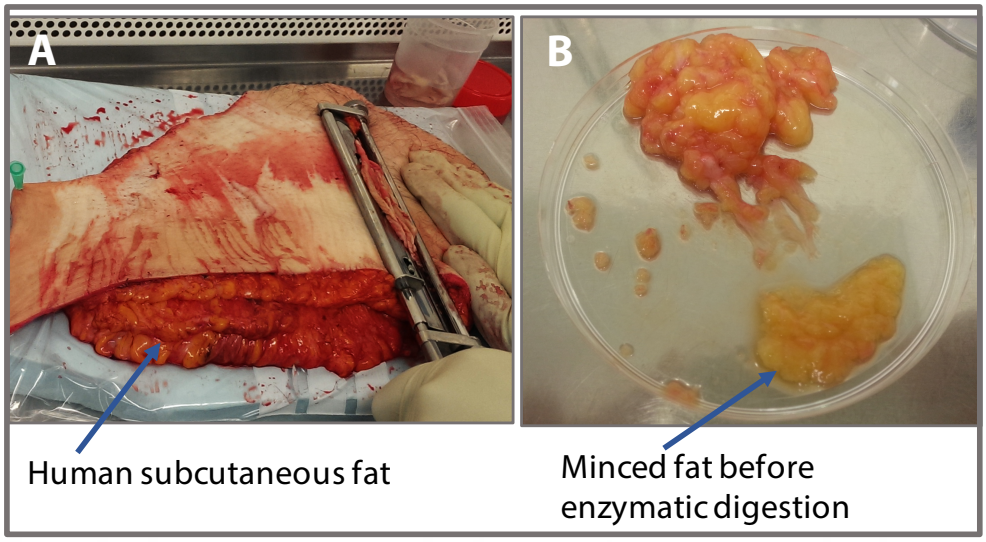

Figure 2.8 ADSC isolation procedure from human fat tissue. A) Human subcutaneous fat as a source of adipose derived stem cells. B) Muscular tissue was removed and remaining fat tissue was minced before enzymatic disaggregation.

2.2.2.5.1.2 Characterization of human adipose derived stem cells (ADSCs) with flow cytometry

The isolated subcutaneous human adipose cells of passages 0 and 5 were analyzed by flow cytometry. Cells were washed with PBS and were detached by incubation with trypsin for 5 min at 37ºC. After trypsinization, cells were centrifuged (3000 rpm, 5 min) pellets were resuspended in ADSC media. 125,000 cells were transferred to flow cytometer tubes. Cells were then fixed with paraformaldehyde (1 mL) and washed with BSA solution (0.1% v/v in PBS) to block nonspecific unions between Ab and other regions.

Fixed cells were stained with mouse IgG1 anti-human monoclonal antibodies (Biolegend, USA) against CD31 (#303110), CD45 (#304017) and CD90 (#328116) surface markers. Mouse IgG1 monoclonal antibody was used as the negative control for the detection of nonspecific binding. The cell population was gated on the forward and side scatter chart and flow cytometry was performed on 105 cells per sample. Positive expression was defined as the level of fluorescence greater than 50% of the corresponding unstained cell sample. Data was analyzed using Flow Jo software (BD Accuri C6 Plus, USA).

2.2.2.5.1.3 Culture of human umbilical vein endothelial cells (HUVEC)

Human umbilical vein endothelial cells (HUVECs) were used for pre-vascularization studies together with ADSCs in the hydrogels. HUVECs were obtained from PromoCell, UK. Cells were grown in T-flasks at 37^{o}C in a humid atmosphere with 5% CO_2 in endothelial growth medium-2 supplemented with growth medium kit (Lonza, USA) according to manufacturer's instructions. Cells were routinely split at a 1:3 ratio and cultured up to passage 5.

When the HUVECs were seeded into the hydrogels, the medium was EGM-2 that contained hEGF (human endothelial growth factor), hydrocortisone, GA-1000 (Gentamicin, Amphotericin-B), FBS (Fetal Bovine Serum), VEGF (vascular endothelial growth factor), hFGF-B (human fibroblast growth factor), R3-IGF-1 (insulin-like growth factor) ascorbic acid and heparin.

2.2.2.5.2 Endothelial and stem cell encapsulation into GelMA/HAMA hydrogels

ADSCs ($5x10^5$, $1x10^6$ or $2x10^6$ cells) were resuspended in GelMA/HAMA solution (200 mL) containing 0.5% (w/v) photoinitiator (Irgacure2959) and the hydrogels were produced as described in Section 2.2.2.3. After crosslinking with UV, cell loaded hydrogels were cultured without direct contact with TCPS by using cell culture inserts (CellCrown 12 well plate inserts), 2 mL of growth medium was added into each well and plates were incubated at 37°C and 5% CO_2 (Eke et al. 2017).

In some tests, vascular endothelial growth factor (VEGF, 100 ng/hydrogel) was added into the hydrogel composition as a positive control of ADSC presence.

In order to achieve *in vitro* pre-vascularization, HUVEC and ADSCs were co-cultured in GelMA/HAMA hydrogels at a concentration of $5x10^5$ and $1x10^6$, respectively. After UV crosslinking and release from the molds, hydrogels were cultured in the EGM:DMEM-HAMF12 1:1 medium for 3 weeks.

2.2.2.5.3 Viability of ADSCs in the hydrogels assessed by Live-Dead assay

Hydrogels loaded with ADSCs were cultured for 3 weeks, washed with PBS and double stained with calcein AM (4 mM in PBS) and ethidium homodimer-1 (10 mM in PBS) for 20 min. Excess stain was removed, gels were washed with PBS, and examined by confocal microscopy (CLSM, Zeiss LSM 9100, Germany).

2.2.2.5.4 Cell proliferation by DNA quantification assay

The DNA of the ADSCs was isolated at each time point using a Genomic DNA Purification Kit according to the manufacturer's protocol (Promega, USA). Briefly, hydrogels were decomposed in a medium containing collagenase (150 µL, 0.1 g/mL) at 37^{o}C for 1 h. After centrifugation, cells were collected and resuspended in 350 µL of RLT lysis buffer. Then, 10 µL of the sample was diluted 10 folds in DNase-free water. Finally, 5 µL of this sample was added in 200 µL working buffer (199 µL of the Quant-IT dsDNA buffer and 1 µL Quant-IT dsDNA reagent prepared for each sample), after which the sample was shortly vortexed and incubated at room temperature for 5 min. Total DNA isolated was quantified (n=5) with PicoGreen dsDNA Assay. The samples and DNA standards (1 mL) were incubated with PicoGreen reagents, fluorescence was measured at λ_{ex}: 560 λ_{em}: 590 nm, and DNA content was determined from the calibration curve (**Appendix B**).

2.2.2.5.5 Assessment of ADSC behavior in the GelMA/HAMA hydrogels

Behavior of ADSCs in the hydrogels at different time points was studied with CLSM. Cytoskeleton and nuclei of the cells were stained with Alexa488 (λ_{ex}: 495 nm, λ_{em}: 519 nm) and Draq5 (λ_{ex}: 646 nm, λ_{em}: 697 nm), respectively and studied with 20x and 40x objectives.

2.2.2.5.6 Assessment of pre-vascularization with HUVECs in the GelMA/HAMA hydrogels

For the capillary formation (pre-vascularization) *in vitro*, HUVEC and ADSCs were co-cultured in the hydrogels, and studied with CLSM at different time points.

HUVECs were stained with CD31 antibody (λ_{ex}: 590 nm, λ_{em}: 617 nm). Cytoskeleton and nuclei of the cells were stained as mentioned in *Section 2.2.2.5.5* and studied with 20x objectives.

2.2.2.6 *Ex ovo* studies

The angiogenic potential of the ADSC and VEGF containing hydrogels was studied with 2 different assays, chick chorioallontoic membrane (CAM) assay and chick aortic arch assay. *In vivo* hydrogel degradation was also studied with CAM assay.

2.2.2.6.1 Preparation of the eggs

Pathogen-free fertilized white leghorn chicken eggs (Gallus gallus domesticus) were obtained from Henry Stewart Co. Ltd (UK). Care was consistent with the guidelines of the Home Office, UK. Fertilized chicken, Gallus domesticus, Medeggs, UK) eggs were received on the same day of dispatch. Dirt, feathers and excrement from the egg shells were cleaned with ethanol (20%) by spraying. Eggs could be stored at +10^{o}C for up to 7- 10 days after arrival.

2.2.2.6.2 Incubation of the eggs

The eggs were placed in the Automatic Egg Incubator horizontally on Day 0, then incubated at 37.5^{o}C and 60% humidity while rotating 12 times a day (Incubator does this automatically). The upper surfaces of the eggs were marked with a permanent pen to spot the embryo since the embryo resists rotation to a certain extent.

2.2.2.6.3 Ex ovo culture

On day 3, the weighing boats were sterilized by dipping them in a bath of 70% ethanol and dried in a laminar flow cabin. PBS supplemented with Pen/Strep (2 mL, 5%) was added into each weighing boat. The eggs were cracked at the edge of a beaker and embryos transferred into a weighing boat. Heart beat was checked to ensure that the embryo is alive (**Figure 2.9A**). These *ex ovo* cultures were kept in a 37.5^{o}C sterile incubator having 60% humidity. During incubation, the chick embryos were checked if they were developing properly in accordance with their chronological age (chronological age [HH] = developmental age (days)) (Hamburger and Hamilton. 1951). Dead embryos were discarded (by checking the heart beat) immediately to avoid infections (**Figure 2.9B**). Embryo survival was assessed daily and the rate of the embryo survival is presented in **Appendix C**.

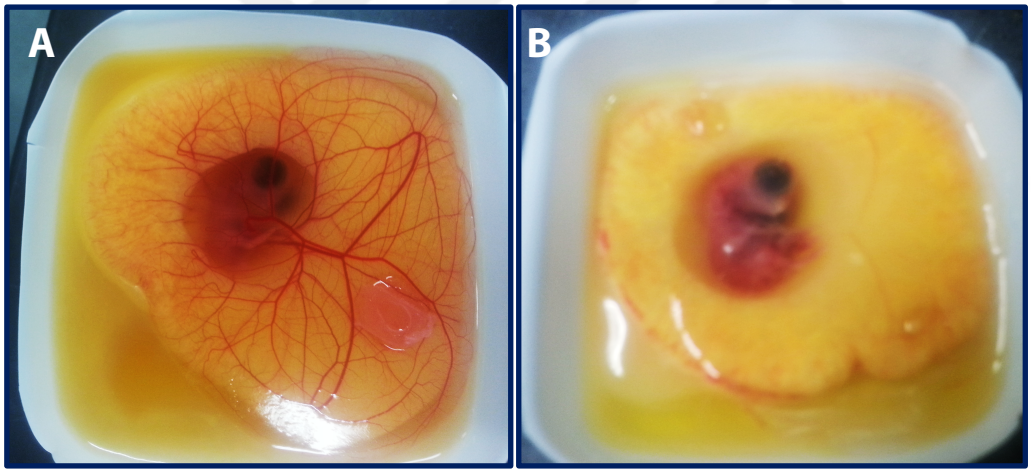

Figure 2.9 CAM of the embryos on Day 8. A) CAM of a healthy embryo. There are blood vessels and they are bright, glossy, moist and even the smallest vessels contain some blood. B) Cam of the dead embryos. The blood vessels are barely visible as there is no circulation at all.

2.2.2.6.4 Assessing the effects of the hydrogels on tissue response and angiogenesis

The angiogenic properties of the ADSC or VEGF-loaded GelMA/HAMA hydrogels, and the tissue response of the embryos was tested with the CAM Assay. After transfer of the chick embryos into Petri dishes, they were kept until Day 8 at 37.5^{o}C in a humidified egg incubator. On day 8, samples (cell or VEGF loaded and control hydrogels) were introduced to *ex ovo* cultures. The samples were placed halfway between the embryo and the outer border of the CAM and in between two large vessels (**Figure 2.10A**). All samples were identical in terms of shape and size.

After samples were placed, the embryos were incubated at 37°C in the humidified incubator for 14 days. Angiogenesis and tissue response were quantified by taking light microscope pictures of the CAM between days 10 and 14 prior to hydrogel retrieval, and by histology of the retrieved scaffold (Ribatti et al. 2000; Zudaire and Cuttitta 2012). Histology of a control CAM was shown in **Figure 2.10B**.

On Day 14, test samples were retrieved with 0.5 mm margin by spring scissors and placed in paraformaldehyde (3.7%). Then the chick embryos were sacrificed by cutting the vitelline artery with spring scissors.

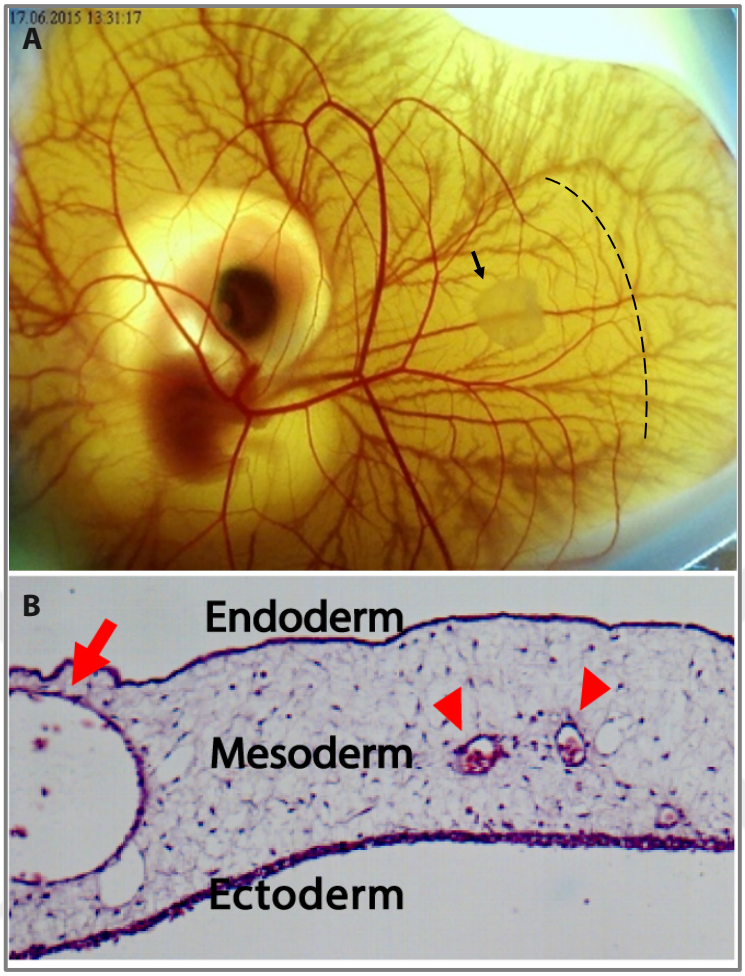

Figure 2.10 Photographs showing how the angiogenic effects of the constructed GelMA and HAMA hydrogels were evaluated by CAM assay. A) Proper placement of a test sample on the CAM on Day 8 of embryonic development. Arrow shows the test sample and the dashed line the border of the CAM. B) Histological section of a control CAM showing three embryonic layers. Red arrows and arrow heads represent large blood vessels and capillaries, respectively.

2.2.2.6.5 Morphometric quantification of angiogenesis

Angiogenesis was quantified using the digital images taken at embryonic development day (EDD) 14 from 6 samples of each group. A semi - automated process was then run using the Image J software and a free online plug in NeuronJ. The images were converted to grayscale (8-bit) and sharpened twice before tracing all discernible vessels in the image with the Neuron J tracing tool. Total vessel length, total number of blood vessels and vasculogenic index were then calculated (Barnhill and Ryan 1983). All discernible blood vessels-capillaries, arterioles, venules- traversing a 1 mm annulus about the 2 mm imaginary circle drawn around the scaffold material were counted provided that they formed an angle of less than 45° with a line radiating from the center. Vessels branching within the annulus were counted as 1 vessel, whereas those branching outside the annulus were considered 2 vessels (Seidlitz et al. 2004; Domenico Ribatti et al. 2006; Zudaire and Frank Cuttitta 2012).

2.2.2.6.6 In vivo degradation of GelMA/HAMA hydrogels

The hydrogels were placed in the *ex ovo* cultures as mentioned in Section 2.2.2.6.4. The decrease in the sizes of the hydrogels were quantified by taking light microscope images of the CAM between Days 10 and 14 prior to hydrogel retrieval. Percent decrease in hydrogel area until Day 14 was calculated by Image J (NIH).

2.2.2.6.7 The chick aortic arch assay

Chicken embryos were sacrificed on embryonic development day (EDD) 14, aortic arches were removed, aortic branches were cut into 1 mm rings under a stereomicroscope. Aortic rings were embedded in 50 mL of Matrigel® (Basement Membrane Matrix, Corning®) in a 24 well plate.

After 30 min of incubation, DMEM (2 mL, supplemented with 2.5% FCS, 50 units/mL penicillin and 50 mg/mL streptomycin) was added into each well and incubated in an incubator at 37^{o}C and 5% CO_2. With the aid of a transparent tissue culture insert the aortic rings were co-cultured with unloaded or ADSC loaded GelMA/HAMA hydrogels ($2.5x10^5$, $5x10^5$ and $10x10^5$ ADSCs were loaded in the hydrogels). The endothelial sprouts were observed under an inverted microscope on Day 5 and the longest sprout length for each sample was calculated (Stratman et al. 2012). Endothelial cells were characterized by immunofluorescence staining with Griffonia Simplicifolia Lectin I, isolectin B4.

2.2.2.7 Histology

The hydrogels and surrounding CAM were retrieved, washed twice with PBS, fixed with formaldehyde (10%), embedded in paraffin and 6 mm sections were cut. Conventional haematoxylin and eosin (H&E) staining as mentioned in *Section 2.2.1.6.1* was performed. Slides were examined under light microscopy to see blood vessels and the inflammatory response in the CAM adjacent to hydrogels. Blood vessels were also stained with a conjugated alpha smooth muscle actin antibody (α-SMA) together with a 4,6-diamidino-2-phenylindole dihydrochloride (DAPI) nuclei staining. Slides were observed under an epi-fluorescence microscope (Olympus, Japan) and the area of α-SMA stained blood vessels were measured (n=6).

2.2.3 Drug Delivery studies into human skin model

Retinyl palmitate loaded PHBV nanoparticles were used to study the penetration through the human skin, and rhodamine loaded nanoparticles were used to study penetration studies through the tissue engineered skin constructs.

2.2.3.1 Preparation of Retinyl Palmitate loaded PHBV nanoparticles

Retinyl palmitate (RP) loaded nanoparticles were prepared with the oil-in-water (o/w) technique (Eke et al. 2015). For this purpose, RP was added in 1.2 mL of solution of PHBV in dichloromethane (DCM; 10%, w/v). This solution was added into an aqueous solution of PVA (4 mL, 4% w/v), sonicated in an ice bath (Ultrasonic Homogenizer, 4710 series, Cole-Parmer Instruments, USA), further dilution was made by adding PVA solution (100 mL, 0.3% w/v), stirred overnight at room temperature to remove the solvent, and centrifuged (rotor: 15156-H Sigma, 3K30). The precipitate was washed twice with distilled water (dH_2O), freezed at -80^oC and then lyophilized.

2.2.3.2 Preparation of Rhodamine loaded PHBV nanoparticles

Rhodamine (Rho) loaded PHBV nanoparticles were prepared as mentioned in *Section 2.2.3.1*. This time, Rhodamine was (0.5 mg/mL) added into the PHBV solution instead of RP.

2.2.3.3 Characterization of the nanoparticles

2.2.3.3.1 Nanoparticle topography with SEM

Aqueous suspension of RP and Rho loaded nanoparticles were added onto carbon tapes attached to scanning electron microscope (SEM) stubs, dried at room temperature, and then sputter coated with Au-Pd before examining with SEM (Quanta 400F Field Emission SEM, The Netherlands). The surface topography was examined from the images and sizes were measured with Image J software, NIH (USA)..

2.2.3.3.2 Size distribution analysis

The size distribution of RP and Rho loaded PHBV particles were studied with the Zeta Potential and Mobility Measurement System (Malvern Nano ZS90, UK).

2.2.3.3.3 Loading and encapsulation efficiencies of Retinyl Palmitate and Rhodamine

The concentration of RP in PHBV particles (10 mg) was determined after dissolving the particles in DCM (3 mL) and measuring the absorbance at 326 nm with UV spectrophotometer.

Rho concentration encapsulated in PHBV particles were determined with measuring the fluorescence with spectrofluorometer (λ_{ex}: 528 nm, $\lambda_{em:}$ 551nm) after dissolving the particles in DCM (10 mg/ mL).

The percent loading and percent encapsulation efficiency (EE) values of RP and Rho were calculated by using the equations (7) and (8):

(8)

$$Loading(\%) = \frac{Encapsulated\ drug\ amount\ (mg)}{Total\ amount\ of\ nanoparticles\ (mg)} x100$$

$$EE(\%) = \frac{Encapsulated\ drug\ amount\ (mg)}{Input\ amount\ of\ drug\ (mg)} x100$$

2.2.3.4 *In situ* release studies from the nanoparticles

Release kinetics of RP and Rho from PHBV nanoparticles were studied in situ. Nanoparticles (10 mg) were put in Eppendorf tubes, 2 mL PBS was added and incubated at 37°C in a shaking incubator (shaking rate 70 rpm, New Brunswick Scientific, Innova 4000, USA). At various time points the tubes were centrifuged, supernatant removed and the amount of released drugs in the solution were determined with the spectrophotometer (λ_{max}: 326 nm) and spectrofluorometer (λ_{ex}: 528 nm, λ_{em}: 551nm) as described in *Section 2.2.3.3.3*. Then, 2 mL of PBS was added to the Eppendorf tubes, pellets were resuspended and incubation was continued (n=5). Amount of the released drugs were determined from calibration curves in **Appendices D1 and D2**.

2.2.3.5 Studies on penetration through human skin

Skin samples were obtained from a 42-year-old, healthy donor admitted for elective breast surgery (upon patient consent and with METU Human Experiments Local Ethics Committee approval, No:28620816/298-37) (**Appendix E**). Skin samples (2×2 cm^2) were inserted into cell crown holders in 12-well plates exposing the epidermis to air while the dermis is in PBS. Stratum corneum of some samples was mechanically removed to study its inhibitory effect on penetration. RP loaded nanoparticles (0.5 mg) were placed on each skin sample.

After a 24 h incubation period, the particles were gently removed from the skin surface, and the skin samples were put in chloroform (10 mL) and stirred for 72 h for skin and nanoparticle destruction. The RP that dissolved was determined with UV visible (Vis) spectrophotometry (λ_{max}: 326 nm) (n=5) using a calibration curve (**Appendix D2**).

2.2.3.6 Determination of nanoparticle concentration on keratinocytes

Prior to the experiment, keratinocytes were isolated from the patient and cultured as mentioned in *Section 2.2.1.5.1*. Then the keratinocytes were detached from the flask with Trypsin solution and seeded on 6 well plates with the density of $1x10^6$. Rho loaded nanoparticles were then added on keratinocytes with different concentrations in the range 250 - 10 ng/mL.

2.2.3.7 Nanoparticle penetration through tissue engineered skin model

Tissue engineered dermis models were produced as mentioned in *Section 2.2.1.2.2*. The last 2 days of incubation, Rhodamine loaded nanoparticles were seeded on the epidermis layer (on top of the keratinocytes on the air-liquid interface). Nanoparticles were incubated with the dermis models for 48 h (n=3).

2.2.3.7.1 Cryosectioning and immunostaining

Nanoparticle loaded tissue engineered skin models were fixed in paraformaldehyde solution (4%) for 5 min and washed twice with PBS. Samples were placed in a plastic cassette and embedded with Optimal Cutting Temperature (O.C.T) compound (Tissue-Tek). Then the molds were set aside to slow freeze to prevent the crack due to internal

stress build up during rapid cooling. The cryotome (CM 1850, Leica) was set at -25°C and 10 μm sections were cut.

2.2.3.7.2 Microscopy

Using H&E staining, it is not possible to assess whether the nanoparticles were penetrated into the skin models or not. Therefore, nanoparticle loaded samples were stained with fluorescent dyes as follows:

The cryoembedding media was removed from the sections by washing with warm PBS. Then, the samples were incubated for 1 h at 37°C with Alexa Fluor 647 Phalloidin for staining of the actin cytoskeleton. After washing with PBS, the nuclei were stained with DAPI by incubating the samples for 10 min at room temperature.

Fluorescence micrographs of the nanoparticle loaded skin models were obtained using an upright fluorescence microscope under 350 nm, 488 nm, 550 nm, 630 nm LED sources and appropriate filter sets (Zeiss Axio Imager M2, Germany) or with an inverted confocal microscope under 488 nm, 532 nm, 630 nm and UV lasers (Leica DM2500, Germany and Zeiss LSM710, Germany).

2.2.8 Statistical analysis

Statistical analysis was performed with Graphpad Prism6 program. Differences between group means were analyzed with Student's T test when the data was normally distributed. Mann Whitney U test was used for data that was not normally distributed. Comparisons of more than 2 groups were performed with One-way ANOVA with Tukey's post-hoc test, to determine significant differences. All values are represented as the mean ± standard deviation. Differences were taken to be significant for $p < 0.05$.

CHAPTER 3

RESULTS AND DISCUSSION

3.1 Epidermis and Dermis Layer of the Skin Model

Two different scaffolds were produced as dermis layer of the model skin. 1) PLA-PHBV-PLA trilayer electrospun mesh, 2) Collagen sponge/PLA-PHBV bilayer electrospun fiber mesh. As a positive control, de-cellularized de-epidermized dermis (DED) was used. Keratinocytes were seeded on these dermis substitutes to form epidermis. A shematic illustration is presented in **Figure 2.1**.

3.1.1 Characterization

3.1.1.1 Collagen Type I characterization

Collagen type I was isolated from Sprague-Dawley rat tails, as mentioned in *Section 2.2.1.1.1.* After isolation, SDS-PAGE was developed in order to determine the collagen type (**Figure 3.1**). The typical SDS-PAGE band pattern for collagen Type I is a doublet at 115 and 130 kDa and another doublet at 215 and 235 kDa (data sheet from Sigma Aldrich Co.). Three collagen batches isolated at different times were tested. Both the doublet-patterns were obtained with each of the collagen samples, confirming that the collagen isolated (Kilic et al. 2014; Bahcecioglu et al. 2014) was type I.

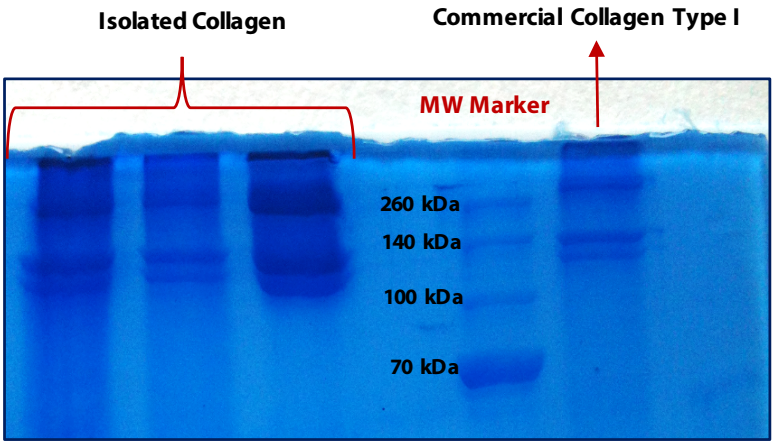

Figure 3.1 SDS-PAGE of collagen isolated from Sprague-Dawley rat tails. Three batches of isolated collagen were tested. The doublet-patterns were confirming the type I collagen. The control in commercial collagen Type I purchased from Sigma (US).

3.1.1.2 Wettability and degradation of collagen sponges

The interaction between the collagen sponge and aqueous environment was assessed by determining the contact angles. Static water contact angles of the lyophilized collagen were measured as 92.81±5.47º showing the hydrophobicity of the collagen sponges in their dry form (**Figure 3.2A**).

Since collagen is a hydrophilic protein (Leikin, Rau, and Parsegian 1995), however, the production methods and fibrous nature of the collagen scaffolds result in a change of the surface properties of the product, suggesting surface morphology and crosslinking induces the hydrophobicity. Ghaeli et al reported a water contact angle of 97.14° and showed the nano roughness of the surfaces in the SEM images of crosslinked collagen films (Ghaeli et al. 2017). Elliot et al. coated surfaces of the

substrates with collagen Type I. The surface collagen coat thickness resulted in an increase of water contact angle from ~39° to ~106° (Elliott et al. 2003). These all support that crosslinking of collagen and surface roughness change the surface contact angle and therefore wettability.

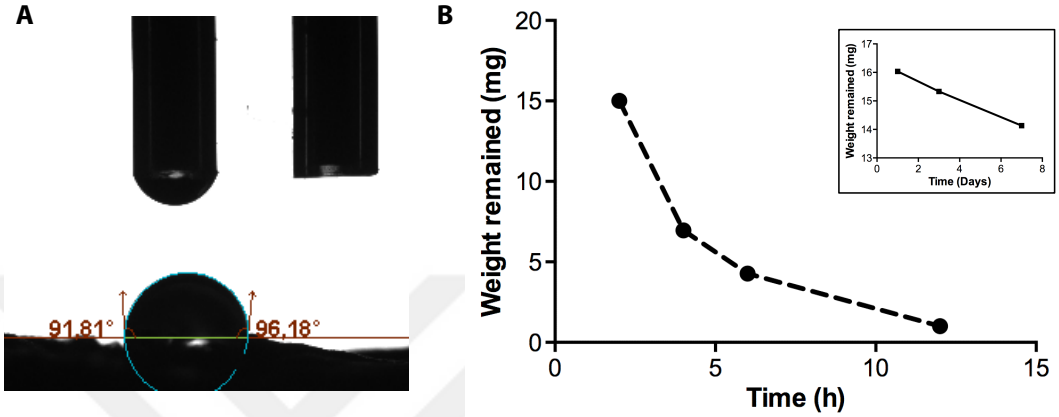

Figure 3.2 Contact angle and degradation profile of the collagen sponges. A) Representative micrograph of contact angle measurements to determine scaffold wettability. B) Enzymatic degradation of the collagen sponges. Degradation was completed in 12 h with the presence of collagenase enzyme and degradation was almost complete in 1 week in PBS. Inset shows the scaffold degradation in PBS without the presence of the enzyme.

A crucial point that should be considered while designing a tissue engineered scaffold is the degradation rate of the material used, in order to understand how long the scaffold will stay in the body. The presence or absence of ECM-secreting cells influence this rate significantly. Therefore, the *in situ* degradation of the collagen sponges in PBS and in enzymatic medium were studied for 1 week.

Collagen sponges showed a very rapid weight loss in the first 6 h (72%) in the collagenase solution (**Figure 3.2B)**. The final weight that remained after 12 h was about 97% and 6.2% after 12 h. The degradation profile in PBS is given in **Figure 3.2B** inset. In contrast, the total weight remaining was 19 % after 1 week in PBS. According to the results collagen sponge is not very stable, degrades too fast and does not allow sufficient time for integration with the surrounding tissue.

3.1.1.3 Morphology analysis with SEM

Structure collagen sponges, the PLA/PHBV/PLA trilayer electrospun mesh and the collagen/PLA/PHBV bilayer fiber mesh constructs were were studied using SEM (**Figure 3.3**).

Coll sponge: The sponge was highly porous which may also affect fibroblast cell secretion (**Figure 3.3A**). Porosity, pore size distribution and average pore size of the collagen sponges were measured from the SEM micrographs using ImageJ. Pore size and the porosity of sponges were determined as 213±87.30 nm and 79.42%, respectively.

Trilayer electrospun mesh: Fibers were electrospun according to in *Section 2.2.1.2.2*. Sequential electrospinning provided a method for producing a composite structure where combining the properties of different polymers brought together the best properties of both components. PHBV produces a flat, dense, brittle meshes while PLA spinning produces low density elastic meshes. Both materials support cell attachment (Bye et al. 2013). Therefore, dense PHBV mat was designed as a basal membrane whereas elastic PLA mat represented the epidermis and dermis layers (**Figure 3.3B**). Sequential spinning resulted in microbeads on the fiber surfaces.

Coll sponge/fiber mesh bilayer construct: PLA/PHBV bilayer fiber mesh was attached onto the surface of collagen sponges. Since collagen sponge has large pores that would allow fibroblast migration towards the keratinocyte layer the bilayer fiber mesh was introduced to provide a separation between the two cells types (**Figure 3.3C**). This layer is less porous for keratinocyte culture. Fibroblasts were therefore seeded on the collagen sponge and keratinocytes on the opposite side of the fiber mesh thus physically separating the two cell types but allowing exchange of chemicals across the barrier.

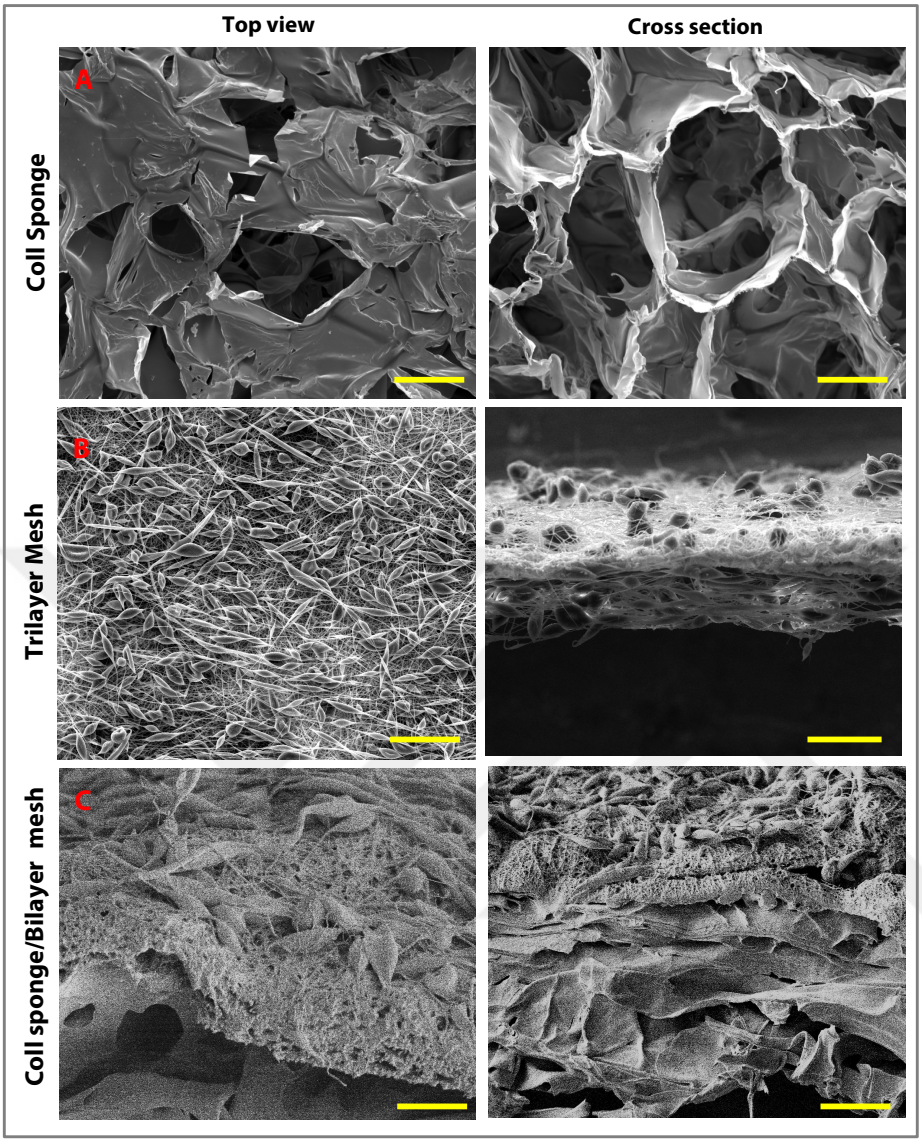

Figure 3.3 Surface topography and vertical section of skin models A) Collagen sponges. A smooth skin layer with pores was formed (x100). The interconnected pores allow fibroblast ingrowth. B) PLA/PHBV/PLA electrospun fiber mesh. Sequential electrospinning results in microbeads. C) Collagen sponge/bilayer mesh. Fibroblasts seeded on the collagen sponge and keratinocytes on the opposite side of the fiber mesh to separate the cells while allowing exchange of chemicals (Scale bars 100 μm).

3.1.1.4 Mechanical properties of the scaffolds

Young's modulus (E) is calculated as the slope of the stress-strain curve (**Figure 2.4**). This is the Elastic Region of the plot for a viscoelastic material. The higher the slope, the stiffer is the material. This parameter is also called elastic modulus, because, the elongation of the material during this linear slope is elastic deformation allowing recoil to its original size. After the linear portion, the elongation observed is plastic deformation; complete recovery of the deformation is not possible (**Figure 2.4**). The other 2 parameters to describe the tensile properties of a material are the ultimate tensile strength (UTS) and the strain at UTS which shows the maximum elongation of the material.

All samples were prepared in size (5 mm x 20 mm) and thickness were measured by a micrometer. Stress-strain data from each sample was normalized before assessing the mechanical properties. Native human skin and DED were tested as positive controls. Statistics were analyzed compared to the native healthy human skin. No major differences were observed between unseeded dermis and cell seeded dermis (allograft) in terms of UTS (3.69 vs 5.67 MPa) and strain (0.70 vs 0.72) compared to natural human skin. In their dry state, trilayer electrospun mesh had approximately 70 times higher modulus (3.46 MPa vs 0.05) values compared to collagen sponges (3.47 MPa vs 0.05 MPa) (**Figure 3.4**). Young's Modulus of native human skin (10.91 MPa) was significantly higher than all the other scaffolds.

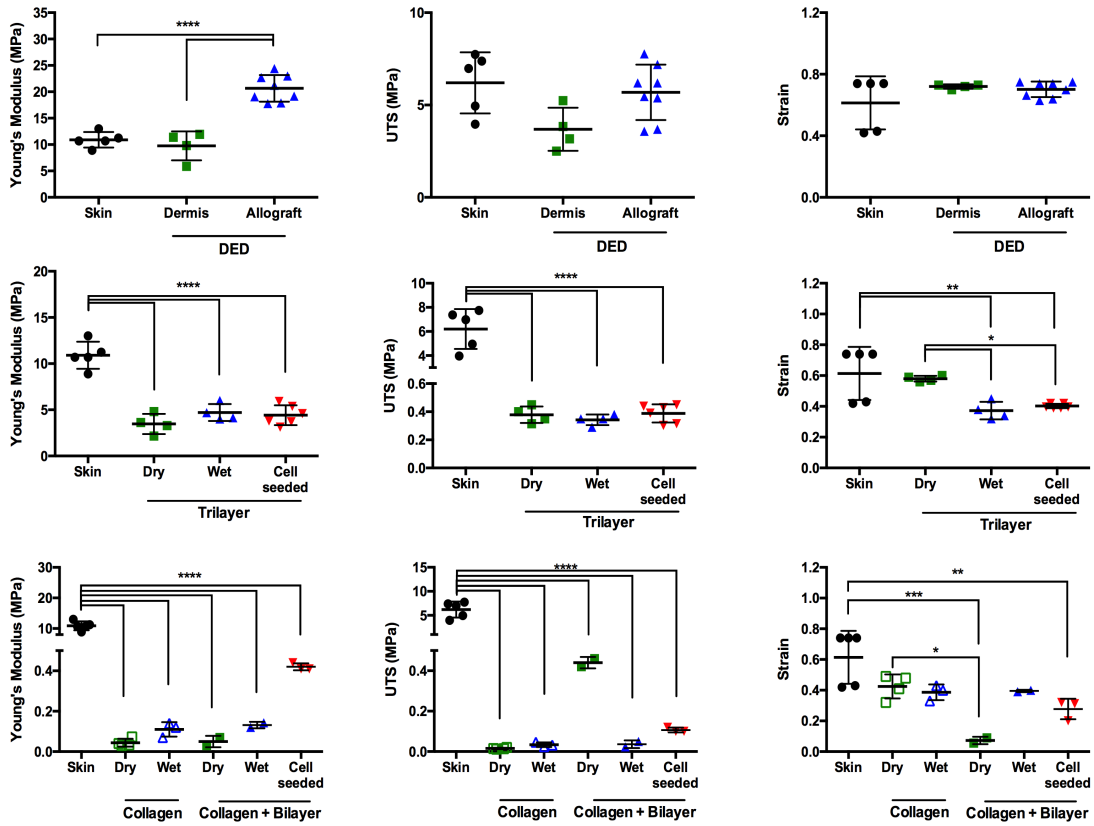

Figure 3.4 Mechanical properties of the scaffolds in their dry and wet state, unseeded and cell (keratinocytes and fibroblasts) seeded (incubation for 30 days) states. Error bars are 95% CI. The values in the y axis are given as mean (±SD) for Modulus, UTS and ultimate strain (ns $p > 0.05$, *$p \leq 0.05$, **$p \leq 0.01$, ***$p \leq 0.001$, ****$p \leq 0.0001$).

Collagen sponge had significantly lower modulus and UTS values compared to the other scaffolds in their wet and dry state. When wet, the strain values between the collagen sponge, coll/bilayer mesh and skin were non-significant. Cell seeding on dermis significantly increased the mechanical properties. On the other hand, cell seeding on trilayer mesh did not significantly change the mechanical properties when compared to their wet and dry states (**Table 3.1**).

Quantitive measurements of the mechanical characteristics of human skin reflect the skin structure (Alexander and Cook 1977). Consequently, an ideal tissue-engineered scaffold designed to act as a model skin should be mechanically comparable to the natural skin. Scaffold type (sponge, fibers or films), porosity, surface wettability and material types affect mechanical properties (Kumbar et al. 2008). The fast biodegrading rate and the low mechanical strength of the collagen scaffold are the crucial problems that limit the further use of this material. In line with these results and literature stating the disadvantages, collagen sponges were not tested further for skin tissue model. They were employed in *in vitro* testing when they were combined with the bilayer mesh only.

Table 3.1 Mechanical properties of the scaffolds designed as dermis layer [mean (±SD) values for UTS (Ultimate Tensile Strength), Strain and E (Young's modulus)] (ns $p > 0.05$, * $p \leq 0.05$, ** $p \leq 0.01$, *** $p \leq 0.001$, **** $p \leq 0.0001$).

Sample Type	**Dry state**			**Wet state**			**Cell seeded (30 days of incubation)**		
	E(MPa)	*UTS(MPa)*	*Strain*	*E(MPa)*	*UTS(MPa)*	*Strain*	*E(MPa)*	*UTS(MPa)*	*Strain*
Human skin	-	-	-	10.908	6.202	0.614	-	-	-
(SD)	-	-	-	(1.311)	(1.480)	(0.154)	-	-	-
De-epidermized dermis (DED)	-	-	-	9.750^{****}	3.687^{ns}	0.720^{ns}	20.657^{****}	5.686^{ns}	0.701^{ns}
(SD)	-	-	-	(2.369)	(1.013)	(0.012)	(2.360)	(1.402)	(0.047)
Trilayer mesh	3.467^{****}	0.378^{****}	0.576^{****}	4.813^{****}	0.360^{****}	0.383^{**}	5.418^{****}	0.388^{****}	0.402^{**}
(SD)	(0.945)	(0.049)	(0.017)	(0.789)	(0.032)	(0.049)	(0.975)	(0.059)	(0.012)
Collagen sponge	0.047^{****}	0.015^{****}	0.306^{ns}	0.112^{****}	0.034^{****}	0.38^{ns}	-	-	-
(SD)	(0.017)	(0.003)	(0.021)	(0.029)	(0.009)	(0.042)	-	-	-
Coll sponge/bilayer mesh	0.069^{****}	0.441^{****}	0.073^{ns}	0.131^{****}	0.036^{****}	0.395^{ns}	0.502^{****}	0.12^{****}	0.285^{**}
(SD)	(0.012)	(0.020)	(0.017)	(0.010)	(0.013)	(0.005)	(0.143)	(0.024)	(0.057)

3.1.2 *In vitro* studies

3.1.2.1 Histology

The simplest method of assessing histological changes was to use H&E staining (*Section 2.2.1.6*). This combination stains cell nuclei in purple, cytoplasm and connective tissue pink. **Figure 3.5** shows allograft, trilayer electrospun mesh and collagen sponge/bilayer fiber mesh morphology after incubation with keratinocytes and fibroblasts. Human skin was also used as a control. Fibroblasts were seeded on the dermis layer 10 days prior to the keratinocyte seeding. After 14 days of incubation with keratinocytes stratified squamous epithelium was formed. When these cells were seeded on the trilayer mesh, it is evident that fibroblasts and keratinocytes have migrated through the PLA mesh, and each side of the PHBV fiber mesh shows both cell types. PHBV acts as a basal membrane between two PLA fiber layers. After 7 days of culture with fibroblasts on one face of the PHBV and culture with keratinocytes on the opposite face, the cells remain segregated as can be seen in **Figure 3.5.** PHBV has been successful at both supporting cell attachment and keeping the two cell types separated for at least 14 days.

Darker color of dermis shows the fibroblasts located throughout the dermis and mostly under the basal membrane for all the scaffold types. After 14 days of incubation with keratinocytes stratified squamous epithelium was formed. The keratinocytes were well differentiated with a good keratin layer. The progression from nucleated cells in the stratum basale to flattened non-nucleated keratinocytes in the stratum corneum could clearly be seen. The basal keratinocytes were orientated in planar forms. Full

differentiation of the epidermal component was demonstrated with a pink eosin stained stratum corneum as per *in vivo* skin.

Dermal morphology and fibroblast penetration were better for the trilayer electrospun mesh scaffolds. On the other hand, the keratinized layer and the dermo-epidermal junction in the scaffolds are thicker than the allograft and the human skin appearances.

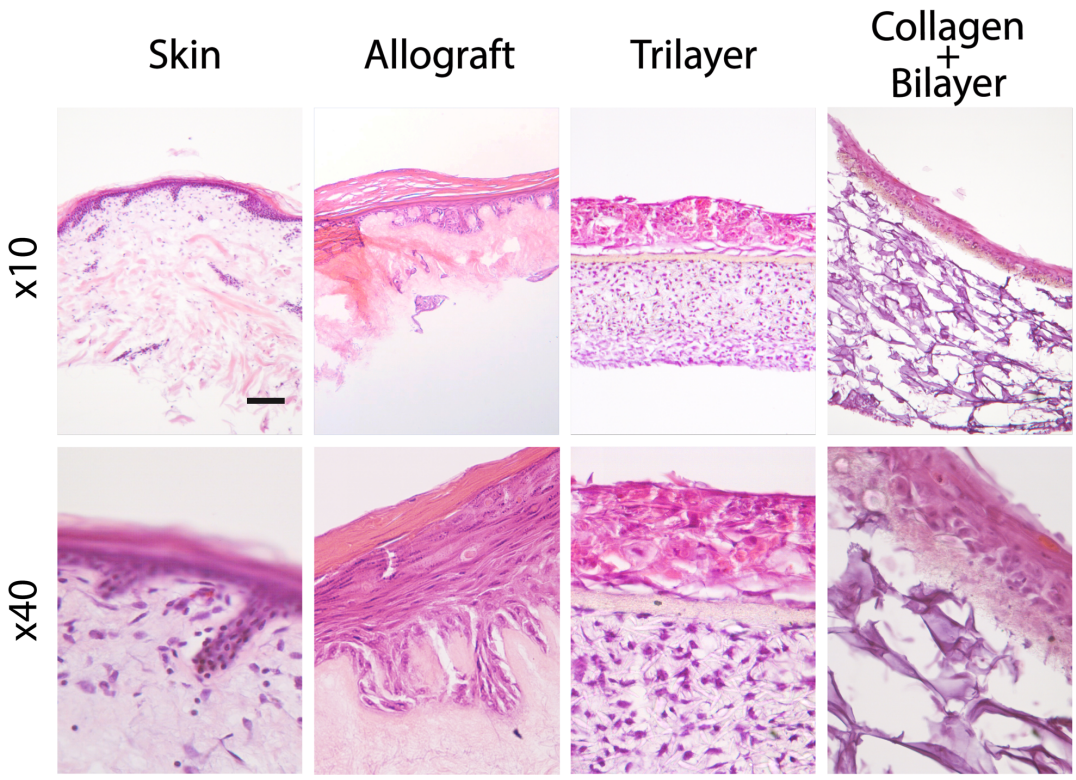

Figure 3.5 H&E staining of human skin, allografts, trilayer mesh and collagen sponge+bilayer mesh after 3 weeks of incubation with fibroblasts and keratinocytes. Sections with 10 µm thickness were cut with cryotome. Samples were incubated with fibroblasts for 10 days prior to the keratinocyte seeding. A thick epidermis and a basal layer of cells beneath epidermis was formed after 14 days of incubation with keratinocytes. Scale bar 0.1 mm.

3.1.2.2 Immunohistochemistry

3.1.2.2.1 Involucrin staining

As a marker of disordered keratinocyte differentiation, immunohistochemistry was performed for Involucrin. **Figure 3.6** shows the effect of Involucrin expression on skin, allografts, trilayer electrospun mesh and collagen sponge/bilayer fiber mesh after 3 weeks of incubation with fibroblasts and keratinocytes. Brown color throughout the entire epidermis shows the involucrin expression is confined to the stratum granulosum and the basal keratinocytes. The basal keratinocyte layer was firmly attached at the dermo-epidermal junction for all types of scaffolds and strong staining was observed in the upper epidermal strata.

3.1.2.2.1 Collagen IV staining

The basement membrane is made up mainly of collagen IV and the glycoprotein laminin, as well as heparan-sulphate proteoglycans (HSPGs) and nidogen/entactin. Coll IV is secreted from the dermal fibroblasts. The immunostaining shows that the fibroblasts had been able to produce coll IV after 3 weeks of incubation prior to the keratinocyte seeding. Collagen IV staining covers all of the dermal compartment of all types of samples (**Figure 3.7**). For the trilayer mesh, Intense regions are also present at the top and bottom faces of the PHBV layer, but not at the center. Apart from the PHBV layer, the dermal layer is showing the brown color where the fibroblasts are located.

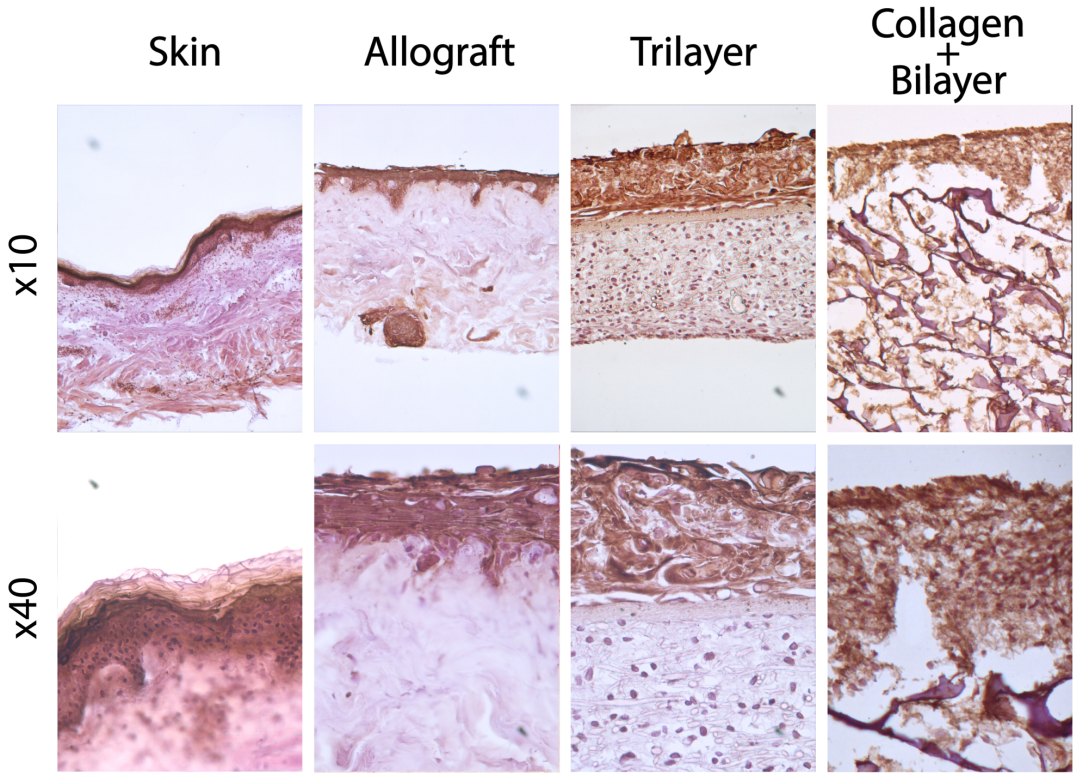

Figure 3.6 Involucrin staining showing the differentiated keratinocytes on the epidermal layer of human skin, allografts, trilayer mesh and collagen sponge/bilayer fiber mesh after 3 weeks of incubation with fibroblasts and keratinocytes. Sections with 10 µm thickness were cut with cryotome. Samples were incubated with fibroblasts for 10 days prior to the keratinocyte seeding. A thick epidermis and a basal layer of cells beneath epidermis was formed after 14 days of incubation with keratinocytes. Brown color on the epidermis shows the involucrin produced by the keratinocytes. Scale bars 0.1 mm.

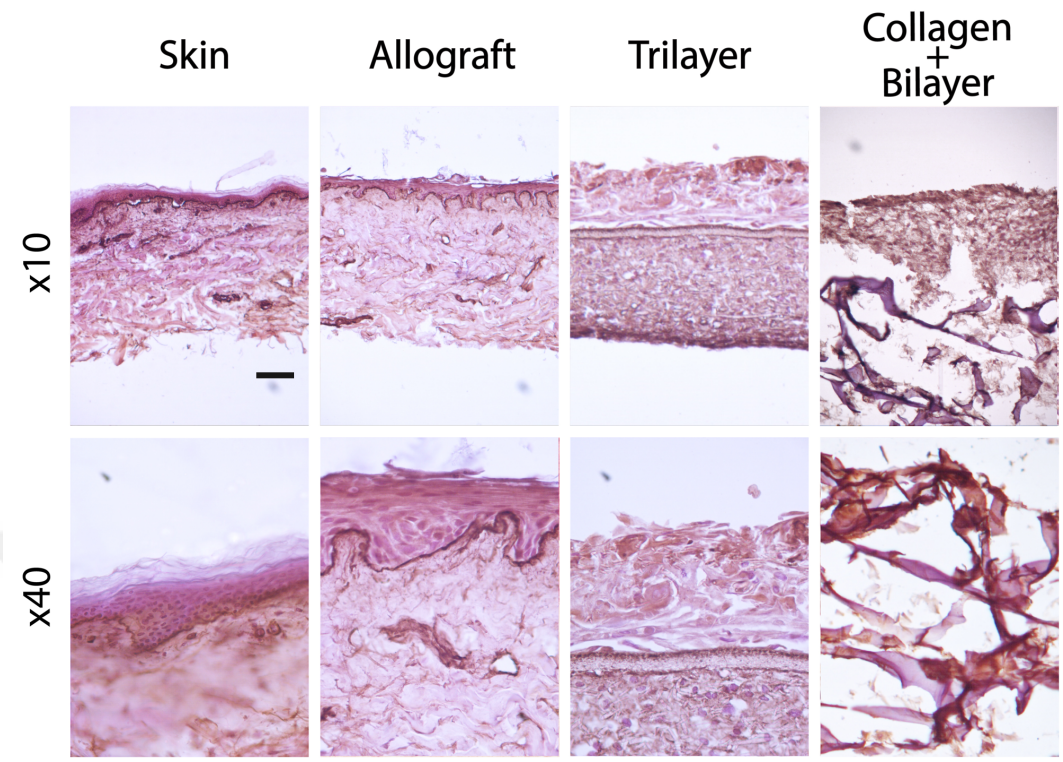

Figure 3.7 Collagen IV staining showing the collagen IV produced by the fibroblasts on the dermal layer of human skin, allografts, trilayer mesh and collagen sponge/bilayer fiber mesh after 3 weeks of incubation with fibroblasts and keratinocytes. Sections with 10 µm thickness were cut with cryotome. Samples were incubated with fibroblasts for 10 days prior to the keratinocyte seeding. A thick epidermis and a basal layer of cells beneath epidermis was formed after 14 days of incubation with keratinocytes. Brown color on the dermis shows the coll IV produced by the fibroblasts. Scale bars 0.1 mm.

3.2 Subcutaneous Tissue of the Skin Model

As the subcutaneous layer for the skin substitute, a gelatin/hyaluronic acid based UV crosslinkable hydrogel that allows effective incorporation of stem cells was synthesized and characterized. This hydrogel was synthesized from methacrylated gelatin and methacrylated hyaluronic acid polymers where methacrylate groups were used for crosslinking with exposure to UV and designed to deliver cells to stimulate new blood vessel formation *in vivo*.

3.2.1 Characterization of the hydrogels

Hydrogel characterization was studied in terms of methacrylation degree, morphology, mechanical properties, transparency, swelling and degradation rate of the hydrogels.

3.2.1.1 Methacrylation of gelatin and hyaluronic acid

The degree of methacrylation of gelatin was calculated from the peaks of the proton NMR at 7.4 ppm for the aromatic amino acid residues of gelatin, and the peaks at 5.5 ppm and 5.7 ppm for the double bonds of the methacrylate groups (Nichol et al., 2010; Shin, Olsen and Khademhosseini, 2012) (**Figure 3.8**). The methacrylation reaction of hyaluronic acid showing the methacrylate peaks at 6.1, 5.6, and 1.85 ppm (**Figure 3.8B**) presents a proton NMR spectrum characteristic for this reaction (Messager et al. 2013). The degree of methacrylation was calculated from the relative integrated intensities of the methacrylate protons and methyl protons in hyaluronic acid (peak at 1.9 ppm). NMR results demonstrated that gelatin was 63% methacrylated and hyaluronic acid 25% methacrylated (**Figures 3.8A and B**). Thus, the efficiency of gelatin methacrylation was about 2.5-fold higher than that of hyaluronic acid.

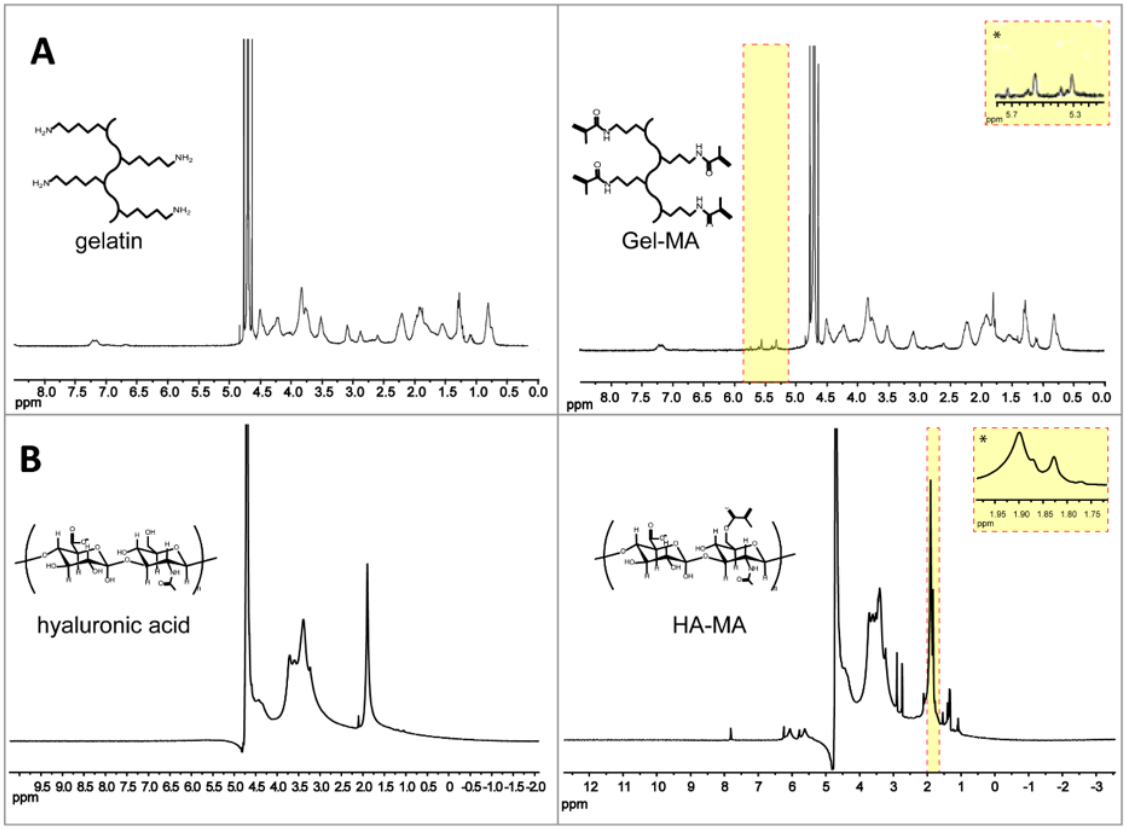

Figure 3.8 ^{1}H NMR spectra of gelatin, hyaluronic acid and their methacrylamide forms prepared in D_2O at room temperature. A) ^{1}H NMR spectra of gelatin (left) and gelatin methacrylamide (Gel-MA) (right). The expanded region in Gel-MA between 5 and 6 ppm (shown with an asterix) is presented as insets which show the methacrylation of gelatin. B) ^{1}H NMR spectra of hyaluronic acid (left) and hyaluronic acid methacrylamide (right). The expanded region between 1.5 and 2 ppm (shown with an asterix) represents the increase in the peaks because of methacrylation as shown at the inset.

Hydrogel properties are affected by types of polymer, their concentration, ratios if they are blends and the degree of methacrylation and crosslinking. The reaction conditions such as temperature, solvent content, the initiator concentration and duration of UV exposure affect the physical and mechanical properties of the hydrogel by changing the degree of methacrylation and crosslinking of hyaluronic acid and gelatin. A high degree of methacrylation was reported when the reaction was carried out at low temperatures or in the presence of solvent (DMF). It was reported that the methacrylation degree of hyaluronic acid was 14% at 45^{o}C but 23% at a lower temperature (25^{o}C) (Dantzer and Braye 2001). Keeping the temperature constant and increasing the DMF concentration to 50% resulted in 90% methacrylation before reaching the solubility limit of the hyaluronic acid (Hasirci et al. 2016).

3.2.1.2 Morphology of GelMA/HAMA hydrogels

Hydrogels were obtained after the methacrylated gelatin and hyaluronic acid solutions were mixed and crosslinked with UV (**Figure 3.9**). The GelMA and HAMA solutions were free flowing before UV exposure (**Figure 3.9A, left**), and gelled after crosslinking by exposure to UV (**Figure 3.9A, right**). The freezedried form of GelMA/HAMA hydrogels are shown to be highly porous (**Figure 3.9B**). The average pore size was 120 ± 76 μm and had a porosity of 79% (n=75). Such pore size and the porosity are very suitable for tissue engineering applications.

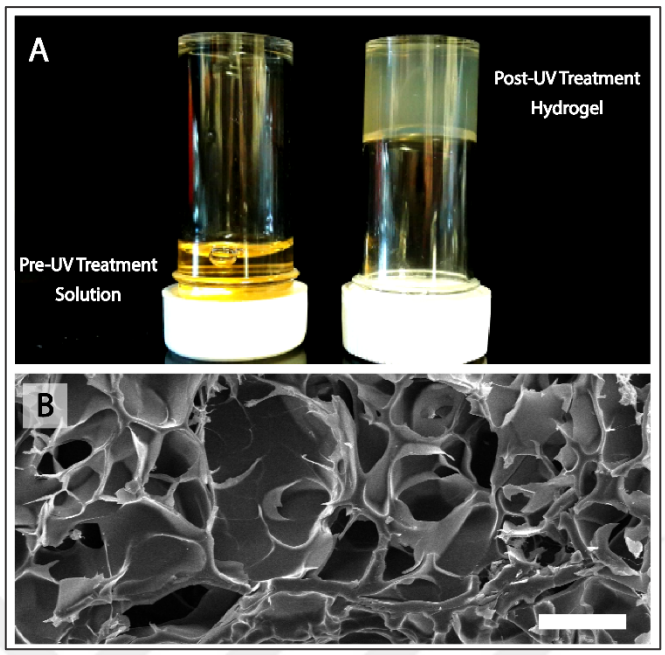

Figure 3.9 Characterization of GelMA/HAMA hydrogels. A) The gel solution before (left) and after (right) 40 s of UV treatment, B) SEM of the vertical cross-section of the hydrogels (scale bar: 100 μm).

3.2.1.3 Water contact angle measurements

Wettability was tested to study the interaction between the hydrogel surface and fluids. Static water contact angles were measured in order to evaluate the wettability of the hydrogel as a result from UV curing. The contact angle of the GelMA/HAMA hydrogel was 13.79±1.57^{o} which was in accordance with the literature. The contact angles of GelMA hydrogels were 10^{o} and 12^{o}, respectively (Aubin et al. 2010; Tan et al. 2013). As a result, high hydrophilicity might increase the diffusivity thus compensate the effect on water and nutrient entry into the hydrogel. Therefore, this amount of hydrophilicity would not affect the cell viability.

3.2.1.4 Transparency

The transmittance analysis of cell-free and ADSC loaded GelMA/HAMA hydrogels showed that the unloaded hydrogels had a light transmittance of 85% (**Fig. 3.10A and B**) and upon loading with $1x10^6$ ADSCs, the transmittance did not change significantly. However, the transmittance decreased to 56% when 2 million cells were loaded. All these samples transmitted UV to a very low degree (320-400 nm UVA, and 290-320 nm, UVB) which made them inherently protective against UV radiation.

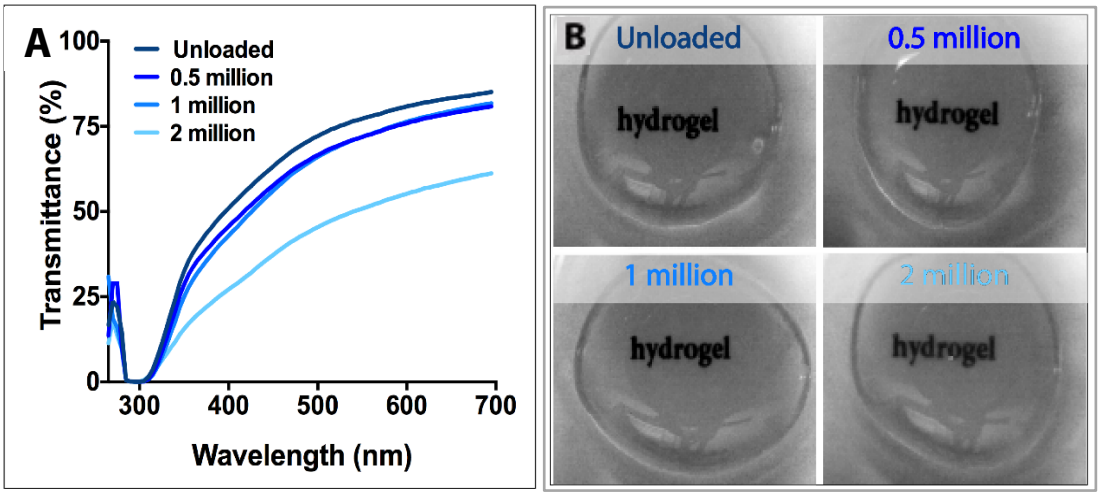

Figure 3.10 Transparency of the unloaded and stem cell loaded hydrogels. A) Up to 2 million cells in the hydrogel presented satisfactory level of transparency of the gel. The hydrogel does not transmit light in the ultraviolet region making it inherently UV protective. B) A decrease in the transparency of the hydrogels was observed upon the number of cells. Opacity increases with the loading of 2 million cells.

In case of wound dressing applications, it is important to have a therapeutic device that is transparent when wet and thus allows the clinicians follow up of the healing process without removing the dressing (Sherman and Kennedy 1998).

3.2.1.5 Manual handling of the hydrogel and its mechanical properties

A round 1 cm diameter piece of the GelMA/HAMA hydrogel could easily be manipulated using surgical forceps without breaking and deformation showing that it was robust enough for handling (**Figure 3.11A**).

In compression mechanical testing, the hydrogels were stable until compression with a load of 12.86 ± 1.23 kPa (ultimate compressive stress) and had a modulus of 6.17 ± 2.05 kPa. A representative stress-strain curve of the GelMA/HAMA hydrogel presented in **Appendix A**. In the literature, GelMA hydrogels with GelMA concentration and degrees of methacrylation similar to that used in this study had a compressive modulus of about 10 kPa showing that our results are in line with previous published studies (Kinikoglu, Damour, and Hasirci 2015; Tsou et al. 2016). Also, these hydrogels proved easy to manipulate which will be important in their handling in the laboratory and in the clinic in future.

3.2.1.6 Swelling and *in situ* degradation

Hydrogels are crosslinked networks of hydrophilic polymers that can swell in water to capture many times their original mass. The hydrogels prepared in this study reached equilibrium swelling after about 48 h with the degree of swelling (DS) of 227% ± 11 (n=5).

The weight loss over time was used as a measure of degradation. Hydrogels were incubated in PBS and at certain time points the gels were removed from the PBS,

freeze-dried and weighed. Degradation was slow in the first week and about 90% of the weight was remained and in the second and third weeks the degradation rate was significantly increased and samples lost about 60% of their initial weights (**Figure 3.11B**).

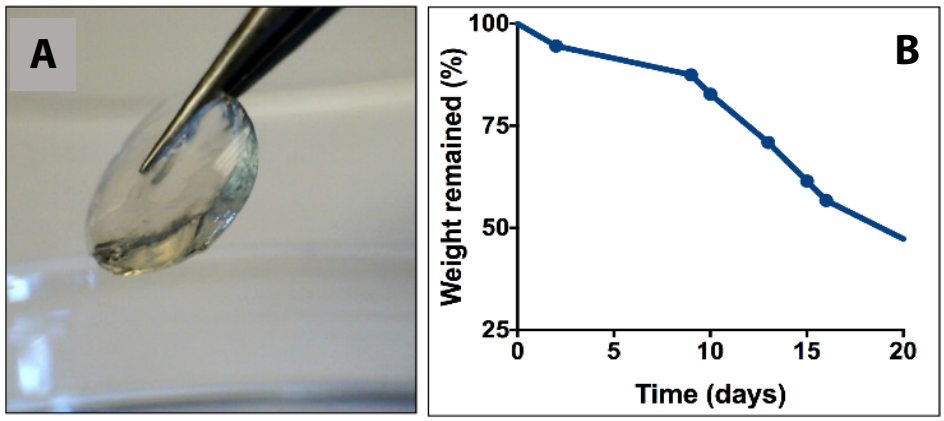

Figure 3.11 Handling and degradation of the hydrogels A) Photograph showing ease of handling and mechanical stability of the GelMA/HAMA hydrogel with surgical forceps, B) *In situ* weight loss o the hydrogel during 21 days of incubation.

Studies with the commercial dermal product Integra showed that it takes at least 3 weeks or more for new blood vessels to grow into the product from the underlying wound (Bhargava et al. 2008; Oudshoorn et al. 2007). Therefore, this rate of hydrogel degradation will be appropriate for it acting as a dermal substitute and also a biological wound dressing for stimulating chronic wounds to heal.

3.2.2 *In vitro* studies

3.2.2.1 Characterization of adipose derived stem cells (ADSCs)

The expression of surface markers of the cells isolated from adipose tissue were studied in order to verify their mesenchymal stem cell nature. Passages 0 and 5 were used for characterization. Isolated cells were expanded in tissue culture flask in growth media.

They were analyzed using flow cytometry for the expression of surface markers CD90, CD45 and CD31. CD90 (Thy-1) is a surface protein responsible for cell-cell and cell-ECM interactions (Deans and Moseley 2000). Hematopoetic CD45 (Leukocyte common antigen) and endothelial CD31 (PECAM) markers are absent on ADSCs and are used as negative markers (Crisan et al. 2008). In order to detect any nonspecific interaction between the cell surface, cells were also incubated with the IgG1κ isotype control and the fluorescence intensity was compared with the unstained cells (**Figure 3.12**).

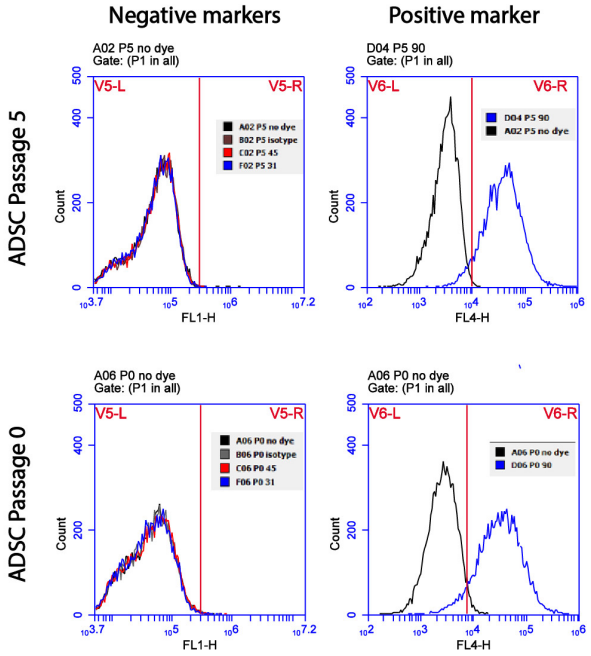

ADSC Passage 5	Negative quadrant	Std. Dev.	Positive quadrant	Std. Dev.
No dye	99.95%	4.0 10^{-4}	0.05%	4.0 10^{-4}
Isotype control	99.97%	0.0 10^{-4}	0.03%	0. 10^{-4}
CD45	99.97%	1.7 10^{-4}	0.03%	1.6 10^{-4}
CD31	99.98%	1.6 10^{-4}	0.02%	0.5 10^{-4}
CD90	6,54%	44.5 10-4	94.81%	26.0 10^{-4}

ADSC Passage 0	Negative quadrant	Std. Dev.	Positive quadrant	Std. Dev.
No dye	99.86%	3.3 10^{-4}	0.14%	3.4 10^{-4}
Isotype control	99.86%	8.4 10^{-4}	0.14%	8.4 10^{-4}
CD45	99.86%	2.4 10^{-4}	0.12%	4.2 10^{-4}
CD31	99.86%	7.1 10^{-4}	0.11%	8.3 10^{-4}
CD90	5,19%	26.0 10^{-4}	93.47%	44.5 10^{-4}

Figure 3.12 ADSC phenotype characterization. P0 and P5 were tested for antigen expression. Representative example of antigen expression of human ADSC by flow cytometry analysis. Expression of each antigen is also indicated as percentage.

Nonspecific binding was not detected as the fluorescence intensity of cells stained with isotype control highly overlapped (over 99.8% for both passages). Stem cells were negative (<0.12%) for the negative markers CD45 (0.12%for p0 and 0.03% for p5) and CD31 (0.11% for p0 and 0.02% for p5), while they displayed positive expression (>93%) for the mesenchymal marker CD90 (93.47% for p0 and 94.81% for p5). The expression profiles were consistent with other studies reporting ADSCs positive for CD90 but negative for CD31 and CD45 (De Toni et al. 2011).

3.2.2.2 Viability and DNA quantification of ADSCs in the hydrogels

Viability of stem cells was determined with Live-Dead Assay. Live cell (green) coverage was 99, 97, 94 and 96% on days 3, 7, 14 and 21, respectively (**Figure 3.13A**) showing that more than 90% of the cells were alive, able to elongate and move freely in the hydrogels for at least 3 weeks.

The proliferation and DNA amount of ADSCs in of *in vitro* culture was determined by quantification of the DNA with Picogreen staining (**Figure 3.13B**). Same amount of cells ($1x10^6$) were seeded on TCPS and the hydrogels. It was observed that ADSCs in the hydrogels proliferated at a rate similar to that in 2D culture (TCPS). There was a gradual increase in the amount of DNA over the 21 days of culture both in the GelMA/HAMA hydrogels and in TCPS showing that the 3D environment is very suitable for ADSC growth.

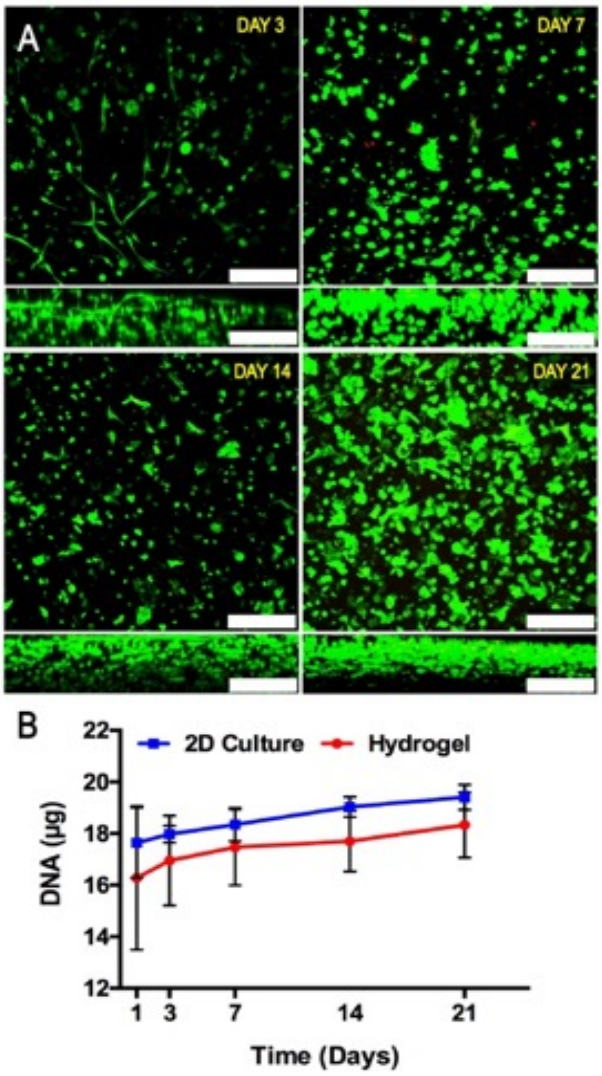

Figure 3.13 Live-Dead analysis and DNA quantification of ADSC in the hydrogels over 3 week period. A) Live-Dead analysis of ADSCs using CLSM, on the hydrogels at different time points (3-21 days). Hydrogels stained with calcein AM (green) for live and ethidium homodimer-1 (red) for dead cells (Magnification x10). The z-stacks show that the penetration of the ADSCs into the hydrogel is almost homogenous (Scale bar: 250 µm). B) Quantification of DNA content by staining with Picogreen (Anova One-Way Tukey test, p: 0.014).

GelMA and HAMA undergo photocrosslinking to form the hydrogel used. In this study, the Live-Dead Assay shows that more than 90% of ADSCs were alive for 21 days and the DNA count showed no negative effect of UV exposure on cell proliferation. There is a decrease compared to the control TCPS, which arises from the fact that cell growth in a hydrogel is less than on a TCPS surface.

According to the literature, low duration of UV exposures at 365 nm are accepted and found to be safe in terms of cell damage (Klotz et al. 2016; Yue et al. 2015; Nichol et al. 2010). Also, Masuma et al., 2013 studied toxicological effects of different wavelengths (250, 270, 290, and 310 nm) and doses of UV irradiation on cell viability, DNA structure, and DNA damage repair. Among these 4 wavelengths, the proportion of cyclobutane pyrimidine dimer (CPD) formation, which induces mutations, was highest at 250 nm and lowest at 310 nm. These show both cell viability and DNA damage (as shown by CPD formation) are very low, indicating that these conditions are safe (Masuma et al. 2013).

3.2.2.3 ADSC morphology in the hydrogels

After 3 days in culture, ADSCs entrapped in the GelMA/HAMA hydrogels started to spread and form protrusions within the hydrogels (**Figure 3.14A**). On Day 14, they were more elongated, and by Day 21 they formed interconnected networks among the neighboring cells.

Pore size and porosity of the hydrogels were measured from their SEM using NIH imageJ program. Average pore size increased from 130 ± 72 μm on Day 3 to 210 ± 98 μm on Day 21 (**Figure 3.14B**) indicating the degradation of the hydrogel.

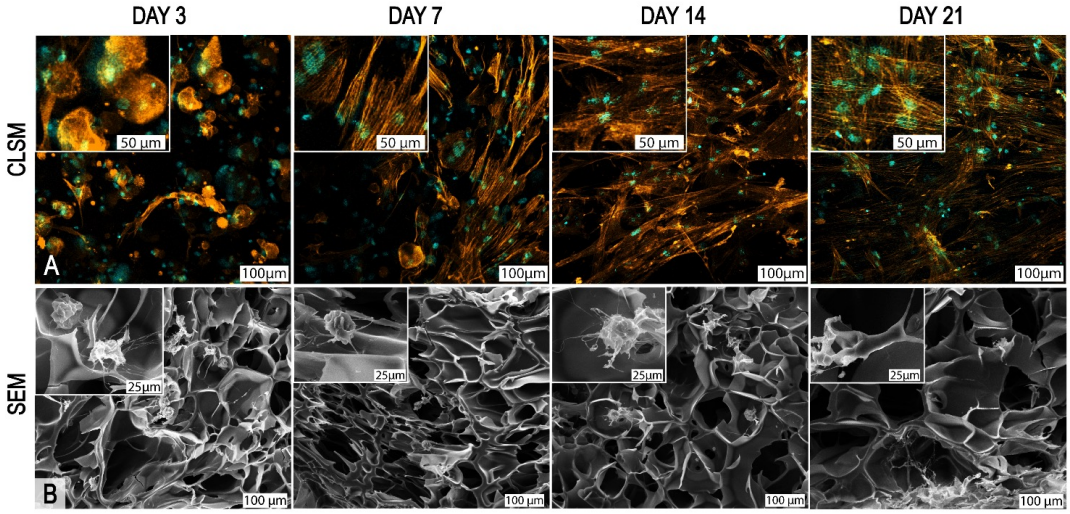

Figure 3.14 Behavior of ADSCs in the hydrogels at different time points as studied with CLSM and SEM. A) CLSM images of ADSC loaded hydrogels. Orange (Alexa488, cytoskeleton) and cyan (Draq5, nucleus). Filopodia were observed starting from Day 7 (Magnification x20). Inset micrographs show that the cells change from spherical to spindle like morphology. B) SEM micrographs show the cross section of ADSC loaded hydrogels. Individual cells could be seen starting from Day 7. Insets show the change in cell morphology at different time points.

3.2.2.4 Organization of endothelial cells into a 3D prevascular network

Endothelial cells, co-cultured with ADSCs organized into a prevascular network *in vitro* in 21 days. HUVECs stained positive for the endothelial marker CD31 while positive staining was not observed in control samples seeded only with ADSCs (**Figure 3.15A**). The formation of the prevascular network was promoted by seeding HUVEC: ADSC 5:95 ratio. **Figure 3.15B** shows the cells are connected to each other and form a 3D prevascular network of endothelial cells (stained green).

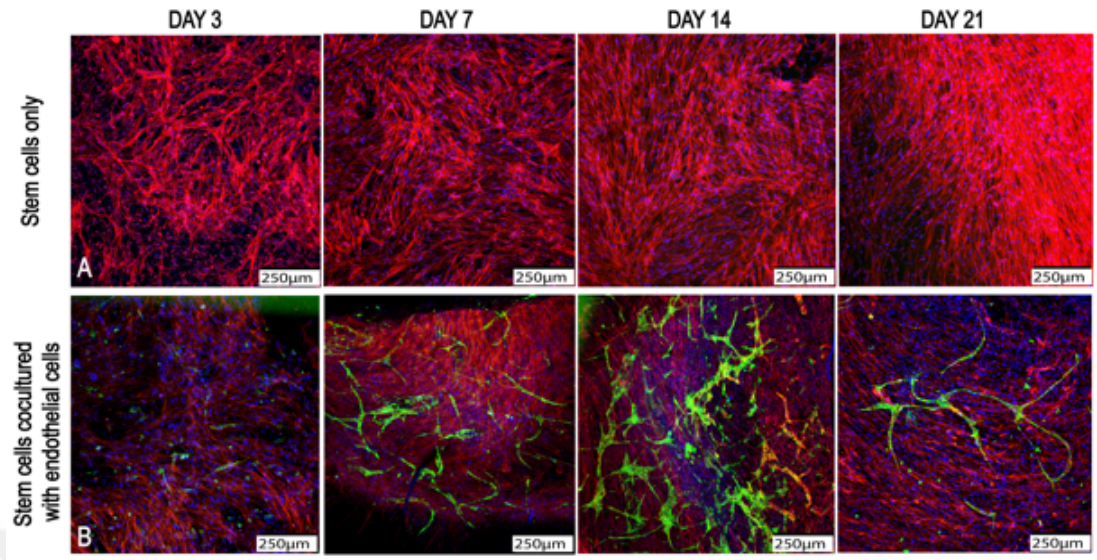

Figure 3.15 Formation of a prevascular network in the hydrogels during 3 weeks of incubation. A) CLSM images of ADSC loaded hydrogels were used as controls. Stains were cytoskeleton (red, AlexaFluor532) and nucleus (blue, To-pro-3). ADSCs are homogenously distributed in the hydrogel. B) CLSM images of HUVEC and ADSC co-cultured in hydrogels. The additional stain is for endothelial cells (green, CD31). After 3 days of co-culture, endothelial cells were round and separated throughout the hydrogel. The endothelial cells organized into elongated, vessel-like structures by days 14 and 21 (x10).

The endothelial cells showed organized, elongated, vessel-like structures after Day 7. This finding is a strong indication that in vitro prevascularization is a promising strategy to improve implant vascularization in skin tissue engineering.

In designing the cell based hydrogel dressing to stimulate blood vessel formation it is important to consider cell behavior and morphology, how long they need to be in place and the fate of the hydrogel in the long term.

Adipose derived stem cells secrete a wide variety of pro-angiogenic factors such as vascular endothelial growth factor (VEGF), fibroblast growth factor 2 (FGF-2), and interleukin-6 (IL-6) that are influential at different steps of angiogenesis (Jiang, Mao and Gao 2015; Camci-Unal et al. 2013). Co-culture of the endothelial cells (HUVEC) with the stem cells promoted the formation of tubular like structures which shows the *in vitro* pre-vascularization has occurred within the hydrogels.

3.2.3 *Ex ovo* studies

3.2.3.1 Ex ovo degradation

GelMA/HAMA hydrogels were placed onto chorioallantoic membrane of Day 8 chick embryos as mentioned in Section 2.2.2.6.4. Decrease in the hydrogel size was measured at different time points as a measure of hydrogel degradation. Degradation of the hydrogels were quantified by taking light microscope images of the CAM between Days 10 and 14 as shown in **Figure 3.16A.** The hydrogels lost their 30% of their surface area in 4 days with respect to their initial counterparts (**Figure 3.16B**). The *ex ovo* degradation rate was higher than the *in situ* conditions showing the enzymatic activity surpasses hydrolytical degradation.

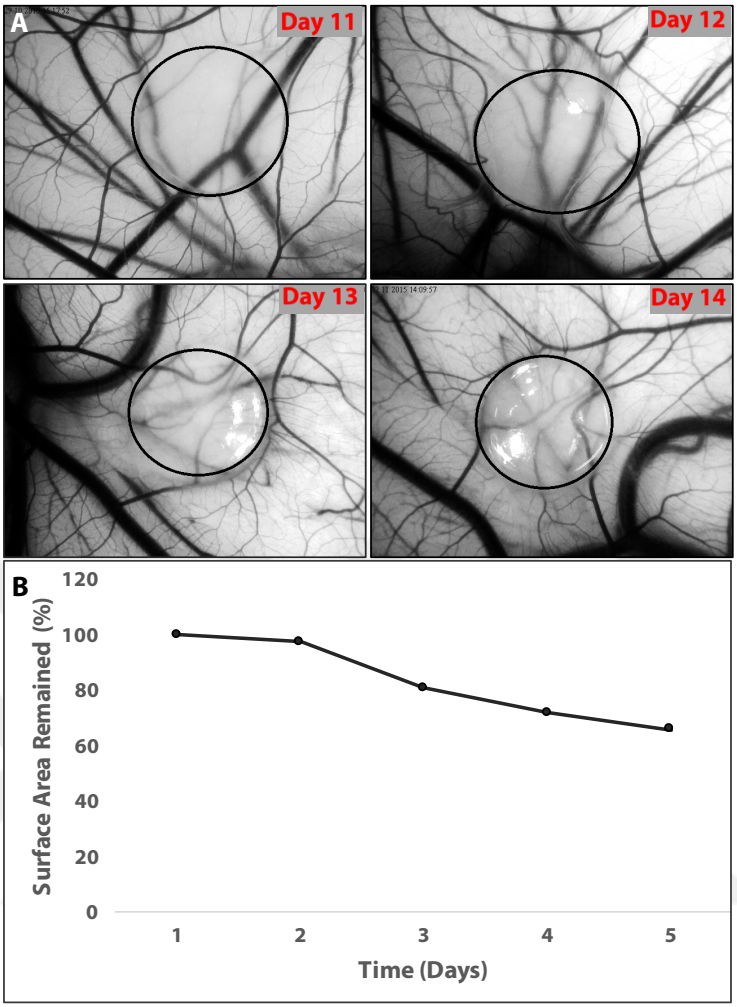

Figure 3.16 *Ex ovo* degradation of the GelMA/HAMA hydrogels. A) Stereomicroscopic images of the hydrogels which were incubated on chick embryo CAM (day 10-14). Circles indicating the hydrogel edges. B) The change in hydrogel area. The percent area was measured and analyzed with Image J. The hydrogels lost their 30% of their surface area in 4 days.

3.2.3.2 The angiogenic potential of the GelMA/HAMA hydrogels

The sprouting blood vessel-like tubular structures observed in the chick aortic ring assay were identified as endothelial cells as they stained positively with the endothelial cell marker Isolectin B4 (**Figure 3.17A**). A significant increase was observed in the length of the tubular sprouts when co-cultured with ADSC loaded hydrogels whereas the unloaded hydrogels did not present any such structures (**Figure 3.17B**). Also, an effective cell seeding density for ADSCs to increase endothelial cell sprouts was found to be between $5x10^5$ - $1x10^6$ (**Figure 3.17C**).

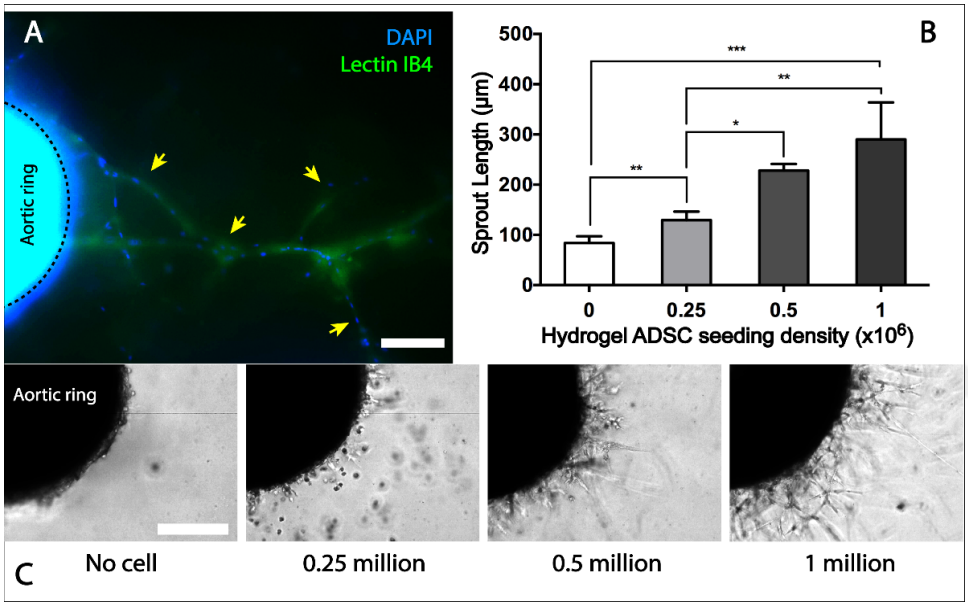

Figure 3.17 ADSC loaded hydrogels were co-cultured with chick aortic arches to evaluate endothelial cell proliferation and sprouting on day 5 of culture. A) Endothelial cell sprouts as observed with epifluorescence microscopy. Lectin IB4 positive endothelial cells are stained green, nuclear components stained blue (DAPI). Arrows show endothelial cell sprouts. B) The change in the length of endothelial sprouts with

the seeding density of ADSCs. C) Sprout length measurements used in the calculation of data for Figure 6B (scale bars represent 250 μm).

The CAM assay clearly demonstrated newly growing blood vessels towards hydrogels loaded with ADSC or VEGF where unloaded hydrogels served as controls (**Figure 3.18A**). The total number and length of blood vessels growing on the CAM tissue adjacent to the VEGF loaded and ADSC loaded hydrogel were significantly higher compared to unloaded ones. Also, the vasculogenic index (number of vessels growing towards the gel in a spoke-wheel pattern) was highest for VEGF loaded hydrogels and ADSC loaded hydrogels was the second highest with unloaded hydrogels being the lowest (**Figure 3.18B**).

This experiment shows that the GelMA/HAMA hydrogels themselves had no effect on angiogenesis but when loaded with ADSC they increased the angiogenic response, however, ADSCs were less effective than VEGF (used as a positive control here) (**Figure 3.18**).

Currently the vasculogenic potential of tissue engineered materials are mainly evaluated by in vivo studies which do not allow direct visualization of the blood vessels, besides the materials are expensive and the process is time consuming. The *ex ovo* CAM assay used in this study allows direct visualization of the newly forming vessels, is relatively rapid (2 weeks), and inexpensive. Also, this method can potentially be used as a rapid, simple and low cost screening tool to test the initial tissue response to biomaterials, as a pre *in vivo* method (Xiao et al. 2011).

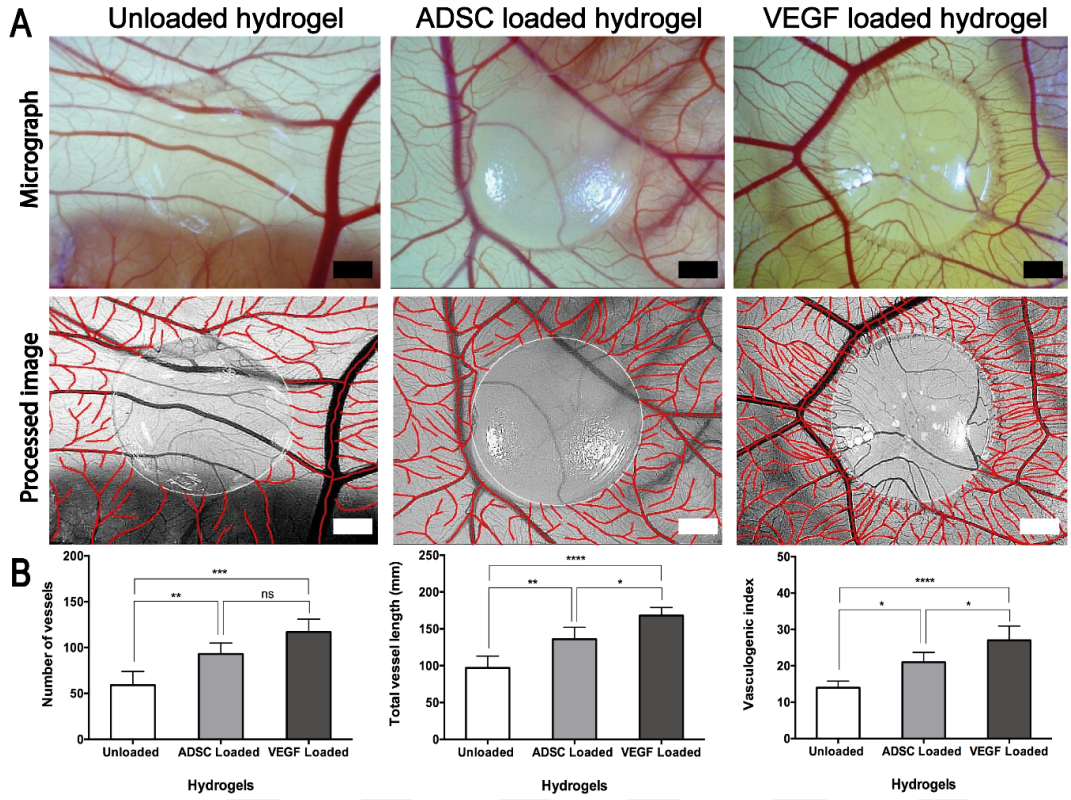

Figure 3.18 Evaluation of the angiogenic properties of the hydrogels in the chick chorioallantoic membrane (CAM) assay. A) Micrographs (upper row) and semi-automatic processed images (lower row) of the hydrogel, hydrogel containing ADSCs and hydrogel containing VEGF (positive control), taken on day 14 of embryonic development. B) The change in total number of vessels, total vessel length and vascularisation index of ADSC and VEGF loaded hydrogels calculated from processed images ($p<0.005$, $n_{unloaded}=5$, $n_{adsc\ loaded}=4$, $n_{VEGF\ loaded}=5$, One-way ANOVA, pairwise comparison Tukey's post-hoc test, *: $p<0.05$, **: $p<0.01$, ***: $p<0.005$, ****: $p<0.001$, ns: nonsignificant). Scale bars 2 mm.

3.2.3.3 Histological evaluation of angiogenesis and initial *in vivo* tissue response to hydrogels

Histological and immunohistological evaluation of normal CAM structure on Day 14 is shown in **Figure 3.19A**. Immunohistological study showed an increase in α-SMA positive blood vessels in CAM tissue with the VEGF loaded hydrogels compared to the unloaded hydrogels (**Figure 3.19B**). Stem cell loaded hydrogels had moderately increased the number of blood vessels.

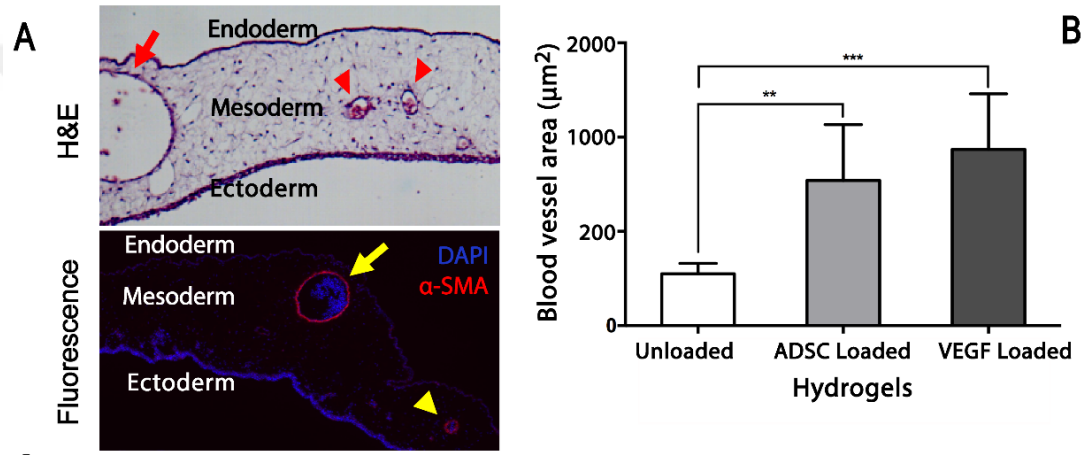

Figure 3.19 Histological and immunohistological evaluation of angiogenic properties of GelMA/HAMA hydrogels on CAM on day 14. A) Normal appearance of CAM structure on haematoxylin & eosin (H&E) staining and fluorescence staining of CAM vessels with alpha-smooth muscle actin (α-SMA) and 4,6-diamidino-2-phenylindole dihydrochloride (DAPI). Arrows and arrow heads indicate large and small blood vessels, respectively. B) Bar chart showing quantification of α-SMA positive blood vessel area (n=5) where ADSC loaded hydrogels had significantly increased vessel area compared to unloaded hydrogel (One-way ANOVA, pairwise comparison Tukey's post-hoc test, **: $p<0.01$, ***: $p<0.005$).

The H&E staining of the samples demonstrated almost no inflammation in the CAM underneath the hydrogel and VEGF loaded hydrogel whereas a mild inflammatory response together with infiltration of inflammatory cells in the perivascular area was observed consistently in the ADSC loaded hydrogel group (**Figure 3.20A**). Histologic examination of CAM-hydrogel complex has confirmed a significantly increased area of α-SMA positive blood vessels in CAM tissue under and adjacent to the VEGF loaded hydrogel compared to the hydrogel alone whereas ADSC loaded hydrogel was associated with a moderate increase in the number of blood vessels (**Figure 3.20B**).

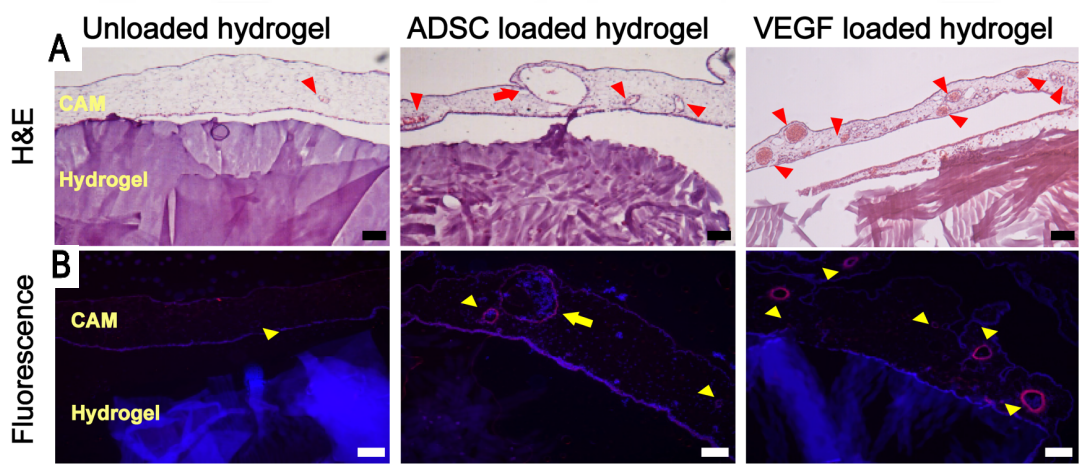

Figure 3.20 Histological evaluation of angiogenesis and initial *in vivo* tissue response to GelMA/HAMA hydrogels loaded with ADSC or VEGF A) Representative images from each group stained with H&E demonstrating no inflammation and slight perivascular inflammatory cell infiltration on CAM tissue adjacent to unloaded and VEGF loaded and ADSC loaded hydrogels, respectively. B) Fluorescent α-SMA stained micrographs showing blood vessel periphery in red color. Fluorescent images demonstrate α-SMA stained blood vessels on the CAM underneath ADSC loaded and VEGF loaded hydrogels (Scale bars: 100 μm).

The link between neo-angiogenesis and inflammation has long been established (Bender et al. 2011; Nowak-Sliwinska et al. 2010; Vargas et al. 2007; Richardson et al. 2005). It is important to rule out inflammation as a trigger in angiogenesis, especially when xenogenic cell sources are studied. The chick embryo lacks a mature immune system, especially in the first 11 days of the embryonic development which appears as an advantage of using the CAM assay (Lee et al. 2009; Nai-Chen et al. 2017). These histology results in this study proved that the hydrogels loaded with stem cells or VEGF did not cause any inflammation on the CAM tissue. There is no tissue integration was also observed during the study.

3.3 Drug delivery studies into the dermal skin model

3.3.1 Characterization of nanoparticles

3.3.1.1 Particle Morphology, Size and Size Distribution

PHBV nanoparticles were produced as mentioned in Section *2.2.3.1*. SEM micrographs of Retinyl palmitate (RP) and Rhodamine (Rho) loaded particles were similar in terms of average size and shape. The shape of these nanoparticles was spherical and the size was considerably uniform, as shown in **Figures 3.21A and B**. The average diameters of the RP and Rho loaded particles were in the range of 190-900 nm, and 70-450 nm, respectively (**Table 3.2**). CLSM was used to determine the fluorescence intensity Rhodamine where red color represents Rhodamine (**Figure 3.21C**).

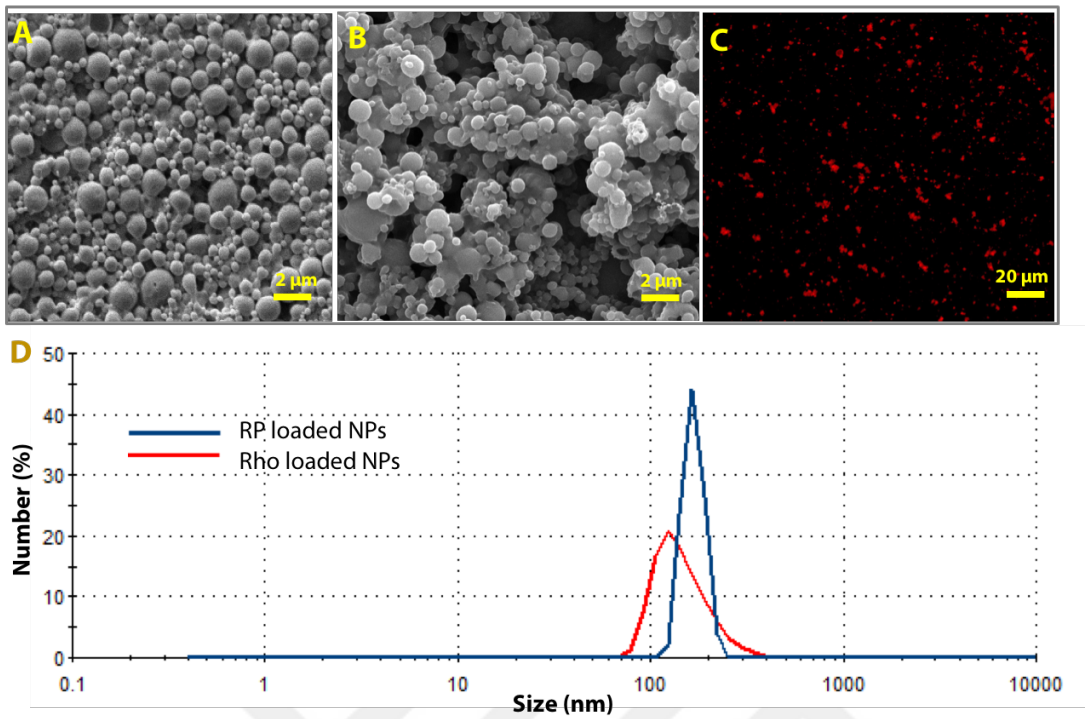

Figure 3.21 Characterization of RP and Rho loaded PHBV nanoparticles. A) SEM micrograph of the RP loaded, and B) Rho loaded particles. Magnification 20,000x. Scale bar: 2 µm. B) CLSM microscopy of the Rho loaded particles. Red color represents Rhodamine (x40). Scale bar: 20 µm C) Size distribution of the RP and Rho loaded nanoparticles (n=5).

In this study, all the particles were smaller than 3 µm (**Figure 3.21D**) in all formulations and this range is suitable for transdermal penetration. The particle size should be smaller than 500 nm for penetration into the cells, and 85% of our particles were in this range indicating that the all particles could penetrate the skin and a large fraction is suitable for endocytosis (Eke et al., 2014).

3.3.1.2 Loading and Encapsulation Efficiency (EE) for RP and Rho

EE and loading of RP in PHBV nanoparticles determined using UV-Vis spectrophotometry as 18.5% and 11.5%, respectively. These values for Rho were 54% and 42% (**Table 3.2**).

Table 3.2 Sizes, encapsulation efficiency and loading of drugs in nanoparticles.

Sample / Property	Unloaded	RP loaded	Rho loaded
Mean Diameter, nm	206.5 ± 22.1	251.7 ± 53.8	213.8 ± 49.7
PDI	0.2 ± 0.1	0.3 ± 0.1	0.3 ± 0.1
Size range, nm	184 - 228	198 - 306	144 - 262
Detection method	-	UV-Vis spectrophotometry; $\lambda_{max:}$ 326 nm	spectrofluorometer; λ_{ex}:528 nm, λ_{em}:551 nm
EE (%)	-	18.5 ± 0.2	54 ± 23%
Loading (%)	-	11.3 ± 0.1	42 ± 17%

The loading process of hydrophobic drugs in hydrophobic particles is reported to involve hydrophobic interactions between the drug and the polymeric chains of the particles (Lalatsa et al. 2012). In the literature, 3.4% RP loading in poly(l-lactic acid) (PLLA) nanoparticles, and 1% and 0.94% retinoic acid loading in PLGA and PHBV nanoparticles, respectively, were reported (Errico et al. 2009; Sane and Limtrakul 2011). The results obtained in this study are higher but are comparable to those in the literature and were used in the following release studies.

3.3.2 Release Kinetics

Drug in the surface of the nanoparticles is dissolved first and then diffuses out of the matrix. For this system, the rate of dissolution of drug within the matrix is faster than the diffusion rate of dissolved drug leaving the matrix. The equation, which describe the rate of the released drugs dispersed in an inert matrix system have been derived by Higuchi (Higuchi 1961).

The release behaviors of Rho and RP from the PHBV nanoparticles were plotted as 'percent released of drugs vs. time' (% vs. t) and also according to Higuchi Equation (M_t/M_∞ vs. t), where M_t is the amount of drugs released at a given time and M_∞ is the initial amount. The results are presented in **Figure 3.22**.

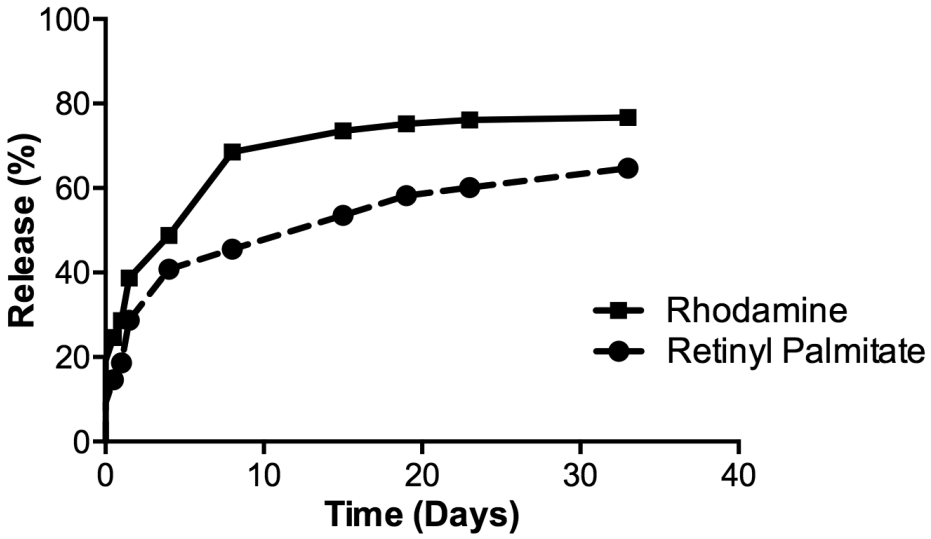

Figure 3.22 Release profiles of Rhodamine and Retinyl palmitate from the PHBV nanoparticles in PBS. Nanoparticles prepared by the current method released these drugs in a gradual manner.

Rho and RP have comparable release rates since they are both hydrophobic molecules. It was found that PHBV nanoparticles tended to release Rho faster than RP. For Rho, 65% of the content was released in the first week and release reached 78% in 35 days. For RP, nanoparticles released 40% of their content in the first week and on Day 35, the cumulative release was 60%. These burst release rates were acceptable since a high drug concentration in the beginning of treatment saturates the system with the burst and later low rate of release maintains the drug level.

3.3.3 Penetration of RP loaded nanoparticles into human skin

In the literature, RP has been shown to repair skin damaged by chronological aging or photoaging (Hyojung Kim et al. 2008) and it has been reported that photoaging of skin may be decreased by using a cream containing retinoid derivatives (Varani et al. 2000). Topical application of retinyl palmitate is a pragmatic strategy for loading the skin with vitamin A. Retinyl palmitate is reported to penetrate to the epidermis and dermis (Kim et al. 2018).

Human skin samples were used for in the penetration studies and RP loaded nanoparticles were used for being a derivative of vitamin A. They were applied on the upper layer of the skin samples. Epidermis was exposed to air and dermis was immersed in PBS. As expected, no RP could be detected in PBS. RP amount in the skin was determined as 1.2 ± 0.4% and 6.4 ± 1.5% in the presence and absence of stratum layers (when the stratum layer was removed), respectively. This was in accordance with the literature; for CdSe quantum dot-loaded PEG particles, penetration increased by 4-fold when the SKH-1 hairless mouse skin was abraded (Gopee et al. 2009). It is also reported that FITC-conjugated polystyrene nanospheres

dispersed in an aqueous gel were clearly visualized within pilosebaceous structures of full-thickness hairless rat and human skin after 2 h of passive permeation.

In vivo skin penetration studies also showed that 4 h of PHBV sphere application on the dorsal region of BALB/c mice was adequate for particles to penetrate through the skin and the amount of particles decreased for 10 days after application (Jeong et al. 2003; Eke et al. 2015). Therefore, it can be stated that less than 24 h is sufficient for skin penetration of the polymeric materials.

3.3.4 Determination of Nanoparticle Concentration on Keratinocytes

Different amount of drug loaded nanoparticles were used to determine the ideal concentration of drug for the penetration through the skin model. 2D keratinocyte culture was used for these experiments.

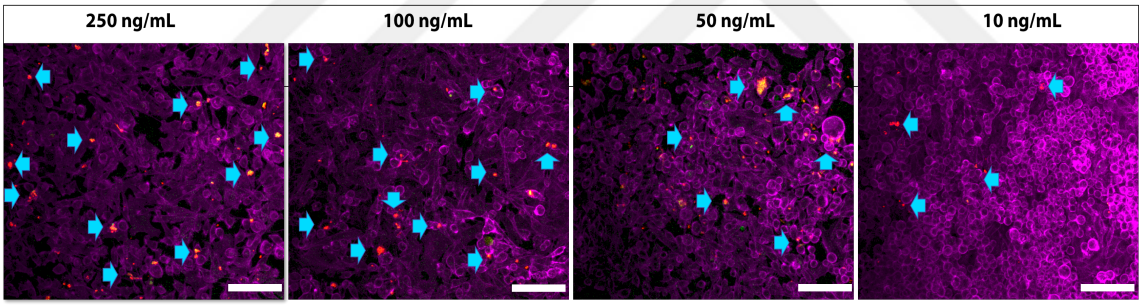

Figure 3.23 Effect of drug loaded nanoparticles on keratinocyte cell culture. Arrows show nanoparticles penetrated to the cells. Red color represents nanoparticles and keratinocytes are shown by purple. Scale bar 100 μm.

Keratinocytes were seeded in a TCPs with the density of $1x10^6$/well. Rhodamine loaded nanoparticles were then added on keratinocytes with different concentrations

in the range 250-10 ng/mL. The cell morphology was examined with CLSM. Morphology of the cells seemed to be damaged with the presence of a high concentration of nanoparticles (100-250 ng/mL, 1 mL).

Cell numbers were also seemed to be decreased with the increasing amount of the nanoparticles according to the confocal micrographs (**Figure 3.23**). According to these results, the ideal nanoparticle concentration was selected as 50 ng/mL per sample.

3.3.5 Penetration of Rho loaded nanoparticles into tissue engineered skin

Considering degradation, mechanical testing and immunohistochemistry results, PLA-PHBV-PLA trilayer electrospun mesh was selected for the nanoparticle penetration studies. The penetration behavior of fluorescent tagged nanoparticles (av. d 213.8 ± 49.7 nm) was investigated (**Figures 3.24 and 3.25**). Rhodamine loaded nanoparticles were seeded on the upper part (epidermis part having keratinocytes) of the trilayer mesh prepared as skin model. After 48 h, the top epidermis side (where keratinocytes are located) and the bottom dermis side (where fibroblasts are located) were studied with CLSM. Trilayer mesh not treated with nanoparticles was used as the control. Cytoskeleton and nuclei of the cells were stained with FITC-labeled phalloidin (green) and Topro3 (red), respectively. The fluorescent stain, rhodamine was shown in blue.

It was found that the rhodamine loaded nanoparticles were localized on the upper most layers of keratinocyte which was shown in blue color (**Figure 3.24**). On the other hand, rhodamine was released from the particles and penetrated much deeper to the bottom side of the skin model where fibroblasts were placed (**Figure 3.25**).

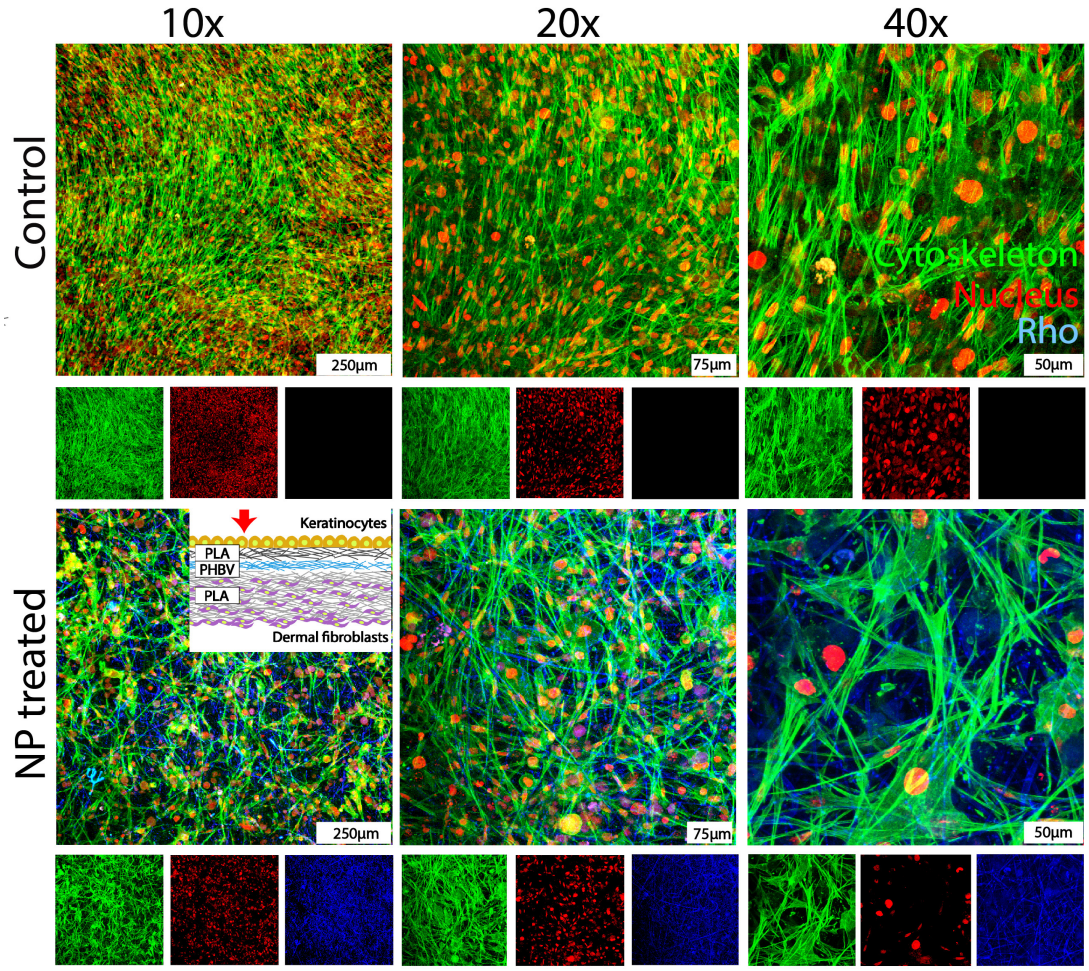

Figure 3.24 Confocal microscopy of the top layer (keratinocyte layer) of PLA-PHBV-PLA trilayer mesh skin model treated with Rhodamine loaded nanoparticles. Cytoskeleton and nuclei of keratinocytes were stained with FITC-labeled phalloidin (green) and Topro3 (red), respectively. The skin model not treated with nanoparticles was used as a control. Blue color shows the rhodamine which was not observed in the control samples. Inset represents the illustration of the skin model and red arrow indicates the direction of the imaging.

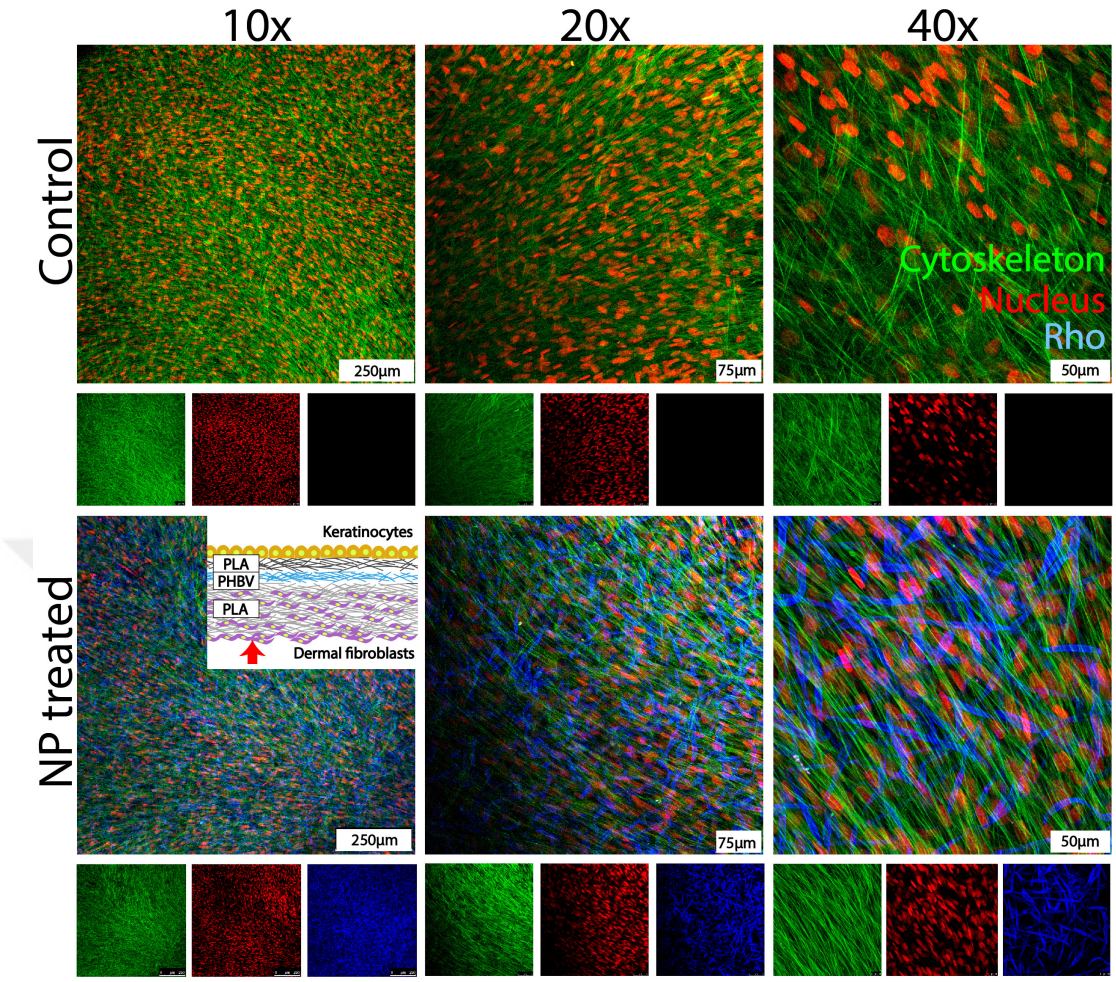

Figure 3.25 Confocal microscopy of the bottom layer (fibroblasts) of PLA-PHBV-PLA trilayer mesh skin model treated with Rhodamine loaded nanoparticles. Cytoskeleton and nuclei of keratinocytes were stained with FITC-labeled phalloidin (green) and Topro3 (red), respectively. The skin model not treated with nanoparticles was used as a control. Blue color shows the rhodamine which was not observed in the control samples. Inset represents the illustration of the skin model and red arrow indicates the direction of the imaging.

3.3.6 Histology of the Rhodamine loaded nanoparticles into tissue engineered skin

Penetration depth of the rhodamine loaded nanoparticles were studied with the sections of the constructs using SEM and CLSM (**Figure 3.26**). Rhodamine loaded nanoparticles were seeded on the top keratinocyte layer and incubated for 48 h. Control samples were not treated with the nanoparticles (**Figure 3.26A**). In the SEM image of the cross section, trilayer electrospun mesh was observed with stratified epidermal keratinocytes on top. In the close-up image (**Figure 3.26A1**) individual fibers were observed. CLSM images of the control sample showed a confluent layer of keratinocytes on top of the construct (green, cytoskeleton) but no rhodamine signal (blue) (**Figure 3.26A**, bottom row). On the other hand, there were spherical structures resembling the nanoparticles (**Figure 3.26B**) on the nanoparticle treated constructs on the magnified images (**Figure 3.26B1**). This result was interpreted as the penetration of the nanoparticles to the first layer of the trilayer electrospun mesh. CLSM images were in agreement with the SEM findings such that, the highest rhodamine signal (blue) was observed at the top electrospun layer where keratinocytes resided (green, cytoskeleton) (**Figure 3.26B**, bottom row) showing the nanoparticles were mostly located on the top layer.

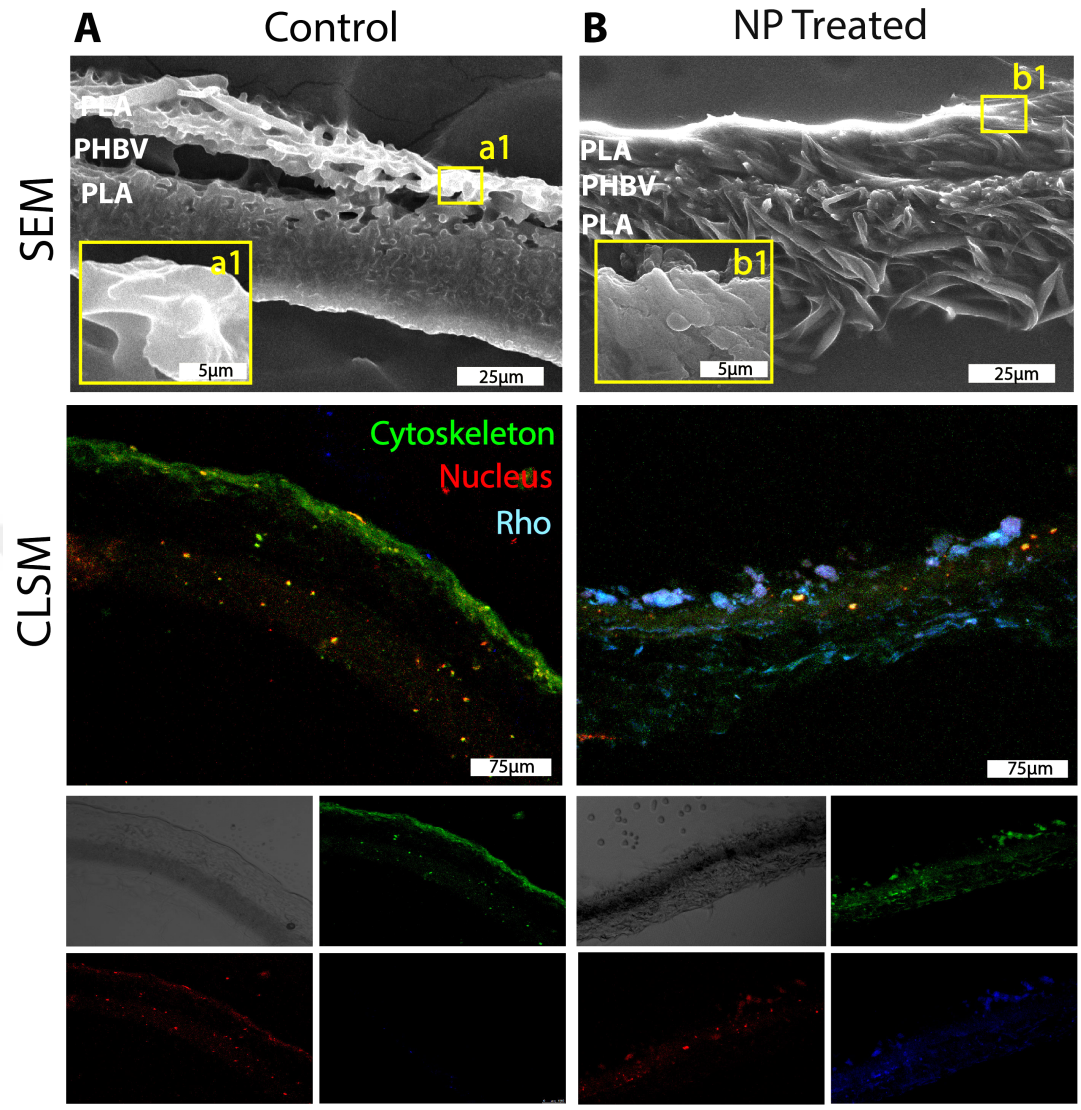

Figure 3.26 SEM and CLSM micrographs of A) control and B) rhodamine loaded nanoparticle treated PLA/PHBV/PLA trilayer mesh skin models. Sections were cut in 6 µm thickness with cryotome. Cytoskeleton and nuclei of the cells were represented in green and red, respectively. Nanoparticles loaded with rhodamine were shown in blue.

Fluorescence intensity analysis of the rhodamine release to the skin model were also studied with CLSM of the sections. Samples were embedded and cross sectioned without further staining and analyzed for Rho fluorescence emission at 540-600 nm. DIC images demonstrates top PLA, middle PHBV and bottom PLA layers (**Figure 3.27**). The control sample (no nanoparticles) showed no fluorescence emission throughout the three layers of the scaffold at the given wavelengths (**Figure 3.27**, left panel). On the other hand, nanoparticle loaded construct showed Rhodamine emission (**Figure 3.27**, right panel). Fluorescence intensity analysis were conducted for all three layers of the construct and top PLA and PHBV layers had the highest signals with significance ($p<0.0001$) (from top to the bottom average signal intensities were 13.5±3.00 au, 30.0±5.52 au, 6.33±2.65 au, respectively). These results were in agreement with the previous analysis where Rhodamine signal overlapped the keratinocyte locations. According to the histology results and SEM micrographs of the sections, nanoparticles were mostly located on the top layer, however rhodamine was released throughout the construct.

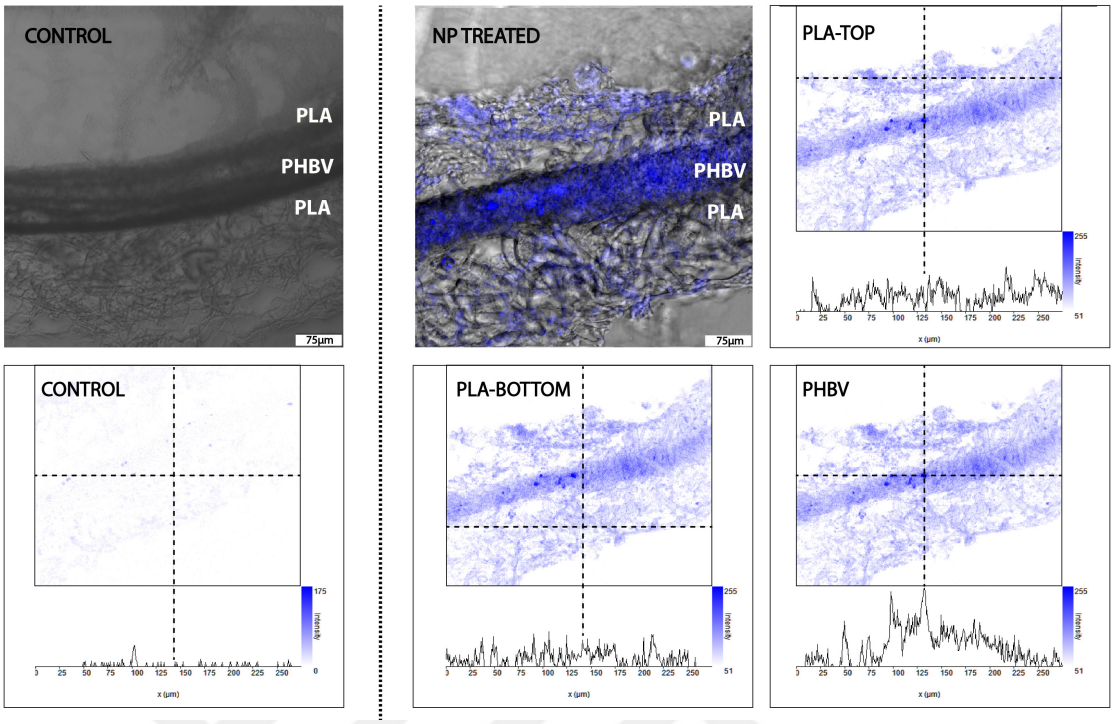

Figure 3.27 Fluorescence intensity analysis of the rhodamine release to the control and rhodamine loaded nanoparticle treated PLA/PHBV/PLA trilayer mesh skin models. Sections were cut in 6 µm thickness with cryotome.

Drugs for transdermal delivery have three pathways to cross the epidermis: intercellular (or paracellular, in between the keratinocytes), intracellular (or transcellular, across the keratinocytes), and through the appendageal shunt (transappendageal) (Barry 2001). Intracellular pathway is longer than the normal stratum corneum thickness, therefore, the most commonly preferred route for the application of the nanoparticles and drugs is intercellular route.

CHAPTER 4

CONCLUSIONS

In this study, it was possible to construct a viable skin equivalent and a model using the principles of tissue engineering. Two different scaffolds were produced as dermis layer of the model skin; PLA-PHBV-PLA trilayer electrospun mesh, collagen sponge/PLA-PHBV bilayer mesh. In skin tissue engineering applications, two or three-dimensional biomaterials are used for the replacement of the skin's dermal layer. To form epidermis, keratinocytes are exposed to air, differentiate and form epidermis layer themselves. Both scaffolds have shown to act as a split-thickness skin model by introducing fibroblasts and keratinocytes. Both fibroblasts and keratinocytes are previously shown to improve the compatibility of the scaffolds. Successful synthetic skin models were produced to stimulate epidermis, dermis and most importantly basal membrane junction on cultured fibroblasts and keratinocytes by two different types of scaffolds and human allograft.

As a subcutaneous tissue substitute, a hydrogel was synthesized from methacrylated gelatin and methacrylated hyaluronic acid polymers where methacrylate groups were used for crosslinking with the application of UV. Among other chemical and physical crosslinking methods, UV crosslinking has the advantage of being rapid and reliable. Hydrogel types and degradation time play a key role in host response (formation of granulation tissue following the acute and chronic inflammation processes) to the

implanted material which then determines the occurrence of complications such as erosion and exposure. The other attractive feature of the GelMA/HAMA hydrogel is its optical transparency. Further, the fact that the hydrogels are reasonably transparent even when loaded with cells will enable clinicians to view the wound bed under the hydrogel and see the extent of new blood vessel formation. Additionally, it was observed a growing number of endothelial cell sprouting from the chick aorta in response to an increasing number of ADSCs when they are co-cultured. Taken together these data suggest that the stem cell loaded hydrogel which was designed to act as a subcutaneous tissue promotes angiogenesis.

Finally, drug loaded nanoparticles of PHBV were developed for drug delivery studies into the skin model. The bioactive agent selected was retinyl palmitate, and rhodamine was used as a fluorescent stain for the penetration studies.

The skin penetration results showed that the retinyl palmitate loaded nanoparticles penetrated into the human skin. Fluorescent-tagged (Rhodamine) PHBV nanoparticles were also transported to the inner parts of the skin model (trilayer electrospun mesh). It was also observed that these particles penetrate into the cellular membrane. This shows that the effectiveness of the application would be high without the potential damage due to the nanoparticle accumulation because of the biodegradability of the particles. For specific diseases, particular drugs are needed to be encapsulated in these particles to achieve the optimum healing if not a complete cure. In this context, the systems developed become personalized implants and treatment tools.

Future Work

Finding strategies to combat the primary problem of 'contraction' which occurs after transplantation of the tissue engineered skin constructs to real patients: Several novel approaches that might help to decrease the contraction of the model skins have been developed, the most promising strategy so far appears to be introducing the skin cells together with the hydrogel on the skin model. These experiments need to be further optimized to find the most favorable cell- hydrogel interaction to prevent contraction.

Evaluating the angiogenic potential of the split-thickness dermis models: Angiogenic potential of the hydrogels will be tested by the CAM assay together with initial tissue response to the constructed dermis models. Angiogenic potential and tissue response of the subcutaneous tissue model (GelMA/HAMA hydrogels) was presented in this thesis. However, the patients, who have superficial burns, only require a dermis layer. Therefore, angiogenic potential of the tissue engineered dermis layer will be studied using a similar approach with the hydrogel studies using CAM assay.

Long term *in vivo* tissue response: Although subcutaneous tissue model has initial tissue response with chorionic allantoic chick membrane. Still, these initial results need further evaluations which will mainly involve the type of inflammatory response (M1/M2 macrophage ratio) *in vivo*.

REFERENCES

Aksoy A, Umran E.A, Kara F, and Hasirci N. 2015. "Heparin/Chitosan/Alginate Complex Scaffolds as Wound Dressings: Characterization and Antibacterial Study against S. Epidermidis." *Journal of Biomaterials and Tissue Engineering* 5: 104–13. doi:10.1166/jbt.2015.1296.

Alexander H, and Cook T.H. 1977. "Accounting for Natural Tension in the Mechanical Testing of Human Skin." *Journal of Investigative Dermatology* 69 (3). Elsevier: 310–14. doi:10.1111/1523-1747.EP12507731.

Aubin H, Nichol J.W, Hutson C.B, Bae H, Sieminski A.L, Cropek D.M, Akhyari P, and Khademhosseini A. 2010. "Directed 3D Cell Alignment and Elongation in Microengineered Hydrogels." *Biomaterials* 31 (27). Elsevier: 6941–51. doi:10.1016/J.BIOMATERIALS.2010.05.056.

Auxenfans C, Fradette J, Lequeux C, Germain L, Kinikoglu B, Bechetoille N, Braye F, Auger F.A, and Damour O. 2009. "Evolution of Three Dimensional Skin Equivalent Models Reconstructed in Vitro by Tissue Engineering." *European Journal of Dermatology* 19 (2): 107–13. doi:10.1684/ejd.2008.0573.

Bahcecioglu G, Buyuksungur A, Kiziltay A, Hasirci N, and Hasirci V. 2014. "Construction and in Vitro Testing of a Multilayered, Tissue-Engineered Meniscus." *Journal of Bioactive and Compatible Polymers* 29 (3): 235–53. doi:10.1177/0883911514529688.

Barnhill R.L, and Ryan T.J. 1983. “Biochemical Modulation of Angiogenesis in the Chorioallantoic Membrane of the Chick Embryo.” *J Invest Dermatol*.

Barry B.W, 2001. “Novel Mechanisms and Devices to Enable Successful Transdermal Drug Delivery.” *European Journal of Pharmaceutical Sciences* 14 (2). Elsevier: 101–14. doi:10.1016/S0928-0987(01)00167-1.

Bello Y, and Falabella A. 2003. “The Role of Graftskin (Apligraf) in Difficult-to-Heal Venous Leg Ulcers.” *Journal of Wound Care* 11 (5): 182–83.

Bender C, Ivo Partecke L, Kindel E, Döring F, Lademann J, Dieter Heidecke C, Kramer A, and Olaf Hübner N. 2011. “The Modified HET-CAM as a Model for the Assessment of the Inflammatory Response to Tissue Tolerable Plasma.” *Toxicology in Vitro* 25 (2). Elsevier Ltd: 530–37. doi:10.1016/j.tiv.2010.11.012.

Beumer G.J, Blitterswijk C.A, and Ponec M. 1994. “Biocompatibility of a Biodegradable Matrix Used as a Skin Substitute: An in Vivo Evaluation. 1994; 28: 545-52.” *J Biomed Mater Res* 28: 545–52.

Bhardwaj N, Chouhan D, and Mandal B.B. 2018. “3D Functional Scaffolds for Skin Tissue Engineering.” In *Functional 3D Tissue Engineering Scaffolds*, 345–65. Elsevier. doi:10.1016/B978-0-08-100979-6.00014-8.

Bhargava S, Patterson J.M, Inman R.D, MacNeil S, and Chapple C.R. 2008. “Tissue-Engineered Buccal Mucosa Urethroplasty-Clinical Outcomes.” *European Urology* 53 (6): 1263–71. doi:10.1016/j.eururo.2008.01.061.

Böttcher-Haberzeth S, Biedermann T, and Reichmann E. 2010. “Tissue Engineering of Skin.” *Burns : Journal of the International Society for Burn Injuries* 36 (4). 450–60. doi:10.1016/j.burns.2009.08.016.

Boyandin A.N, Prudnikova S.V, Filipenko M.L, Khrapov E.A, Vasil'ev A.D, and Volova T. 2012. "Biodegradation of Polyhydroxyalkanoates by Soil Microbial Communities of Different Structures and Detection of PHA Degrading Microorganisms." *Applied Biochemistry and Microbiology* 48 (1): 28–36. doi: 10.1134/S0003683812010024.

Boyce S, Goretsky M.J, Greenhalgh D.G, Kagan R.J, Rieman M.T, and Warden G.D. 1995. "Comparative Assessment of Cultured Skin Substitutes and Native Skin Autograft for Treatment of Full-Thickness Burns." *Annals of Surgery* 222 (6): 743–52. doi:10.1097/00000658-199512000-00008.

Boyce S.T, Kagan R.J, Meyer N.A, Yakuboff K.A, and Warden G.D. 1999. "THE 1999 CLINICAL RESEARCH AWARD Cultured Skin Substitutes Combined With Integra Artificial Skin* to Replace Native Skin Autograft and Allograft for the Closure of Excised Full-Thickness Burns." *Journal of Burn Care and Research* 20 (6): 439–40. doi:10.1097/00004630-199920060-00006.

Broughton G, Janis J.E, and Attinger C.E. 2006. "The Basicdcience of Wound Healing." *Plastic and Reconstructive Surgery* 117 (7): 12–35. doi:10.1097/01.prs.0000225430.42531.c2.

Bye F, Bissoli J, Black L, Bullock A, Puwanun S, Moharamzadeh K, Reilly G, Ryan A.J, and MacNeil S. 2013. "Development of Bilayer and Trilayer Nanofibrous/microfibrous Scaffolds for Regenerative Medicine." *Biomaterials Science* 1 (9): 942. doi:10.1039/c3bm60074b.

Camci-Unal G, Cuttica D, Annabi N, Demarchi D, and Khademhosseini A. 2013. "Synthesis and Characterization of Hybrid Hyaluronic Acid-Gelatin Hydrogels." *Biomacromolecules* 14: 1085–92. doi:DOI: 10.1021/bm3019856.

Chakrabarty K:H, Dawson R, Harris P, Layton C, Babu M, Gould L, Phillips J, et al. 1999. "Development of Autologous Human Dermal-Epidermal Composites Based on Sterilized Human Allodermis for Clinical Use." *British Journal of Dermatology* 141 (5): 811–23. doi:10.1046/j.1365-2133.1999.03153.x.

Contard P, Bartel R.L, Jacobs L, Perlish J.S, Douglas MacDonald E, HandlerE, Cone D, and Fleischmajer R. 1993. "Culturing Keratinocytes and Fibroblasts in a Three-Dimensional Mesh Results in Epidermal Differentiation and Formation of a Basal Lamina-Anchoring Zone." *Journal of Investigative Dermatology* 100 (1). Elsevier: 35–39. doi:10.1111/1523-1747.EP12349952.

Cooper M, Hansbrough J.F, Spielvogel R.L, Cohen R, Bartel R.J, and Naughton G. 1991. "In Vivo Optimization of a Living Dermal Substitute Employing Cultured Human Fibroblasts on a Biodegradable Polyglycolic Acid or Polyglactin Mesh." *Biomaterials* 12 (2). Elsevier: 243–48. doi:10.1016/0142-9612(91)90207-Q.

Cotsarelis G. 2006. "Epithelial Stem Cells: A Folliculocentric View." *Journal of Investigative Dermatology* 126 (7). Elsevier: 1459–68. doi:10. 1038/SJ.JID.5700376.

Crisan M, Yap S, Casteilla L, Chen C.W, Corselli M, Park T.S, Andriolo G, et al. 2008. "A Perivascular Origin for Mesenchymal Stem Cells in Multiple Human Organs." *Cell Stem Cell* 3 (3). Cell Press: 301–13. doi:10.1016/ J.STEM.2008.07.003.

Dantzer E, and Braye F.M. 2001. "Reconstructive Surgery Using an Artificial Dermis (Integra): Results with 39 Grafts." *British Journal of Plastic Surgery* 54 (8): 659–64. doi:10.1054/bjps.2001.3684.

Deans R.J, and MoseleyA.B. 2000. “Mesenchymal Stem Cells: Biology and Potential Clinical Uses.” *Experimental Hematology* 28 (8): 875–84. doi:10.1016/S0301-472X(00)00482-3.

Demidova-Rice T, Hamblin M.R, and Herman I.M. 2012. “Acute and Impaired Wound Healing: Pathophysiology and Current Methods for Drug Delivery, Part 1: Normal and Chronic Wounds: Biology, Causes, and Approaches to Care.” *Advances in Skin and Wound Care* 25 (7): 304–14. doi: doi.org/10.1097/01.ASW.0000416006.55218.d0.

Dogan S, Demirer S, Kepenekci I, Erkek B, Kiziltay A, HasirciN, Müftüoğlu S, et al. 2009. “Epidermal Growth Factor-Containing Wound Closure Enhances Wound Healing in Non-Diabetic and Diabetic Rats.” *International Wound Journal* 6 (2): 107–115. doi:10.1111/j.1742-481X.2009.00584.x.

Duangjit S, Opanasopit P, Rojanarata T and Ngawhirunpat T. 2011. “Characterization and In Vitro Skin Permeation of Meloxicam-Loaded Liposomes versus Transfersomes.” *Journal of Drug Delivery* 2011 (Figure 1): 418316. doi:10.1155/2011/418316.

Eke G, Kuzmina A, Goreva A, Shishatskaya E.I, Hasirci N, and Hasirci V. 2014. “In Vitro and Transdermal Penetration of PHBV Micro/nanoparticles.” *Journal of Materials Science. Materials in Medicine* 25 (6): 1471–81. doi:10.1007/s10856-014-5169-5.

Eke G, Goni-de-Cerio F, Suarez-Merino B, Hasirci N, and Hasirci V. 2015. “Biocompatibility of Dead Sea Water and Retinyl Palmitate Carrying poly(3-Hydroxybutyrate-Co-3-Hydroxyvalerate) Micro/nanoparticles Designed for Transdermal Skin Therapy.” *Journal of Bioactive and Compatible Polymers* 30

(5): 455-47. doi: 10.1177/0883911515585183.

Eke G, Mangir, Hasirci N, Macneil S, and Hasirci V. 2017. “Development of a UV Crosslinked Biodegradable Hydrogel Containing Adipose Derived Stem Cells to Promote Vascularization for Skin Wounds and Tissue Engineering.” *Biomaterials* 129. 188–198. doi:10.1016/j.biomaterials.2017.03.021.

Elliott J.T, Tona A, Woodward J.T, Jones P.L, and Plant A.L. 2003. “Thin Films of Collagen Affect Smooth Muscle Cell Morphology.” *Langmuir* 19 (5): 1506–14. doi:10.1021/la026216r.

Errico C, Bartoli C, Chiellini F, and Chiellini E. 2009. “Poly(hydroxyalkanoates)-Based Polymeric Nanoparticles for Drug Delivery.” *Journal of Biomedicine and Biotechnology* 2009: 1–10. doi:10.1155/2009/571702.

FinkA.Z, Gittler J.K, Nakrani R.N, Alis J, Blumfield E, and Levin T.L. 2018. “Imaging Findings in Systemic Childhood Diseases Presenting with Dermatologic Manifestations.” *Clinical Imaging* 49. Elsevier: 17–36. doi:10.1016/ J.CLINIMAG.2017.10.015.

Fischer A.H, Jacobson K, Rose J, and Zeller R. 2008. “Hematoxylin and Eosin Staining of Tissueand Cell Sections.” *Cold Spring Harbor Protocols* 3 (5): 4986–88. doi:10.1101/pdb.prot4986.

Freed L, Vunjak-Novakovic G, Biron R.J, Eagles D.B, Lesnoy D.C, Barlow S.K, and Langer R. 1994. “Biodegradable Polymer Scaffolds for Tissue Engineering.” *Nature Biotechnology* 12 (July). Nature Publishing Company: 689. http://dx.doi.org/10.1038/nbt0794-689.

Ghaeli I, Moraes M.A, Beppu M, Lewandowska K, Sionkowska A, Ferreira-Da-Silva, Ferraz M.P, and Monteiro F.J. 2017. “Phase Behaviour and Miscibility Studies of Collagen/silk Fibroin Macromolecular System in Dilute Solutions and Solid State.” *Molecules* 22 (8). doi:10.3390/molecules22081368.

Gopee N.V, Roberts D.W, Webb P, Cozart R, Siitonen P.H, Latendresse J.R, Warbitton A.R, et al. 2009. “Quantitative Determination of Skin Penetration of PEG-Coated CdSe Quantum Dots in Dermabraded but Not Intact SKH-1 Hairless Mouse Skin.” *Toxicological Sciences* 111 (1): 37–48. doi:10.1093/toxsci/kfp139.

Groeber F, Holeiter M, Hampel M, Hinderer S, and Schenke-Layland K. 2011. “Skin Tissue Engineering - In Vivo and in Vitro Applications.” *Advanced Drug Delivery Reviews* 63 (4). Elsevier B.V.: 352–66. doi:10.1016/j.addr.2011.01.005.

Haddow D, Steele D.A, Short, R.D, Dawson R.A, and Macneil S. 2003. “Plasma-Polymerized Surfaces for Culture of Human Keratinocytes and Transfer of Cells to Anin Vitro Wound-Bed Model.” *Journal of Biomedical Materials Research* 64A (1): 80–87. doi:10.1002/jbm.a.10356.

Halim A, Khoo T.L, and Yussof S.J.M. 2010. “Biologic and Synthetic Skin Substitutes: An Overview.” *Indian Journal of Plastic Surgery* 43: 23.

Hamburger V, Hamilton H. 1951. “A Series of Normal Stages in the Development of the Chick Embryo.” *Jounal of Morphoogy.* 81 (1): 49–92. doi: 10.1002/aja.1001950404.

Harrison C, Layton C, Z Hau, Bullock A, Johnson T.S, and MacNeil S. 2007. “Transglutaminase Inhibitors Induce Hyperproliferation and Parakeratosis in Tissue-Engineered Skin.” *The British Journal of Dermatology* 156 (2): 247–57.

doi:10.1111/j.1365-2133.2006.07641.x.

Hasirci N, Kilic C, Komez A, Bahcecioglu G, and Hasirci V. 2016. “Hydrogels in Regenerative Medicine.” In *Handbook of Polymer Applications in Medicine and Medical Devices*, edited by Mohammad R. Abidian, Umut A. Gurkan, and Faramarz. Edalat, 2nded., 1–52. USA: Worls Scientific. doi:10.1016/B978-0-323-22805-3.00012-8.

Hasirci V, Vrana N.E, Zorlutuna P, Ndreu A, Yilgor P, Basmanav B, and Aydin E. 2006. “Nanobiomaterials: A Review of the Existing Science and Technology, and New Approaches.” *Journal of Biomaterials Science. Polymer Edition* 17 (11): 1241–68.

Hasirci V, Yilgor P, Endogan T, Eke G, and Hasirci V. 2017. “Polymer Fundamentals: Polymer Synthesis.” In *Comprehensive Biomaterials*, edited by P Ducheyne, K Healy, and DE Hutmacher, 2nd ed., 349–71. Amsterdam: Elsevier.

Hermans M. 1989. “Clinical Experience with Glycerol-Preserved Donor Skin Treatment in Partial Thickness Burns.” *Burns* 15 (1). Elsevier: 57–59. doi:10.1016/0305-4179(89)90074-0.

Hesketh M, Sahin K, West Z, and Murray R.Z. 2017. “Macrophage Phenotypes Regulate Scar Formation and Chronic Wound Healing.” *International Journal of Molecular Sciences* 18 (7): 1–10. doi:10.3390/ijms18071545.

Higuchi T. 1961. “Rate of Release of Medicaments from Ointment Bases Containing Drugs in Suspension.” *Journal of Pharmaceutical Sciences* 50 (10): 874–75. doi:10.1002/jps.2600501018.

Jarman-Smith, M, T Bodamyali, C Stevens, J Howell, M Horrocks, and J Chaudhuri. 2004. “Porcine Collagen Crosslinking, Degradation and Its Capability for Fibroblast Adhesion and Proliferation.” *Journal of Materials Science: Materials in Medicine* 15 (8): 925–32.

Jean J, Lapointe M, Soucy J, and Pouliot R. 2009. “Development of an in Vitro Psoriatic Skin Model by Tissue Engineering.” *Journal of Dermatological Science* 53 (1). Elsevier: 19–25. doi:10.1016/J.JDERMSCI.2008.07.009.

Jeong Y, Gyu Song J, Kang S.S, Ryu H, Lee Y.H, Choi C, Shin B.A, Keun Kim, Kyu Youn Ahn, and Jung S. 2003. “Preparation of poly(DL-Lactide-Co-Glycolide) Microspheres Encapsulating All-Trans Retinoic Acid.” *International Journal of Pharmaceutics* 259 (1–2). Elsevier: 79–91. doi:10.1016/S0378-5173(03)00207-2.

Jiang P, Mao Z, and Gao C. 2015. “Combinational Effect of Matrix Elasticity and Alendronate Density on Differentiation of Rat Mesenchymal Stem Cells.” *Acta Biomaterialia* 19: 76–84. doi:10.1016/j.actbio.2015.03.018.

Kilic C, Girotti A, Rodriguez-Cabello C, and Hasirci V. 2014. “A Collagen-Based Corneal Stroma Substitute with Micro-Designed Architecture.” *Biomater. Sci.* 2 (3): 318–29. doi:10.1039/C3BM60194C.

Kim H, Kim J.T, Barua S, Yoo S, Hong S, and Lee K.B. 2018. “Seeking Better Topical Delivery Technologies of Moisturizing Agents for Enhanced Skin Moisturization.” *Expert Opinion on Drug Delivery* 15 (1): 17–31.

Kim H, Kim B, Kim H, Um S, Lee J, Ryoo H, and Hyungil Jung. 2008. "Synthesis and in Vitro Biological Activity of Retinyl Retinoate, a Novel Hybrid Retinoid Derivative." *Bioorganic & Medicinal Chemistry* 16 (12). Pergamon: 6387–93. doi:10.1016/J.BMC.2008.05.005.

Kinikoglu B, Damour O, and Hasirci V. 2015. "Tissue Engineering of Oral Mucosa: A Shared Concept with Skin." *Journal of Artificial Organs* 18 (1): 8–19. doi:10.1007/s10047-014-0798-5.

Klotz B, Gawlitta D, Rosenberg A, Malda J, and Melchels F. 2016. "Gelatin-Methacryloyl Hydrogels: Towards Biofabrication-Based Tissue Repair." *Trends in Biotechnology* 34 (5). Elsevier Ltd: 394–407. doi:10.1016/j.tibtech.2016.01.002.

Kumar R.J, Kimble R.M, Boots R, and Pegg S.P. 2004. "Treatment of Partial-Thickness Burns: A Prospective, Randomized Trial Using Transcyte™." *ANZ Journal of Surgery* 74 (8): 622–26. doi:10.1111/j.1445-1433.2004.03106.x.

Kumbar S, Nukavarapu P, James R, Laksmi N, and Laurencin C. 2008. "Electrospun Poly(lactic Acid-Co-Glycolic Acid) Scaffolds for Skin Tissue Engineering." *Biomaterials* 29 (30). Elsevier: 4100–4107. doi:10.1016/J.BIOMATERIALS.2008.06.028.

Lalatsa A, Schätzlein A.G, Mariarosa Mazza, Thi Bich Hang, and LeIjeoma F.Uchegbu. 2012. "Amphiphilic Poly(l-Amino Acids) — New Materials for Drug Delivery." *Journal of Controlled Release* 161 (2). Elsevier: 523–36. doi:10.1016/J.JCONREL.2012.04.046.

Leikin S, Rau D.C, and Parsegian V.A. 1995. “Temperature-Favoured Assembly of Collagen Is Driven by Hydrophilic Not Hydrophobic Interactions.” *Nature Structural Biology* 2 (3): 205–10. doi:10.1038/nsb0395-205.

Lipkin S, Chaikof E, Isseroff Z, and Silverstein P. 2003. “Effectiveness of Bilayered Cellular Matrix in Healing of Neuropathic Diabetic Foot Ulcers: Results of a Multicenter Pilot Trial.” *Wounds* 15 (7): 230–36.

Lorenti A. 2012. “Wound Healing : From Epidermis Culture to Tissue Engineering” 2012 (December): 17–29.

MacNeil S. 2007. “Progress and Opportunities for Tissue-Engineered Skin.” *Nature* 445 (7130): 874–80. doi:10.1038/nature05664.

Marston W.A, Hanft J, Norwood P, and PollakR. 2003. “The Efficacy and Safety of Dermagraft in Improving the Healing of Chronic Diabetic Foot Ulcers: Results of a Prospective Randomized Trial.” *Diabetes Care* 26 (6): 1701–5. doi:10.2337/diacare.26.6.1701.

Masuma R, Kashima S, Kurasaki M, and Okuno T. 2013. “Effects of UV Wavelength on Cell Damages Caused by UV Irradiation in PC12 Cells.” *Journal of Photochemistry and Photobiology B: Biology* 125. Elsevier B.V.: 202–8. doi:10.1016/j.jphotobiol.2013.06.003.

Messager L, PortecopN, Hachet E, Lapeyre V, Pignot-PaintrandI, Catargi P, Auzely-Velty R, and Ravaine V. 2013. “Photochemical Crosslinking of Hyaluronic Acid Confined in Nanoemulsions: Towards Nanogels with a Controlled Structure.” *Journal of Materials Chemistry B: Materials for Biology and Medicine* 1 (27): 3369–79. doi:10.1039/c3tb20300j.

Metcalfe, Anthony D., and Mark W.J. Ferguson. 2007. "Tissue Engineering of Replacement Skin: The Crossroads of Biomaterials, Wound Healing, Embryonic Development, Stem Cells and Regeneration." *Journal of The Royal Society Interface* 4 (14): 413–37. doi:10.1098/rsif.2006.0179.

Min B, Lee G, KimS, Nam Y, Lee T.S, and Park W.H. 2004. "Electrospinning of Silk Fibroin Nanofibers and Its Effect on the Adhesion and Spreading of Normal Human Keratinocytes and Fibroblasts in Vitro." *Biomaterials* 25 (7–8). Elsevier: 1289–97. doi:10.1016/J.BIOMATERIALS.2003.08.045.

Mutlu G, Calamak S, Ulubayram K, and Guven E. 2018. "Curcumin-Loaded Electrospun PHBV Nanofibers as Potential Wound-Dressing Material." *Journal of Drug Delivery Science and Technology* 43. 185–93. doi: 10.1016/J.JDDST.2017.09.017.

Myers, Simon R, and Ghanem A. 2015. "Wound Healing and Scar Formation," *Plastic and reconstructive surgery Approaches and Techniques* 1st Edn. 3–11.

Nai-Chen, Cheng, Lin Wei-Jhih, Ling Thai-Yen, and Young Tai-Horng. 2017. "Sustained Release of Adipose-Derived Stem Cells by Thermosensitive Chitosan/gelatin Hydrogel for Therapeutic Angiogenesis." *Acta Biomaterialia* 51. Elsevier: 258–67. doi:10.1016/J.ACTBIO.2017.01.060.

Nestle F, Di Meglio P, Qin J.Z, and Nickoloff B. 2009. "Skin Immune Sentinels in Health and Disease." *Nature Reviews Immunology* 9 (10): 679–91. doi:10.1038/nri2622.

Nguyen T, Mobashery S, and Chang M. 2016. “Roles of Matrix Metalloproteinases in Cutaneous Wound Healing.” In *New Insights into Ancient Challenges*, edited by Vlad Alexandrescu, 1sted.

Nichol J, Koshy S.T, Bae H, Hwang C, Yamanlar S, and Khademhosseini A. 2010. “Cell-Laden Microengineered Gelatin Methacrylate Hydrogels.” *Biomaterials* 31 (21). 5536–44. doi:10.1016/j.biomaterials.2010.03.064.

Nowak-Sliwinska P, Ballini J.P, Wagnires G, and Bergh H. 2010. “Processing of Fluorescence Angiograms for the Quantification of Vascular Effects Induced by Anti-Angiogenic Agents in the CAM Model.” *Microvascular Research* 79 (1). Elsevier Inc.: 21–28. doi:10.1016/j.mvr.2009.10.004.

Oudshoorn M, Rissmann R, Bouwstra J.A, and Hennink W. 2007. “Synthesis of Methacrylated Hyaluronic Acid with Tailored Degree of Substitution.” *Polymer* 48 (7): 1915–20. doi:10.1016/j.polymer.2007.01.068.

Park J, Lee J, Kim Y, and Prausnitz R.M. 2008. “The Effect of Heat on Skin Permeability.” *International Journal of Pharmaceutics* 359 (1–2). Elsevier: 94–103. doi:10.1016/J.IJPHARM.2008.03.032.

Prow, Tarl W., Jeffrey E. Grice, Lynlee L. Lin, Rokhaya Faye, Margaret Butler, Wolfgang Becker, Elisabeth M.T. Wurm, et al. 2011. “Nanoparticles and Microparticles for Skin Drug Delivery.” *Advanced Drug Delivery Reviews* 63 (6). Elsevier: 470–91. doi:10.1016/J.ADDR.2011.01.012.

Ribatti D, A Vacca, L Roncali, and F Dammacco. 2000. “The Chick Embryo Chorioallantoic Membrane as a Model for in Vivo Research on Anti-Angiogenesis.” *Current Pharmaceutical Biotechnology* 1 (1): 73–82.

Ribatti D, Nico B, Vacca A, and Presta M. 2006. “The Gelatin Sponge-Chorioallantoic Membrane Assay.” *Nature Protocols* 1 (1): 85–91. doi:10.1038/nprot.2006.13.

Richardson M, Wong D, Lacroix S, Stanisz J, and Singh G. 2005. “Inhibition by Doxycycline of Angiogenesis in the Chicken Chorioallantoic Membrane (CAM).” *Cancer Chemotherapy and Pharmacology* 56 (1): 1–9. doi:10.1007/s00280-004-0955-2.

Ro B.I, and Dawson T.L. 2005. “The Role of Sebaceous Gland Activity and Scalp Microfloral Metabolism in the Etiology of Seborrheic Dermatitis and Dandruff.” *Journal of Investigative Dermatology Symposium Proceedings* 10 (3). Elsevier: 194–97. doi:10.1111/J.1087-0024.2005.10104.X.

Romanelli M, Piaggesi A, Scapagnini G, Dini V, Janowska A, Iacopi E, and Scarpa C. 2017. “EUREKA Study – the Evaluation of Real-Life Use of a Biophotonic System in Chronic Wound Management : An Interim Analysis.” *Drug Design, Development and Therapy*, 3551–58.

Sahin A, Eke G, Buyuksungur A, Hasirci N, and Hasirci V. 2018. “Nuclear Targeting Peptide-Modified, DOX-Loaded, PHBV Nanoparticles Enhance Drug Efficacy by Targeting to Saos-2 Cell Nuclear Membranes.” *Journal of Biomaterials Science. Polymer Edition* 29 (5): 507–519. doi: 10.1080/09205063.2018.1423812.

Sahota P.S, Burn J.L, Heaton M, Freedlander E, Suvarna S.K, Brown N.J, and MacNeil S. 2003. “Development of a Reconstructed Human Skin Model for Angiogenesis.” *Wound Repair and Regeneration* 11 (4): 275–84. doi:10.1046/j.1524-475X.2003.11407.x.

Sane A, and Limtrakul J. 2011. “Co-Precipitation of Asiatic Acid and poly(L-Lactide) Using Rapid Expansion of Subcritical Solutions into Liquid Solvents.” *Journal of Nanoparticle Research* 13 (9): 4001–13. doi:10.1007/s11051-011-0328-9.

Seder C.W, Kubasiak J.C, Pithadia R, Basu S, Fhied C, Tarhoni I, Davila E, et al. 2015. “Angiogenesis Biomarkers May Be Useful in the Management of Patients With Indeterminate Pulmonary Nodules.” *The Annals of Thoracic Surgery* 100 (2). Elsevier: 429–36. doi:10.1016/J.ATHORACSUR.2015.04.018.

Seidlitz E, Korbie D, Marien L, Richardson M, and Singh G. 2004. “Quantification of Anti-Angiogenesis Using the Capillaries of the Chick Chorioallantoic Membrane Demonstrates That the Effect of Human Angiostatin Is Age-Dependent.” *Microvascular Research* 67 (2): 105–16. doi:10.1016/j.mvr.2003.12.005.

Sherman M.A, and Kennedy J.P. 1998. “Novel Polyisobutylene/poly (Dimethylsiloxane) Bicomponent Networks. I. Synthesis and Characterization.” *Journal of Polymer Science Part A: Polymer Chemistry* 36: 1891–99. doi:10.1002/(SICI)1099-0518(199808)36:11<1901::AID-POLA25>3.0.CO;2 H.

Shin H, Olsen B.D, and Khademhosseini A. 2012. “The Mechanical Properties and Cytotoxicity of Cell-Laden Double-Network Hydrogels Based on Photocrosslinkable Gelatin and Gellan Gum Biomacromolecules.” *Biomaterials* 33 (11). Elsevier Ltd: 3143–52. doi:10.1016/j.biomaterials.2011.12.050.

Shishatskaya E.I, Goreva A, Kalacheva G, and Volova T. 2011. “Biocompatibility and Resorption of Intravenously Administered Polymer Microparticles in Tissues of Internal Organs of Laboratory Animals.” *Journal of Biomaterials Science, Polymer Edition* 22 (16): 2185–2203. doi:10.1163/092050610X537138.

Shores J, Gabriel A, and Gupta S. 2007. “Skin Substitutes and Alternatives: A Review.” *Advances in Skin & Wound Care* 20 (9): 493–508.

Sloan Kenneth B, Wasdo S.C, and Rautio J. 2006. “Design for Optimized Topical Delivery: Prodrugs and a Paradigm Change.” *Pharmaceutical Research* 23 (12): 2729–47. doi:10.1007/s11095-006-9108-0.

Sneddon, I.B. 1971. “Advances in Dermatology in the Last 25 Years.” *British Journal of Clinical Practice* 25 (11): 477–84.

Spotorno V.G, Hidalgo A, Barbich M, Lorenti A, and Zabal O. 2006. “Culture of Bovine Hepatocytes: A Non-Perfusion Technique for Cell Isolation.” *Cytotechnology* 51 (2): 51–56. doi:10.1007/s10616-006-9000-0.

Stern R, McPherson M, and Longaker M.T. 1990. “Histologic Study of Artificial Skin Used in the Treatment of Full-Thickness Thermal Injury.” *Journal of Burn Care and Rehabilitation* 11 (1): 7–13. doi:10.1097/00004630-199001000-00003.

Stratman A.N, Kim D.J, Sacharidou A, Speichinger K.R, and Davis G.E. 2012. “The Textbook of Angiogenesis and Lymphangiogenesis: Methods and Applications” 101–26. doi:10.1007/978-94-007-4581-0.

Supp D.M, and Boyce T. 2005. “Engineered Skin Substitutes: Practices and Potentials.” *Clinics in Dermatology* 23 (4). Elsevier: 403–12. doi: 10.1016/J.CLINDERMATOL.2004.07.023.

Tan G, Zhou L, Ning C, Tan Y, Ni G, Liao J, Yu P, and Chen X. 2013. “Biomimetically-Mineralized Composite Coatings on Titanium Functionalized with Gelatin Methacrylate Hydrogels.” *Applied Surface Science* 279. 293–99. doi:10.1016/J.APSUSC.2013.04.088.

Tausche, Anne Kathrin, Skaria M, Böhlen L, Liebold K, Hafner J, Friedlein H, Meurer M. 2003. "An Autologous Epidermal Equivalent Tissue-Engineered from Follicular Outer Root Sheath Keratinocytes Is as Effective as Split-Thickness Skin Autograft in Recalcitrant Vascular Leg Ulcers." *Wound Repair and Regeneration* 11 (4): 248–52. doi:10.1046/j.1524-475X.2003.11403.x.

Toni, Fabienne De, Poglio S, Youcef A.B, Cousin B, Pflumio F, Bourin P, Casteilla L, and Laharrague P. 2011. "Human Adipose-Derived Stromal Cells Efficiently Support Hematopoiesis In Vitro and In Vivo: A Key Step for Therapeutic Studies." *Stem Cells and Development* 20 (12): 2127–38. doi:10.1089/scd.2011.0044.

Tsou, Yung-Hao, Khoneisser J, Huang P.C, and Xu X. 2016. Hydrogel as a Bioactive Material to Regulate Stem Cell Fate." *Bioactive Materials* 1 (1): 39–55. doi:10.1016/j.bioactmat.2016.05.001.

Ulubayram K, Cakar A, Korkusuz P, Ertan C, and Hasirci N. 2001. EGF Containing Gelatin-Based Wound Dressings." *Biomaterials* 22 (11): 1345–56. doi:10.1016/S0142-9612(00)00287-8.

Varani J, Roscoe J, Warner L, Voorhees J, Gharaee-Kermani M, Phan S.H, Kang S, Chung J.H 2000. Vitamin A Antagonizes Decreased Cell Growth and Elevated Collagen-Degrading Matrix Metalloproteinases and Stimulates Collagen Accumulation in Naturally Aged Human Skin." *Journal of Investigative Dermatology* 114 (3). Elsevier: 480–86. doi:10.1046/J.1523-1747.2000.00902.X.

Vargas A, M zeisserlabouebe M, Lange N, Gurny R, and Delile F. 2007. The Chick Embryo and Its Chorioallantoic Membrane (CAM) for the in Vivo Evaluation of Drug Delivery Systems." *Advanced Drug Delivery Reviews* 59 (11): 1162–76.

Velnar, Tomaz, T. Bailey, and V. Smrkolj. 2009. The Wound Healing Process: An Overview of the Cellular and Molecular Mechanisms. ” *Journal of International Medical Research* 37 (5): 1528–42. doi:10.1177/147323000903700531.

Tatiana V, Prudnikova S.V, Vinogradova O.N, Syrvacheva D.A, and ShishatskayaE.I. 2017. Microbial Degradation of Polyhydroxyalkanoates with Different Chemical Compositions and Their Biodegradability. ” *Microbial Ecology* 73 (2). Microbial Ecology: 353–67. doi:10.1007/s00248-016-0852-3.

Wainwright, David, Michael Madden, Arnold Luterman, John Hunt, William Monafo, David Heimbach, Richard Kagan, Kevin Sittig, Alan Dimick, and David Herndon. 1996. Clinical Evaluation of an Acellular Allograft Dermal Matrix in Full-Thickness Burns.” *Journal of Burn Care and Rehabilitation*. doi: 10.1097/00004630-199603000-00006.

Wang, Peng-Hui, Ben-Shian Huang, Huann-Cheng Horng, Chang-Ching Yeh, and Yi-Jen Chen. 2017. Wound Healing. ” *Journal of the Chinese Medical Association*, November. Elsevier. doi:10.1016/J.JCMA.2017.11.002.

Wetering, Petra van de, Andrew T. Metters, Ronald G. Schoenmakers, and Jeffrey A. Hubbell. 2005. Poly(ethylene Glycol) Hydrogels Formed by Conjugate Addition with Controllable Swelling, Degradation, and Release of Pharmaceutically Active Proteins. ” *Journal of Controlled Release* 102 (3). Elsevier: 619–27. doi:10.1016/J.JCONREL.2004.10.029.

Wosicka, Hanna, and Krzysztof Cal. 2010. Targeting to the Hair Follicles: Current Status and Potential. ” *Journal of Dermatological Science* 57 (2). Elsevier: 83–89. doi:10.1016/J.JDERMSCI.2009.12.005.

Wright A, Kathleen B, Nadire, Patricia Busto, Tubo R, McPherson J, and Wentworth B. 1998. Alternative Delivery of Keratinocytes Using a Polyurethane Membrane and the Implications for Its Use in the Treatment of Full-Thickness Burn Injury." *Burns* 24 (1). Elsevier: 7–17. doi:10.1016/S0305-4179(97)00075-2.

Xiao, Wenqian, He J, Jason, Nichol W, Wang L, Hutson C, Wang B, Du Y, Fan H, and Khademhosseini A. 2011. "Synthesis and Characterization of Photocrosslinkable Gelatin and Silk Fibroin Interpenetrating Polymer Network Hydrogels." *Acta Biomaterialia* 7 (6): 2384–93. doi: 10.1016/j.actbio.2011.01.016.

Yin W, Khin, and Si-Shen F. 2005. Effects of Particle Size and Surface Coating on Cellular Uptake of Polymeric Nanoparticles for Oral Delivery of Anticancer Drugs." *Biomaterials* 26 (15). Elsevier: 2713–22. doi: 10.1016/J.Biomaterials.2004.07.050.

Yue K, Grissel Trujillo-de Santiago, Mario Moisés Alvarez, Ali Tamayol, Nasim Annabi, and Ali Khademhosseini. 2015. "Synthesis, Properties, and Biomedical Applications of Gelatin Methacryloyl (GelMA) Hydrogels." *Biomaterials* 73: 254–71. doi:10.1016/j.biomaterials.2015.08.045.

Ziane S, Schlaubitz S, Miraux A, Patwa C, Lalande I, Bilem S, Lepreux B, et al. 2012. "A Thermosensitive Low Molecular Weight Hydrogel as Scaffold for Tissue Engineering." *Cells and Materials* 23: 147–60.

Zudaire S, Enrique M, and Cuttitta F. 2012. *The Textbook of Angiogenesis and Lymphangiogenesis: Methods and Applications: Methods and Applications*. Springer Science & Business Media. doi:10.1017/CBO9781107415324.004.

APPENDICES

APPENDIX A

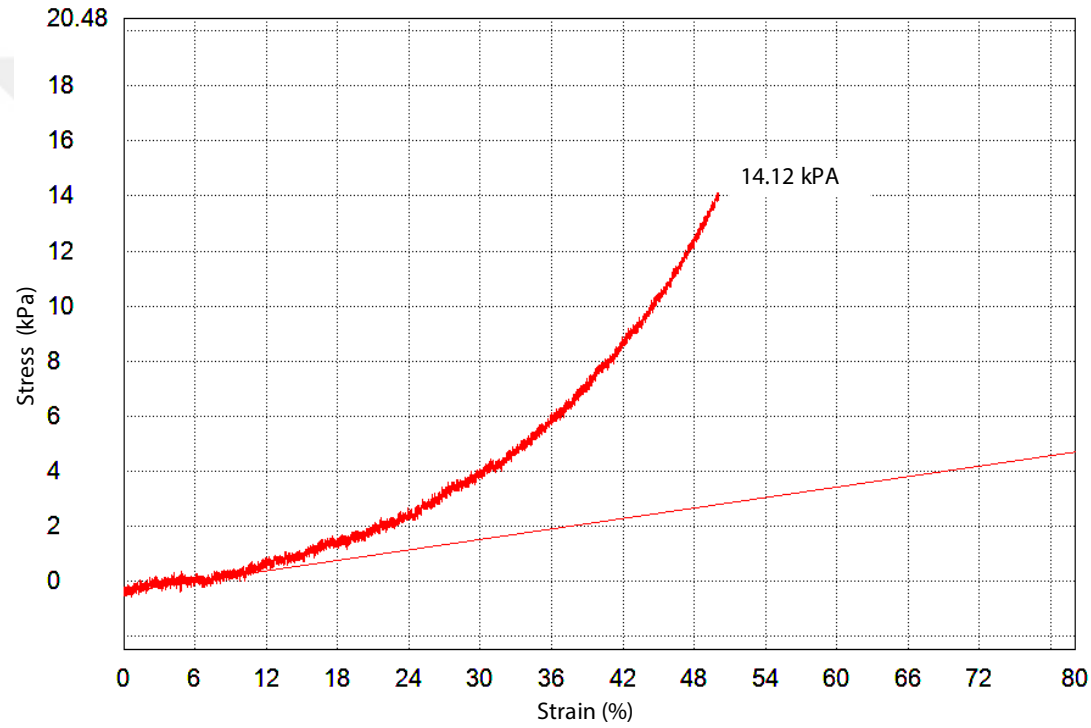

Appendix A: Representative stress strain curve of the hydrogel for compressive test.

APPENDIX B

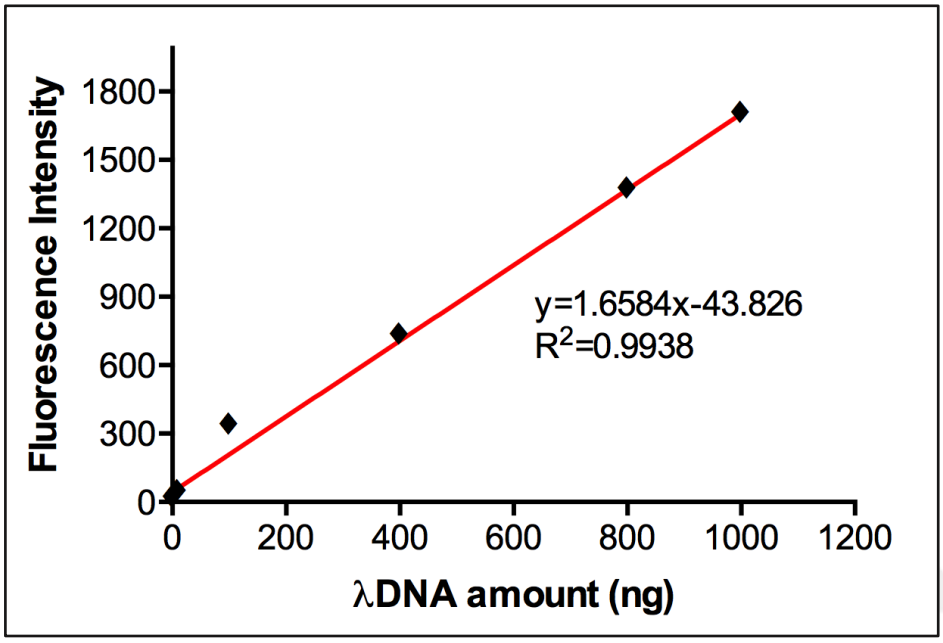

Appendix B: Calibration curve of λDNA-Florescence Intensity for DNA quantification assay.

APPENDIX C

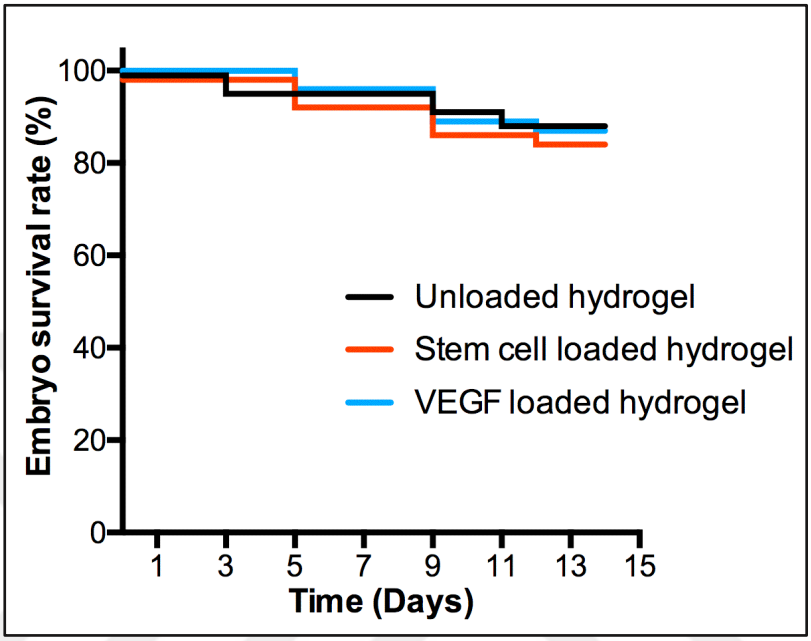

Appendix C: Embryo survival rate in the presence of unloaded, stem cell loaded and VEGF loaded hydrogels.

APPENDIX D

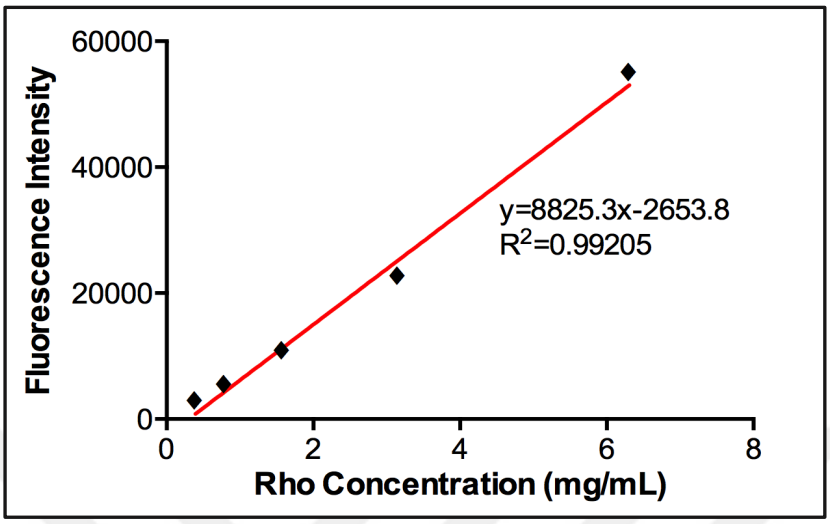

Appendix D1: Calibration curve of Rhodamine Concentration – Fluorescence Intensity for *in situ* Rhodamine release

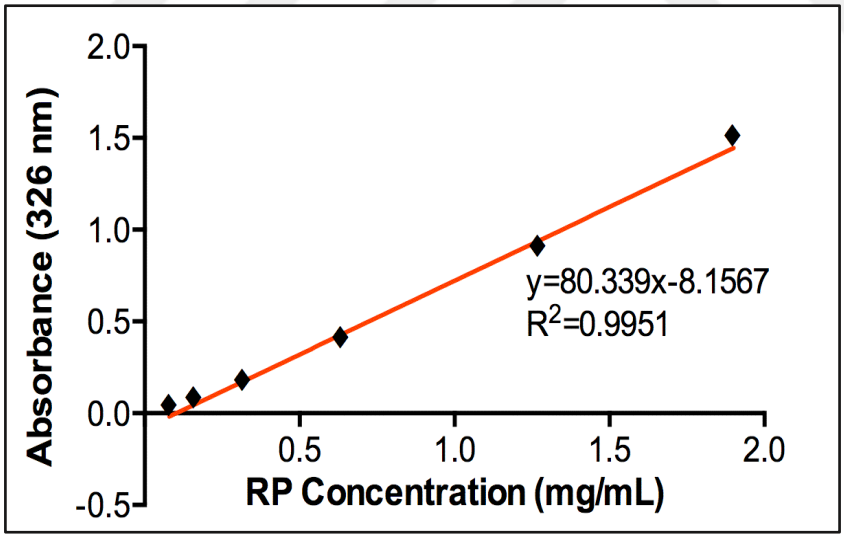

Appendix D2: Calibration curve of Retinyl Palmitate (RP) Concentration – Absorbance for *in situ* Retinyl Palmitate release.

APPENDIX E

UYGULAMALI ETİK ARAŞTIRMA MERKEZİ
APPLIED ETHICS RESEARCH CENTER

ORTA DOĞU TEKNİK ÜNİVERSİTESİ
MIDDLE EAST TECHNICAL UNIVERSITY

DUMLUPINAR BULVARI 06800
ÇANKAYA ANKARA/TURKEY
T: +90 312 210 22 91
F: +90 312 210 79 59
ueam@metu.edu.tr
www.ueam.metu.edu.tr

Sayı: 28620816/298-37

17.06.2014

Gönderilen : Prof. Dr. Vasıf HASIRCI
BİOMATEN

Gönderen : Prof. Dr. Canan Özgen
IAK Başkanı

İlgi : Etik Onayı

Danışmanlığını yapmış olduğunuz Biyoteknoloji Bölümü öğrencisi Gözde Eke'nin "İlaç Yüklü Polimerik Nano Parçacıkların Deri İçine Alımı" isimli araştırması "İnsan Araştırmaları Komitesi" tarafından uygun görülerek gerekli onay verilmiştir.

Bilgilerinize saygılarımla sunarım.

Etik Komite Onayı

Uygundur

17/06/2014

Prof.Dr. Canan Özgen
Uygulamalı Etik Araştırma Merkezi
(UEAM) Başkanı
ODTÜ 06531 ANKARA

Appendix E: Ethical permission was granted by Middle East Technical University Applied Ethics Research Center Ethics Committee.

CURRICULUM VITAE

Homepage: http://biomat.metu.edu.tr/gozde-eke

PERSONAL INFORMATION

Nationality: Turkish (T.C)

Date of and place of birth: 21 March 1984, Ankara, Turkey

Phone: +90 535 712 38 62

Work: +90 312 210 51 89

Fax: +90 312 210 15 42

E-mail: gozdeeke@gmail.com; e168923@metu.edu.tr

EDUCATION

Degree	Institution	Year of Graduation
Ph.D	Middle East Technical University (METU), Dept. of Biotechnology	2018
MS	Middle East Technical University (METU), Dept. of Micro and Nanotechnology	2011
BS	Ankara Univ., Dept. of Chemical Engineering	2007
High School	Ankara H. Omer Tarman High School	2002

ACADEMIC AND WORK EXPERIENCE

Year	Place	Enrollment
2009-cont	Ahi Evran University Faculty of Arts and Sciences Department of Chemistry, Kırşehir	Teaching Assistant
2009-cont	METU, Center of Excellence in Biomaterials and Tissue Engineering (BIOMATEN)	Full Time Researcher
2015 (9 months)	Department of Materials Science and Engineering, University of Sheffield, Kroto Research Institute, Sheffield, England	Visiting Researcher (CAM assay ex ovo and histology studies)
2011 (2 months)	Department of Medical Biology, Siberian Federal University, Krasnoyarsk, Russia	Visiting Researcher (in vivo experiments)
2007-2008	Sanovel Pharmaceutical Company Inc., İstanbul	Stability Expert

FOREIGN LANGUAGES: English (advanced), German (beginner), Russian (beginner)

PUBLICATIONS

Research Articles

1. Sahin A., **Eke G**., Buyuksungur A., Hasirci N., Hasirci V. Nuclear targeting peptide-modified, DOX-loaded, PHBV nanoparticles enhance drug efficacy by targeting to Saos-2 cell nuclear membranes. *Journal of Biomaterials Science, Polymer Edition*. 2018, 1-23. DOI: 10.1080/09205063.2018.1423812

2. **Eke G**., Mangır N., Hasirci N., MacNeil S., Hasirci V. Development of a UV crosslinked interpenetrating network hydrogel containing adipose derived stem cells as a dermal substitute to promote vascularization for tissue engineered skin. *Biomaterials*. 2017, 129, 188-198. DOI: 10.1016/j.biomaterials.2017.03.021.

3. **Eke G**., Goñi-de-Cerio F., Suarez-Merino B., Hasirci N., and Hasirci V. Biocompatibility of Dead Sea Water and Retinyl Palmitate Carrying PHBV Micro/Nanoparticles Designed for Transdermal Skin Therapy. *Journal of Bioactive and Compatible Polymers*. 2015, 30(5) 455-471. DOI: 10.1177/0883911515585183.

4. **Eke G**., Kuzmina A., Goreva A., Shishatskaya E., Hasirci N., and Hasirci V. *In Vitro* and Transdermal Penetration of PHBV Micro/Nanoparticles. *Journal of Materials Science: Materials in Medicine*. 2014, 25(6), 1471-1481. DOI: 10.1007/s10856-014-5169-5.

Book Chapters

1. Hasirci, V., Huri, P. Yilgor, Tanir, T. Endogan, **Eke, G**., and Hasirci, N. Polymer Fundamentals: Polymer Synthesis. In: Ducheyne, P., Grainger, D.W., Healy, K.E., Hutmacher, D.W., and Kirkpatrick, C.J. (eds.), Comprehensive Biomaterials II, 1. pp. 478–506. 2nd Edn. Oxford: Elsevier. 2017; 1-22.
DOI: http://dx.doi.org/10.1016/B978-0-12-803581-8.10208-5

2. Hasirci V., Yilgor P., Endogan T., **Eke G**., Hasirci N. Polymer Fundamentals: Polymer Synthesis, in: Ducheyne P., Healy K., Hutmacher D., Grainger D.W., Kirkpatrick. C.J. Comprehensive Biomaterials 2011; 1: 349-371.

3. Demirbag B., Kardesler S., Buyuksungur A., Kucukturhan A, **Eke G**., Hasirci N., Hasirci V. Nanotechnology in Biomaterials: Nanoparticulates as Drug Delivery Systems, in Bionanotechnology II: Global Prospects, ed D. Reisner. CRC Press/Taylor and Francis. 2011(11); 227-246.

Proceedings

1. **Eke G**., Mangir N., Hasirci N., MacNeil S., Hasirci V. A UV crosslinked IPN hydrogel loaded with ADSC to promote vascularization for tissue engineered skin. Termis European Congress. European Cells and Materials. 20-30 June 2017. 34(1). 1473-1474.

2. **Eke G**., Mangır N., Hasirci N., Chapple C., Hasirci V., MacNeil S. Estradiol releasing hydrogel as a proangiogenic substitute for fat flaps used in urogenital reconstruction. 32nd Annual EAU Congress, 24-28 March 2017, London, United Kingdom. 16(3). e336–e337.

3. Hasirci V., Sahin A., **Eke G**. Delivery of drugs into Cells with PHBV Nanoparticles. 4th TERMIS World Congress, Tissue Engineering Part A. 08-11 September 2015, Boston, USA. 21(1). S349-S349

Oral presentations

1. **Eke G**., Kuzmina A.M., Goreva A.V., Shishatskaya E.I., Hasirci N., Hasirci V. In vitro and In vivo Transport of PHBV Micro/Nanoparticles. European Symposium on Biopolymers (ESBP 2013), 7-9 October 2013, Lisbon, Portugal.

2. **Eke G**., Hasirci N., Hasirci V. In vitro and In vivo Study of Biopolymer Based Micro/nanoparticles with Different Sizes for Transdermal Applications. Summer School on Biomaterials and Regenerative Medicine, 9-13 July 2012, Trento, Italy.

3. **Eke G**., Kucukturhan A., Kardesler S., Yilgor P., Hasirci N., Hasirci V. Nanoparticles as Drug Carriers for the Treatment of Skin Diseases. 6th Nanoscience and Nanotechnology Conference - NANOTR VI, 15-18 June 2010, Izmir, Turkey

Poster Presentations

1. **Eke G**., Kucukturhan A., Yilgor P., Hasirci N., Hasirci V. Polyester Based Nanoparticles as Bioactive Agent Carriers for the Treatment of Skin Diseases. Biomedical Science and Technology Symposium, 28 September - 2 October 2010, Istanbul, Turkey

2. **Eke G**., Hasırcı N., Hasırcı V. Biyopolimerik Nano-mikroparçacıkların İlaç Salım Sistemleri Olarak Deri Hastalıkları Tedavisinde Kullanımı. 3. Ulusal Polimer Bilim ve Teknoloji Kongresi, 12-14 Mayıs 2010, Kocaeli, Turkey.

3. Kardesler S., **Eke G**., Kucukturhan A., Yilgor P., Hasirci N., Hasirci V. Topical Delivery Systems for the Treatment of Skin Diseases. International Symposium of Biotechnology, 27-30 September 2009, Ankara, Turkey.